IJEST

ISSN: 0973-6255
Vol. 14 No.1&2
January - December 2020

Indian Journal of Engineering, Science, and Technology

A Refereed Research Journal

Published by

BANNARI AMMAN INSTITUTE OF TECHNOLOGY

(Autonomous Institution Affiliated to Anna University, Chennai - Approved by AICTE - Accredited by NAAC with "A+" Grade)

Sathyamangalam - 638 401 Erode District Tamil Nadu India | Ph: 04295-226340 - 44 Fax: 04295-226666

E-mail: ijest@bitsathy.ac.in | www.bitsathy.ac.in

Stay Ahead

Indian Journal of Engineering, Science, and Technology

IJEST is a refereed research journal published half-yearly by Bannari Amman Institute of Technology. Responsibility for the contents rests upon the authors and not upon the IJEST. For copying or reprint permission, write to Copyright Department, IJEST, Bannari Amman Institute of Technology, Sathyamanagalam, Erode District - 638 401, Tamil Nadu, India.

Indian Journal of Engineering, Science, and Technology

ISSN: 0973-6255

Volume 14 Number 1&2 **January - December 2020**

CONTENTS

DESIGN AND CHARACTERISTIC STUDY OF HEATING COIL COATED WITH BLYGOLD PLOUAL XT AND ZINC

N. Santhosh[1], Sanjith Muthuvel[2] and M. Srinivasan[3]
[1&2]Department of Mechatronics
[3]Department of Electrical and Electronics Engineering
Bannari Amman Institute of Technology, Sathyamangalam - 638 401, Erode District, Tamil Nadu
E-mail: santhoshmech10@gmail.com

Abstract

The heating coil, or inductor, is a special heating device that is shaped in a spherical design. The coil is made up of ceramic or metal, such as copper, and gets heated when passing an electrical current. The heating coil is subjected to corrosion when it is in contact with water over a prolonged period of time, and this affects the conduction and also reduces the life of the coil. To avoid this, a coating layer of Blygold (Polyurethane impregnated with aluminium) followed by zinc is coated on the surface of the coil. The design and analysis of the proposed coated coil are performed using Intellisute software. The analysis includes both corrosion and the effect of high pressure and stress on the copper coil. Both the coated and non-coated analysis results are compared, and the performance enhancement of the coated copper coil is validated.

Keywords: *Blygold, Corrosion, Heating coil, Intellisute software, Zinc*

1. INTRODUCTION

Nowadays, the heating coil used in water heaters [1-3] is made of copper, which is used to heat the water at high temperatures because it is a good conductor of electricity and has corrosive resistance to water. And at the same time, it can also withstand the pressure and stress of the water very easily without causing any damage to the heating coil. Normally, the corrosion and damage will not occur on the heating coil which is placed in the small water heaters (5 lts to 15 lts) which are used in houses.

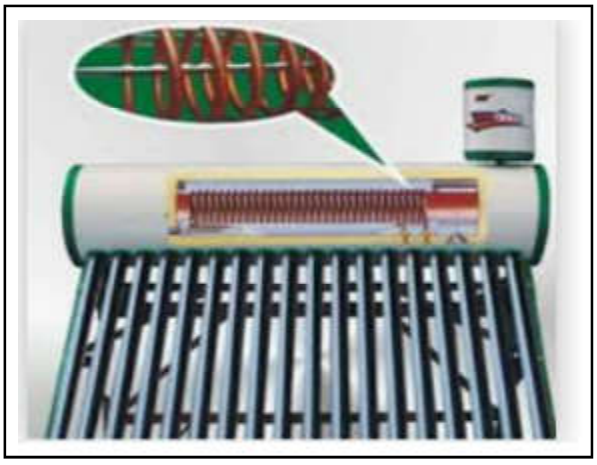

Fig. 1 Water heater with a copper heating coil

But the large capacity water heaters like solar water heaters (100 lts–1000 lts) have a copper heating coil inside that is used to heat the water continuously at a high temperature (60^0 C). These water heaters are mainly used in apartments, colleges, hospitals, hotels, etc. For these kinds of applications, the water heater must be turned on 24/7 to keep the water hot at all times [4]. The coil resists corrosion up to a temperature range of 600^0 °C and can withstand pressure and stress up to 1242 psi and 41 MPa respectively. Generally, the coil is made with a thickness level of 6mm–15mm respectively and corrodes at a rate of 0.25mm per year, but when the coil is used in heating salt water, the coil gets cored at a rate of 0.025mm per year [5–7]. The corrosion of the coil occurs not only due to heating the coil to a high temperature but also due to the pressure and stress developed due to the continuous flow of water. Hence, a detailed analysis is required to determine the rate at which the coil gets corroded. Hence, a suitable simulation is required to find out the optimal coating value required to withstand the corrosion due to the various factors. In this work, the MEMS software is used to perform the simulation operation. A comparative study is performed between the coated and non-coated heating coils, and the optimal coating is obtained from the simulation results.

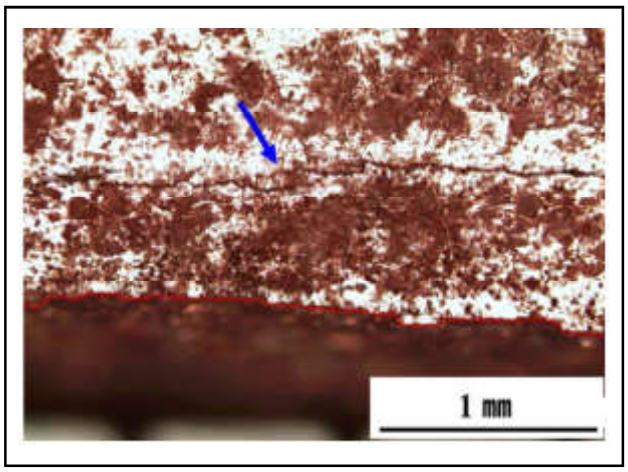

Fig.2 Heating coil crack

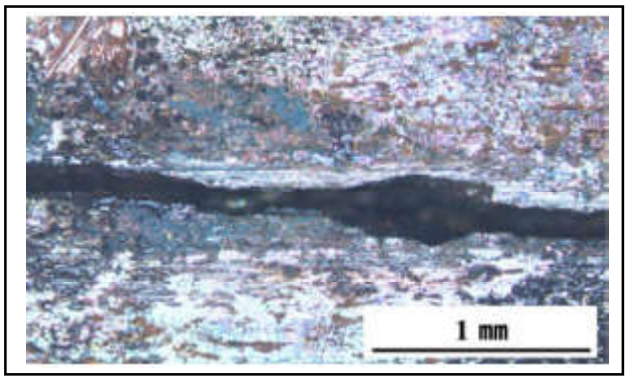

Fig. 3 Heating coil corrosion

Fig. 4 Copper coil corrosion

The crack that occurs on the coil is due to different reasons, such as high temperature (when water is at 100 °C), high pressure, and stress (fig. 2, 3). If there is any salt content present in the water, the coil will be completely corroded and damage the entire system (fig. 4). These are all the problems that will occur in the heating coil when coating is not given to the coil properly and at the same time if the pressure and the stress are too high. To avoid these problems, we created a design of the heating coil in MEMS software (fig. 5) to analyse the amount of corrosion and stress developed in the coil. The analysis of the heating coil is done on three different types of coating (first by using Blygold PoluAl XT, second by using Zinc, and third by using both Blygold and Zinc), and also the non-coated coil. By analysing the coil with different methods of coating, we will be able to compare the range of coatings which are suitable for the coil to avoid corrosion and damage due to high temperature, pressure, and stress.

2. THEORY OF CORROSION

The corrosion that has occurred on the heating coil (which is present in the solar water heater) is caused by high pressure and stress. Consider a 3BHK apartment (4 houses on one floor), which requires 20L of water per floor. If we use a 100-liter capacity solar water heater for that, a huge amount of pressure and stress will occur on the heating coil while heating the water. When the water is heated at a high temperature, the pressure and stress inside the water heater lead to corrosion and can damage the heating coil. This makes the coil corrode very easily. A proper calculation has to be done in order to find the optimal capacity solar water heater. For example, If an apartment requires 800 litres of water, then an 800 litre capacity SWH (Solar Water Heater) is needed. If it is 1000 lts, then a 1000 lt capacity SWH is required. If it is 1400 lts, we need two 700 lts SWH. According to this ratio, the solar water heater must be used.

Another cause of corrosion in the heating coil is that it is constantly submerged in water, and there is no oxygen present inside the solar water heater, which causes corrosion. The corrosion that occurs in the absence of dissolved oxygen is known as anoxic corrosion. In this type of corrosion, hydrogen gas is released as a result of the reaction between copper atoms and water molecules. It is because no proper coating is given to the heating coil, so it makes the coil corrode easily [8-13]. When the coils are heated, the pressure and stress will be generated on the heating coil, which will cause the coil to get corroded and damaged easily. To avoid that problem, two different coatings are coated on the heating coil to avoid corrosion. At the same time, if there is any salt content in the water, the coil will also get corroded very easily. It is because when the water is heated (which may contain salt in it), the generated pressure and stress act on the heating coil, making the

coil corrode and damage the coil easily. The two types of coating that are used to coat the heating coil are Blygold PoluAl XT and Zinc.

2.1 Blygold PoluAl XT Coating

Blygold PoluAl XT is a good coating source for copper coils. It is mainly used for coating copper coils and air-conditioning cooling pipes. The main purpose of using Blygold for coating the copper coil is that Blygold offers a range of solvent-based (if there is any salt content in the water, it will dissolve it easily), and water-based coatings that protect the heating coil from corrosion. At the same time, they can withstand very high temperatures very easily. The corrosion occurred due to a lack of oxygen and the moisture content which is present in the coil. To avoid this problem, Blygold coating is coated on the heating coil to lock in the moisture absorption and to prevent the coil from getting corroded. The thickness of the coating that is needed to be coated on the heating coil is 10m–12m. Even if corrosion occurs, the coating will withstand up to 6–7 years. After that, a new coating can be applied to the heating coil after removing the coating with muriatic acid (hydrochloric acid).

2.2 Zinc Coating

Zinc coatings are also good for coating copper coils. The main purpose of the zinc coating is to provide a protective layer against water to avoid the coil getting corroded. Zinc can form protective layers comprising basic carbonates, oxides, or hydrated surfaces depending upon the nature of the environment. The thickness of the coating that is needed to be coated on the heating coil is 20m–25m. Even if corrosion occurs, the coating will withstand up to 5–6 years (underwater pipes). After that, a new coating can be applied to the heating coil after removing the coating by using diluted muriatic acid (diluted hydrochloric acid).

2.3 Micro Electro Fabrication using MEMS

The blueprint and 3D builder are used to design the copper heating coil in MEMS software. First, we use a blueprint to create the design of the heating coil, which consists of the detailed design of the heating coil, which includes the detailed information of the material to be used. Blygold PoluAl XT (Polyurethane impregnated with Aluminum) at 12m and Zinc at 25m are the coating materials used. After building the model, the appropriate materials are selected. Further meshing is done to ensure that the forces applied, such as pressure, temperature, and stress, are distributed equally. In this, the mechanical meshing is done and, normally, the analysis time mainly depends upon the meshing size, so an optimal meshing is required. In this work, a mesh size of 10m is obtained for analysis. When the modelling is completed, the boundaries of the designs need to be fixed together to get the proper analysis value without any errors in the design. The meshed model is subjected to forces and the analysis is done by the Thermo Electro Mechanical analysis tool.

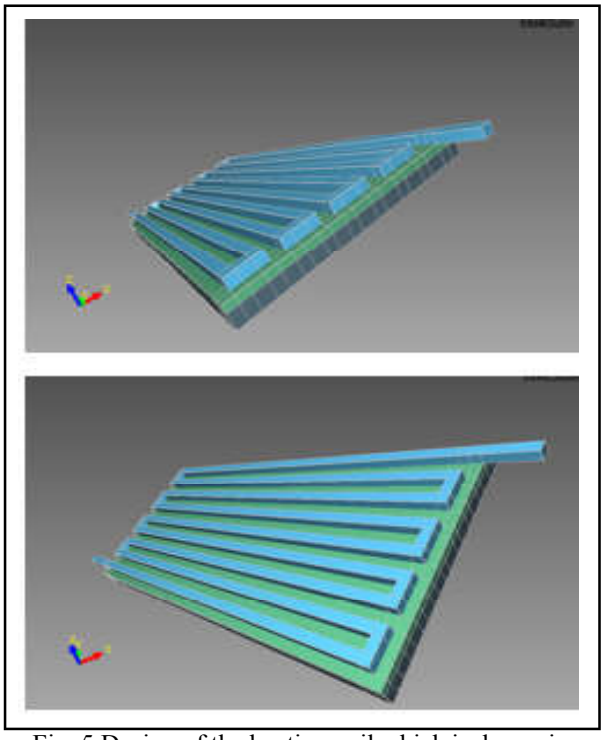

Fig. 5 Design of the heating coil which is drawn in the MEMS software

3. RESULT AND DISCUSSION

After analysing the copper heating coil in MEMS software, we can check the difference between how much pressure and stress the heating coil can withstand before and after coating. It is observed that a comparative study is shown in Table 1 and Fig.7-9, where the impact of pressure and stress for different temperature conditions is monitored for different levels of coatings. It is shown that the pressure and stress impact are greater in the non-coating coil when compared to the coated coil, and among the coated coils, the combination of blygold and zinc gives more preservation to the coil when compared with the blygold and zinc coating separately.

Table 1 Impact of Pressure and Stress on Coating and Non-Coating of Coil at Different Temperature

	Non-coating		Blygold		Zinc		Blygold + Zinc	
Temperature °C	Pressure (psi)	Stress (Mpa)	Pressure (psi)	Stress (Mpa)	Pressure (psi)	Stress (Mpa)	Pressure (psi)	Stress (Mpa)
32.4°C	1134	200	1125	174	1108	161	1014	157
50°C	1209	227	1147	214	1186	203	1152	194
80°C	1269	248	1200	229	1242	231	1193	219

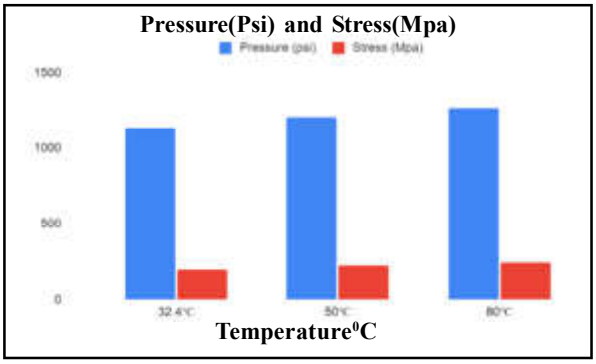

Fig. 6 Pressure vs Stress at different temperature on non-coated coil

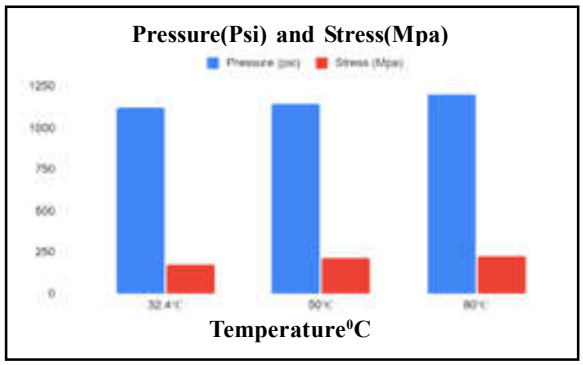

Fig. 7 Pressure vs Stress at different temperature on Blygold coated coil

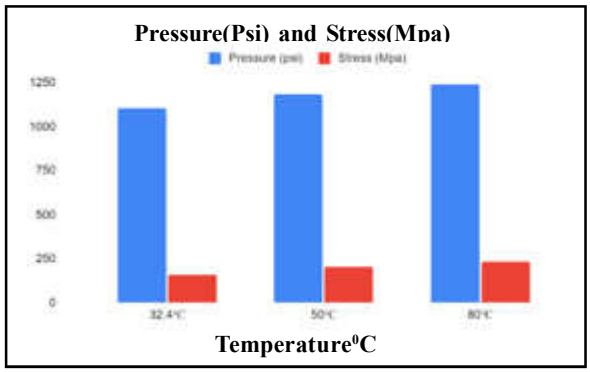

Fig. 8 Pressure vs Stress at different temperature on Zinc coated coil

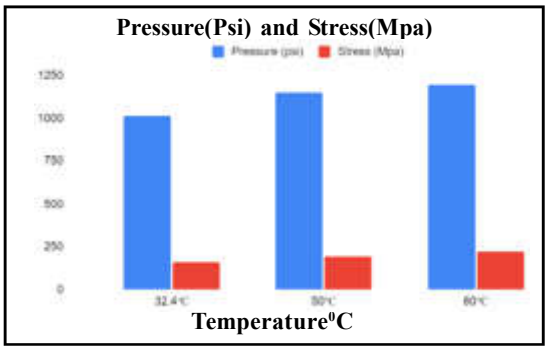

Fig. 9 Pressure vs Stress at different temperature on Blygold+Zinc coated coil

4. CONCLUSION

The heating coil is designed and fabricated in MEMS software in this work, and it is subjected to various pressure and stress conditions at various temperatures.The coils which are subjected to analysis are of different combinations, such as a non-coated coil, a Blygold coated coil, a zinc coated coil, and a combination of both the coatings. It was found that the pressure and stress impact are greater in the non-coating coil when compared to the coated coil and comparing the coated coil the coil with a combined coating of Blygold and zinc performed better when compared to the non-coated and individual coated coils. It is concluded that the combinational coating of Blygold and zinc are best suitable for the fabrication of heating coil.

REFERENCE

[1] Ahmed Elatar, Kashif Nawaz, Bo Shen and Van Baxter "Hydrodynamic Behavior of Wrapped Coil Water Heater Tank", Thermal Science and Engineering Progress, Vol.20, 2020, pp.100741, ISSN 2451-9049,https://doi.org/10.1016/j.tsep.2020.100741.

[2] Sari Farah Dina, Jufrizal, Siti Masriani Rambe, Harry P. Limbong and Edwin H. Sipahutar "Design of Solar Water Heater Using Collector Cylindric Parabolic and Coil Heater as Absorber at Focus Point E3S", Web of Conferences Vol.328,2021.

[3] P.K.Kushwaha, N.K.Sharma, A.Kumar and C.S.Meena, "Recent Advancements in Augmentation of Solar Water Heaters Using Nanocomposites with PCM: Past, Present, and Future", Vol.13, Buildings 2023, pp.79. https://doi.org/10.3390/buildings13010079.

[4] Pooran Singh Dhakar, " A Review Study on Solar Water Heating Systems", JETIR Vol.6, No.6, 2019.

[5] G. Pantazopoulos and G. Tsinopoulos, "Corrosion of a Copper U- Shaped heating Element: Some Morphological and Microstructural Observations", ASM International, 2006.

[6] Hobyung Chae, Huai Wang, "Stress Corrosion Cracking of a Copper Pipe in a Heating Water Supply System", Metals and Materials International, 2019.

[7] L Nelson Farro, P Veleva and I.Copper Marine Corrosion, "Corrosion Rates in Atmospheric and Seawater Environments of Peruvian Port", Open Corrosion Journal, 2009.

[8] Ashoke Kumar Pandey, K. P. Venkatesh and Rudra Pratap "Effect of Metal Coating and Residual Stress on the Resonant Frequency of MEMS resonators" Springer. Vol.651, 2009.

[9] N.Ryan O'Donnell, R. Thomas Powell and S. Zoran Filipi, "Estimation of Thermal Barrier Coating Surface Temperature and Heat Flux Profiles in a Low-Temperature Combustion Engine Using a Modified Sequential Function Specification Approach", Journal of Heat Transfer, 2016.

[10] H.M.Mahmood, Suryanto and Farag Haider "Improvement of Thermal Conductivity by Anodized Copper Coating", IJRTE, 2019.

[11] Stefano Rossi, Massimo Calvi, Domenico Dalpiaz, "The Influence of NIR Pigment on Coil Coating Thermal Behaviors", Department of Industrial Engineering, Italy, 2020.

[12] J. G. Pereyar-Hernandez and I. Rosales-Cadena, "Heat Treatment Effect in the Corrosion Resistance of the Al-Co-Mn Alloys Immersed in 3 M KOH", Research Article, 2021.

[13] M. Korhonen, P. Starck and B. Lofgren, "Characterization of Coil Coating by Thermal Analysis", Journal of Applied Polymer Science, Vol. 87, 2003 Wiley Pero, 2016.

RESUME SCREENING USING NATURAL LANGUAGE PROCESSING

T. Kumaresan[1] and S. Premikkha[2]
[1]Department of Artificial Intelligence and Data science
[2]Department of Computer Science and Engineering
Bannari Amman Institute of Technology, Sathyamangalam -638 401, Erode District, Tamil Nadu
E-mail: kumaresant@bitsathy.ac.in, premikkha.cs19@bitsathy.ac.in

Abstract

As automated recruitment is getting more and more common, manual hiring processes are becoming unproductive. This is due to the fact that recruiting firms get tens of thousands of unstructured resumes from candidates with various levels of expertise. These resumes are too complex to assess manually; yet, an automated recruitment system does so effectively. This makes it easier for recruiters to quickly evaluate, choose, organise, and weed out irrelevant applicants. After the text extraction procedure is finished, the score is calculated using the specifications they provided for the job. The calculated scores are then saved in the local system as a csv file. We utilised a bar chart for better visualisation, and the image of the visualisation is saved as a jpg file on the local computer. To parse the entire resume and to evaluate the resumes, the system makes use of a Natural Language Processing method, NLP toolkit. Phrase Matcher which is provided by NLP toolkit is used to track the frequency of words in various categories. We discovered from the experimental findings that our system operates effectively.

Key Words: *Natural Language Processing, Phrase Matcher. Hiring Process, Python, Resume, Human Resources*

1. INTRODUCTION

For recruiters' talent acquisition is a critical, tedious, and time-consuming process. The size of candidates who are searching for a job is mindboggling. According to LinkedIn, India has the huge percentage of candidates who are "actively searching for a new job [1]." Probably, this is a very liquid and large market, but it also contains a huge irritating inefficiency. The lack of a consistent organisation and format is the most tedious aspect. Shortlisting potential profiles from thousands of resumes for a particular job role is extremely time-consuming and laborious process [2]. To identify the best resumes out of thousands of resumes for a particular job role, effective resume screening and evaluating necessitates domain expertise is required. Selecting or shortlisting the resumes based on the job requirements is difficult for the human resource department because there are huge number of various job roles available nowadays, and also huge number of applications submitted for a job position [3]. India's market is huge. Not only do one million candidates enter into the corporate or MNCs every month, but there is also a huge turnover. This hiring process faces three significant challenges they are:

- Short-listing the applicable individuals from the thousands of individuals: With millions of individuals looking for job in India, screening the resumes and selecting the appropriate individuals is very difficult. This leads to the entire hiring process gradual and inefficient, wasting time for the company.

- Analysing the format of candidate resumes: We all know that CVs that is received from thousands of candidates are not in standard format and this is a second issue. Each and every resume on the market has a different format. Human resource should manually go through the resumes in order to filter out the best individuals for the job description. Obviously, this is time-consuming and also leads to inaccuracy, because a good candidate for the specified job may be overlooked in the process.

- Confirming the candidates are eligible for the particular or specific role before hiring them: The third issue and tedious problem is to evaluate the individuals whether their CV is relevant or matches to the job description in order to identify whether the candidate is capable for the position for which she is being selected

2. RELATED WORK

The Hiring procedure in today's world has witnessed a huge change with the evolution of technologies like the Internet [4]. The following section summarises some of the related work performed in this domain of automated recruiting systems.

The Standard Multiple Linear regression model is aids in predicting the performance of the candidates. Artificial intelligence (AI) has developed as a boon to the human resources (HR) by automating the process of shortlisting and eliminating the CVs. AI based shortlisting and screening helps in automating resume screening process [5]. The Natural Language Processing is implemented to extract required information like skills, education, experience, from the resume from the unstructured resumes. To get better results it is important to check whether the resume matches with the job's description. Cosine – similarity is used to match the resume with the job description. The calculated scores are used to rank the resume of the candidates [6]. The Natural Language Processing is increasingly being used in recruiter's applications, but its purpose for this specific objective is still considered to be limited. The system focuses especially on the task of retrieving information about candidates from raw text data in the form of resumes. And introduces an algorithm to match resumes and job description. NLP has the ability to extract the desired information from the resume. Machine Learning (ML) also has been implemented for analysing the unstructured resume [7]. The ontology mapping is implemented for screening and evaluating candidates for the given job description. It has three phases of function which were the creation of candidate ontology, construction of job description ontology document and then finally mapping of these two to evaluate which individuals are eligible for the job. The job description ontology is mapped to the individual's ontology document and it gives the eligible candidates as output [8]. An automated resume screening system uses different machine learning algorithms and implements Support Vector Regression to create a list of ranked candidates based on job description. The system uses various technologies such as NLP, Spacy, TF-IDF etc., for retrieving the criteria from the LinkedIn profile of the applicants. It uses linguistic analysis to extract the personality characteristics and hence the system also performs personality mining [9]. The Internet and technology caused a considerable impact on the recruitment method through the creation of automated recruiting system that become a primary part or module in most of the corporations. The corporations established job positions on this system, applicants uses this system to send their resumes. Automated recruitment platforms accomplished clear benefits for each HR managers and applicants by reducing the recruiting time and the cost [10].

2.1 System Architecture

The Figure1 shown below is the architecture of the resume evaluator system. It represents the working process of the resume evaluation process. The five modules of the system are, Extraction of Information, Tokenization, Creation of dictionary with key terms, Evaluation and scoring and Results Visualization. The Candidate's resumes and field that is selected by HR are the two inputs to the system and stored in the database for further evaluation. Information extraction is done using NLP Natural language Processing Techniques and PYPDF2 module [11,12]. Scores are calculated for every resume and the results are stored in a data frame and graphical representation of the results are displayed to the users.

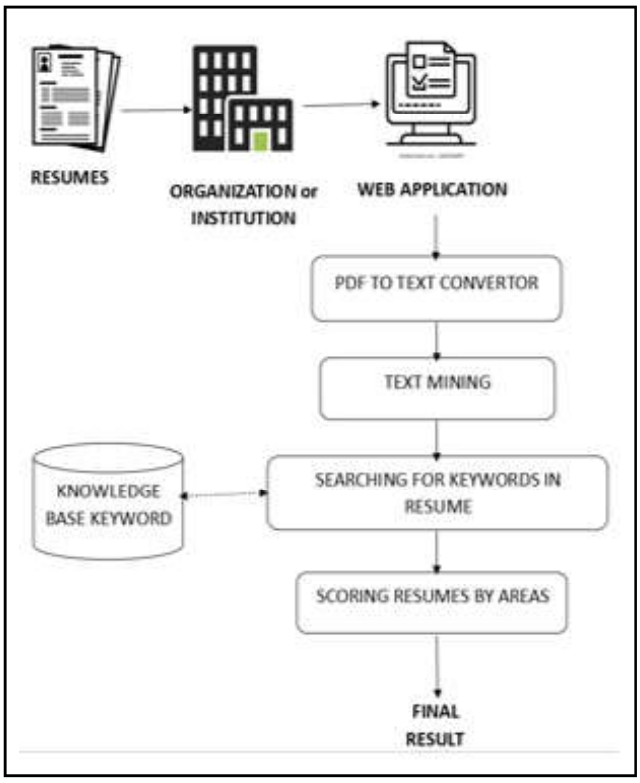

Fig.1 Architecture of our proposed system

3. PROPOSED METHODOLOGY

In this following section, we explain the concepts and methodology that facilitate the construction of the proposed Automated Resume Evaluating System [ARES]. The system functions in the following phases as described below.

3.1 Extraction of Information

The foremost step of our proposed system involves information extraction from the CVs. The data in the resumes is not in a structured or standard format [13]. There are noises, inconsistencies and irrelevant bits of data which is of no use for the recruiting process. The aim is to extract only the relevant keywords from the unstructured textual data in the CVs. Using techniques like Tokenization, Stemming, etc., our system obtains only the required keywords which are important job-description from the uploaded candidate resumes. The resume that are uploaded by the candidates will be in PDF format. For extracting texts from PDF Pages, we have implemented PyPDF2 module. PyPDF2 is a python library used for performing different operations on PDF files such as extracting the specific information, merging the PDF files, splitting the pages of a PDF file, encrypting and decrypting the PDF files [14]. And also, we have used Textract, which provides a single unified command line interface and Python API for extracting text from a various number of file types [15].

3.2. Tokenization

After converting the PDF resume format into text, we start the tokenization process to determine terms that form up a character sequence. This is necessary as through these words, we will be able to obtain meaning from the original text sequence. Tokenization involves dissecting large chunks of text into smaller parts called tokens. This is achieved by eliminating or isolating characters like whitespaces, numbers and punctuation characters. Tokens are sentences and then are further split into individual terms. By performing Tokenization, we can retrieve more information such as the number of words in a text, frequency of a particular word in the text and etc[15]. The tokenization can be implemented in multiple ways such as using Natural Language Toolkit, the SpaCy library, etc [13]. And also, we are converting all strings to lowercase for further process. Tokenization is a important step to get accurate and efficient results.

3.3. Creation of Dictionary with Key Terms

The candidates or engineers should have knowledge and background of each concentration area. It is often recommended for them to undergo a career in a specific concentration area within this field [16]. Additionally, we all know that we are currently on the specialization era, recruiters are more likely to prioritize the applicants with a strong background, knowledge and experience in a specific area or field than "generalist" applicants. Unfortunately, there is a misconception within the applicants between being "excellent and proficient" and being "specialized and highly skilled" in a specific area.
For the following hiring process or method, we have built a resume screening system using Python, which is capable of categorizing keywords into various concentration areas and identifying the one with the highest expertise level in the applicant's resume. For example, let's take the field 'computer science' and the system evaluates and categorizes into different areas (data base man agement, data structure, network and security, AI and data science, Data analytics). The key terms which are included in each area of this following dictionary were relevant to the job description. This dictionary can be customized to add or remove key terms according to the requirements of the job that is required for a specific job role.

3.4. Evaluating the Resume or CVs

The resume is evaluated by calculating the scores per each area. The algorithm scores the resume by counting the occurrences of the keyword in the dictionary in each area and it stores the result of each area which will be used for evaluating them. The scores in each area are stored in a data frame. The scores are displayed in descending order hence the highly skilled area is displayed first. The total score of the resume is also calculated. For a better visualization, the percentage of scores per each area are represented in a graphical form. There are two possible ways of evaluating these results. First is by looking at the score's summary data frame, recruiters can identify how many key terms were included in each concentration area from a given job description. The second way is, by looking at the pie chart which is a graphical format, hiring managers can identify the candidates highly specialization area. The scores will be highly influenced by the number of keywords in each specialization area which is specified in the dictionary.

4. RESULTS AND DISCUSSION

For testing our system, we have used the resumes based of computer science field. We have taken three relevant resume samples from the Internet which is based on computer science field. And those resumes are read by one by one from the folder and undergoes extraction of text from PDF, text cleaning, and finally the evaluation is done. Figure 1 given below shows the sample output after the calculations are performed are get stored inside the data frame.

```
                                score
Data analytics                      4
Database Management                 3
Data Structures and Algorithm       3
Networks and Security               3
AI and Data Science                 2
FullStack Development               1
Evaluation score of the resume: 16
```

Fig 2 Evaluated score of candiadate1

```
                                score
Database Management                18
Data analytics                      7
FullStack Development               3
AI and Data Science                 2
Data Structures and Algorithm       2
Networks and Security               2
Evaluation score of the resume: 34
```

Fig 3 Evaluated score of candiadate2

```
                                score
Networks and Security               5
AI and Data Science                 3
Data analytics                      3
FullStack Development               1
Database Management                 1
Data Structures and Algorithm       1
Evaluation score of the resume: 14
```

Fig 4 Evaluated score of candiadate3

Based on the results, we can analyse that candidate 2 best fits the job posting followed by candidate 1 and candidate 3. The candidates 1 and 3 are having lesser score when compared to candidate 1. The graphical representation of percentage of scores per area of candidates are displayed in figure 5.

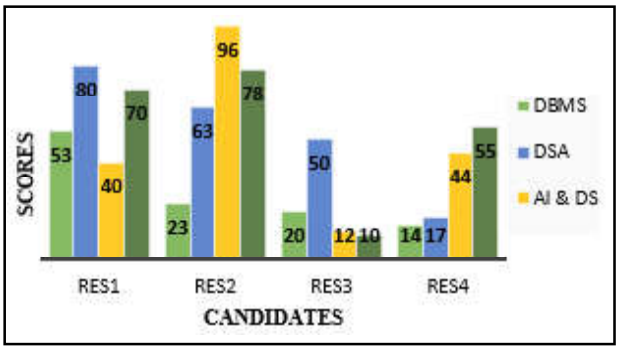

Fig 5. Graphical representation of Evaluated scores

X axis – Candidate's resume
Y axis – Scores of the Candidates

5. CONCLUSION

In this paper, we presented an automated resume evaluating system where complexity of recruitment process is being minimized by eliminating the various problems faced by the hiring managers as they relied on traditional shortlisting of applicants for a given job role. There are two possible ways of evaluating these results. First is by looking at the score's summary data frame, recruiters can identify how many key terms were included in each concentration area from a given job description. The second way is, by looking at the bar chart which is a graphical format, hiring managers can identify the candidates highly specialization area. The scores will be highly influenced by the number of keywords in each specialization area which is specified in the dictionary. The system explores the resume that best fit the particular job role.

REFERENCES

[1] A.Singh, C.Rose, K.Visweswariah, V. Chenthamarakshan and N.Kambhatla, "PROSPECT: A System for Screening Candidates for Recruitment", In Proceedings of the 19th ACM International Conference on Information and Knowledge Management, 2010, pp.659-668.

[2] S. Maheshwary and H. Misra, "Matching Resumes to Jobs Via Deep Siamese Network" Proceedings of The Web Conference, International World Wide Web Conferences Steering Committee, 2018, pp.87-88.

[3] J. Malinowski, T. Keim, O.Wendt and T.Weitzel, "Matching People and Jobs: A Bilateral Recommendation Approach", Proceedings of the 39th Annual Hawaii International Conference on System Sciences (HICSS'06), IEEE, 2006, pp. 137c-137c.

[4] J.L.Howard, G.R.Ferris, "TheEmployment Interview Context: Social and Situational Influences on Interviewer Decisions" Journal of Applied Social Psychology, Vol.26, 1996, pp.112–136.

[5] R. Vedapradha, R. Hariharan and R. Shivakami, "Artificial Intelligence: A Technological Prototype in Recruitment", Journal of Service Science and Management, Vol.12, 2019, pp.382-390.

[6] Chirag Daryani, Gurneet Singh Chhabra, Harsh Patel, Indrajeet Kaur Chhabra and Ruchi Patel, "An Automated Resume Screening System Using Natural Language Processing and Similarity", Intelligent Computing and Industry Design (ICID), Vol.2, No.2, 2020, pp.99-103.

[7] A.K.Sinha, M. Amir Khusru Akhtar and Ashwani Kumar, "A Resume Screening Using Natural Language Processing and Machine Learning: A Systematic Review", Advances in Intelligent Systems and Computing, ISSN: 21945357, eISSN: 21945365, AISC, Vol.1311, 2021, pp.207-214.

[8] V. Senthil Kumaran and A. Sankar, "Towards An Automated System for Intelligent Screening of Candidates for Recruitment Using Ontology Mapping EXPERT", International Journal of Metadata Semantics and Ontologies https://doi.org/10.1504/IJMSO.2013.054184, 2013.

[9] Evanthia Faliagka, Kostas Ramantas and Athanasios Tsakalidis, "Application of Machine Learning Algorithms to an online Recruitment System", International Conference on Internet and Web Applications and Services IARIA, ISBN:978-1-61208-200-4, 2012.

[10] A.Rajaraman, WalmartLabs and J.D.Ullman, "Ch9:Recommendation Systems", Mining of Massive Datasets, California, USA, Stanford University, 2011, pp. 287-321.

[11] M.Allahyari, S. Pouriyeh, M. Assefi, S.Safaei, E.D.Trippe, J.B.Gutierrez and K.Kochut, "A Brief Survey of Text Mining: Classification, Clustering and Extraction Techniques", arXiv preprint arXiv:1707.02919, 2017.

[12] A.Gelbukh, "Computational Linguistics and Intelligent Text Processing", Heidelberg: Springer Berlin Heidelberg, 2014.

[13] S.Jabri, A. Dahbi, T. Gadi and A. Bassir, "Ranking of Text Documents Using TF-IDF Weighting and Association Rules Mining", Fourth International Conference on Optimization and Applications (ICOA), IEEE, 2018, pp.1-6.

[14] P.K. Roy, J.P. Singh and A.Nag, "Finding Active Expert Users for Question Routing in Community Question Answering Sites", International Conference on Machine Learning and Data Mining in Pattern Recognition, Springer, 2018, pp. 440-451.

[15] K.Satheesh, A. Jahnavi, L. Aishwarya, K.Ayesha, G.Bhanu, Shekhar and K.Hanisha, "Resume Ranking Based on Job Description Using SpaCy NER Model", International Research Journal of Engineering and Technology, 2020.

[16] C.Hauff and G. Gousios, "Matching GitHub Developer Profiles to Job Advertisements" Proceedings of the 12th Working Conference on Mining Software Repositories, 2015, pp. 362-366, 2015.

RICE PLANT DISEASES CLASSIFICATION USING DEEP LEARNING ALGORITHM

B. Soundarya[1], C. Poongodi[2], R.Kokiladevi[3], M.Dhivyaa[4] and T. Satheesh[5]
[1.&2] Department of Electronics and Communication Engineering
Bannari Amman Institute of Technology, Sathyamangalam - 638 401, Erode District, Tamil Nadu
[3]Department of Computer Science and Engineering
Karpaga Vinayaga College of Engineering and Technology Chengalpattu - 603 308, Tamil Nadu
[4]Department of Electronics and Communication Engineering
Sri Shanmugha College of Engineering and Technology, Sankari - 637 304, Tamil Nadu
[5] Department of Artificial Intelligence and Data Science
Dr.N.G.P Institute of Technology, Coimbatore - 641 048, Tamil Nadu
E-mail: soundarya@bitsathy.ac.in, poongodic@bitsathy.ac.in, kokilaapcse@gmail.com

Abstract

Agriculture is the backbone of our country's economy. Rice is especially the primary food of our Indian people. Rice production in our country during the year 2021 -22 is 130.23 million tones. Rice production can be reduced by the diseases affecting the rice crop. Numerous major diseases such as blast, brown spot, bacterial blight, sheath blight, etc. are damaging the rice plant. Also minor diseases such as bakanae, false smut, and grain discoloration are affecting the rice crop, therefore reducing the yielding and leading to unprofit. So, in this paper a deep learning algorithm has been used to face this issue. Convolution Neural Network is the pre-eminent method in deep learning algorithms used for object detection and classification. This article focuses on diseases like brown spots caused by fungi and bacterial blight in the rice plant. The proposed CNN classification is implemented with the aid of 1000 samples of data set and obtained 96 % of accuracy.

Keywords: *Bacterial Blight, Brown Spot, CNN, Rice Disease Identification*

1. INTRODUCTION

Three basic needs of human's life: food, clothing and shelter. As food is the basic need of human beings, production of food has to be very large. Rice is especially an important food of our country. In the 1960s, high yielding semi-dwarf rice varieties were introduced by the International Rice Research Institute (IRRI). After that, India reached self- sufficiency in rice production. From then, India exports rice to foreign countries. Though the production of rice increases, diseases affecting the rice plant also increase. The major problem is diseases called brown spots caused by fungi and blight caused by bacteria in rice production. Brown spot: A fungal disease which affects mainly the leaves, leaf sheath of the rice plant. The big brown colored spots appearing on the leaf can destroy the whole plant. Brown spot happens in any stage of crop, but it becomes very dangerous when it occurs in the ripening stage. Figure 1 represents brown spot occurs in the rice plant leaf.

Fig.1 Brown spot in rice plant

Bacterial leaf blight: It is caused by Xanthomonas. When the rice plant is affected by Xanthomonas bacteria, the affected leaves turn yellow into straw colored, finally leading the plant to die. It is one of the severe diseases that take place in rice plants. Bacterial leaf blight occurs in the early stage of crop development means high yielding loss will occur. Figure 2 represents how bacterial leaf blight occurs in rice plant leaves.

Fig. 2 Bacterial leaf blight in rice plant

So, to overthrown these problem essential solutions has to be created. To classify the disease, CNN architecture has been proposed. It has three layers namely, convolution layer, pooling layer and finally fully connected layer. Even though CNN is an efficient algorithm to classify the images, there are some challenges in identifying and classifying the diseases in plant leaf. Quality of leaf image should be very high, leaf color may vary due weather and varieties of diseases are available. Considering these challenges into account, detection of leaf disease has been proposed.

2. LITERATURE REVIEW

For identifying diseases in leaf also to classify those diseases in the leaf, many articles has been proposed with image processing techniques and deep learning algorithms. By analyzing the following articles, modifications would be made to upgrade the performance Convolutional Neural Network (CNN) model.

- Proposed a classification of leaf disease using image processing. It has three steps in the classification of leaf disease such as pre-filtering, features withdrawal and testing of the images. In pre-filtering the image size has been adjusted followed by features of leaf like shape and color are extracted. Finally the unhealthiness of the leaf has been found by applying the image processing techniques.
- Employs a following techniques such as image acquisition, next one is image preprocessing, then image segmentation and feature extraction. Finally k-means algorithm for the classification leaf diseases in paddy.
- Suggested a genetic algorithm to identify and segregate the diseases of plant leaf.[7] proposed a method called k-means clustering for leaf disease diagnosing and classification using SVM, where SVM(Support Vector Machine) has two types of data set, one is test dataset and another one is training data set. By comparing these two dataset, healthiest and unhealthiest leaves are classified.
- Introduced a CNN in soybean leaf. It takes a dataset containing soybean leaves with all kind of leaves including good and unhealthy leaves. This proposed Alex Net and Google Net model provides accuracy of 98.75 % and 96.25% respectively.
- Suggested technique to identify disease in tea leaves. Image augmentation and image preprocessing were done. Also 88% of accuracy is obtained by using this method

3. PROPOSED WORK

Our proposed system uses pre-trained Convolutional neural network (CNN) model to classify the test samples from the trained dataset. Dataset of infected leaf images were collected from the kaggle website. It contains 220 sample dataset of infected leaf images and healthy leaf images. In which 80 were brown spot leaf images, 70 were bacterial blight disease leaf images and 70 were healthy leaf images. Brown spot leaf images were labeled as class A, bacterial blight disease leaf images were labeled as class B and healthy leaf images were named as class C. Summary of the trained and test dataset are given below.

Kagglewebsite:https://www.kaggle.com/datasets/vbookshelf/rice-leaf-diseases

Table 1 Sample dataset of infected leaves

Sl.No.	Disease	Training Dataset	Test Dataset
1	Brown spot	80	20
2	Bacterial blight	70	35
3	Healthy leaves	70	30
Total		**220**	**85**

3.1 Sample Dataset

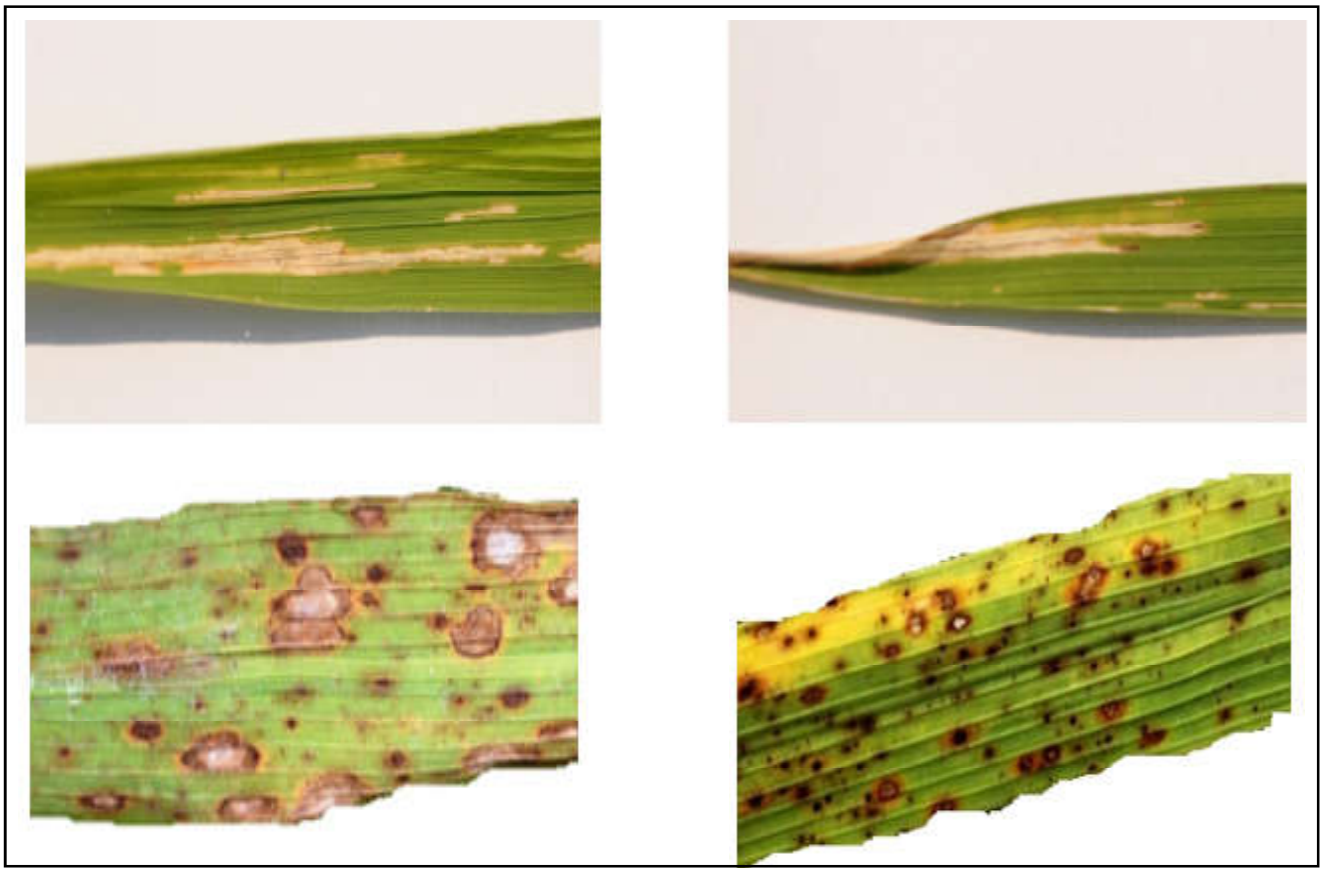

Fig.3 Sample dataset of infected leaves

After collecting a dataset containing **infected** leaf images and healthy leaf images, CNN model has been trained. Images have been preprocessed and these preprocessed images are fed into the pretrained model. Further, the process is carried out by the CNN layers. Architecture of the CNN model has represented in figure 4.

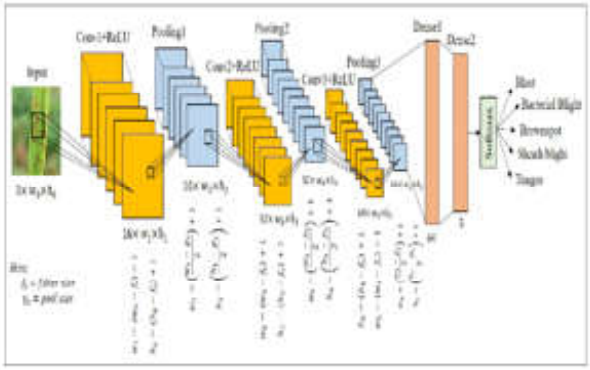

Fig.4 Architecture of CNN

Finally, the disease of the infected leaf has been identified and it is classified.

4. RESULT & DISCUSSION

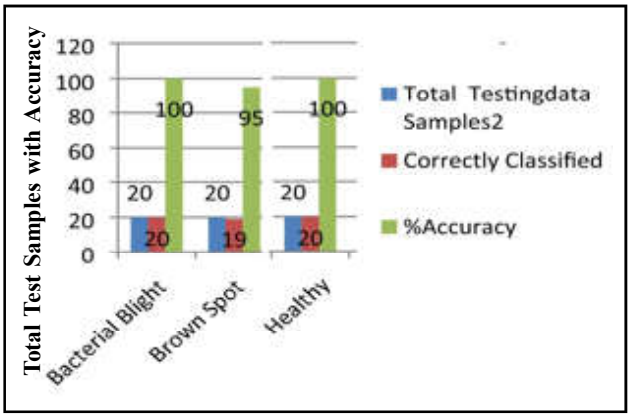

Fig.5 Result

Result has been shown in figure 5. To increase the performance of the CNN, learning rate, mini batch size, epochs, and iteration are slightly changed. Therefore, accuracy of this model 98.33 % is obtained.

5. CONCLUSION

In the proposed work, rice leaf diseases like brown spot and bacterial blight have been examined. With the support of Convolutional neural network models, disease of rice plant has been identified and classified. Also the output is obtained with 98.33 % accuracy rate. In the future, more varieties of diseases which affect the rice plant can be identified using this model.

REFERENCE

[1] C.G.Dhaware and K.H.Wanjale, "A Modern Approach for Plant Leaf Disease Classification Which Depends on Leaf Image Processing", In 2017 International Conference on Computer Communication and Informatics (ICCCI), IEEE, January 2017, pp.1-4.

[2] J.P.Nayak, K.Anitha, B.D. Parameshachari, R. Banu, and P. Rashmi, PCB Fault detection using Image processing. In IOP Conference Series: Materials Science and Engineering,IOP Publishing, August 2017, Vol.225, No.1, pp.012244.

[3] R.P.Narmadha, and G. Arulvadivu, "Detection and Measurement of Paddy Leaf Disease Symptoms Using Image Processing", In 2017 International Conference on Computer Communication and Informatics (ICCCI), IEEE, January 2017, pp.1-4.

[4] V. Singh and A.K.Misra, "Detection of Plant Leaf Diseases Using Image Segmentation and Soft Computing Techniques", Information Processing in Agriculture, Vol.4, No.1, 2017, pp.41-49.

[5] A.A.Esmaeel, "A Novel Approach to Classify and Detect Bean Diseases Based on Image Processing. In 2018 IEEE Symposium on Computer Applications & Industrial Electronics (ISCAIE), IEEE, April 2018, pp.297-302.

[6] S. Hossain, R.M. Mou, M.M.Hasan, S.Chakraborty and M.A.Razzak, "Recognition And Detection of Tea Leaf's Diseases Using Support Vector Machine", In 2018 IEEE 14th International Colloquium on Signal Processing & Its Applications (CSPA), IEEE, March 2018, pp.150-154.

[7] S. Nema and A. Dixit, "Wheat Leaf Detection and Prevention Using Support Vector Machine", In 2018 International Conference on Circuits and Systems in Digital Enterprise Technology (ICCSDET), IEEE, December 2018, pp.1-5.

[8] V. Kanabur, S.S.Harakannanavar, V.I.Purnikmath, P.Hullole and D.Torse, "Detection of Leaf Disease Using Hybrid Feature Extraction Techniques and CNN Classifier", In International Conference On Computational Vision and Bio Inspired Computing, Springer, Cham, September, 2019, pp.1213-1220.

[15] S. Kumar, K.M.V.V.Prasad, A.Srilekha, T.Suman, B.P.Rao and J.N.V.Krishna, "Leaf Disease Detection and Classification Based On Machine Learning", In 2020 International Conference on Smart Technologies in Computing, Electrical and Electronics (ICSTCEE), IEEE, October, 2020, pp.361-365.

[9] M.K.Kaleem, "A ModernApproach for Detection of Leaf Diseases Using ML Based SVM Classifier", Turkish Journal of Computer and Mathematics Education (TURCOMAT), Vol.12, No.13, 2021, pp.3340-3347.

[10] T.Vadivel and R. Suguna, "Automatic Recognition of Tomato Leaf Disease Using Fast Enhanced Learning with Image Processing", Acta Agriculturae Scandinavica, Section B-Soil & Plant Science, Vol.72, No.1, 2022, pp.312-324.

[11] L. Zhu, Z.Li, C.Li, J.Wu and J. Yue, "Vegetable Classification from Images Based on Alexnet Deep Learning Model", International Journal of Agricultural and Biological Engineering", Vol.11, No.4, 2018, pp.217-223.

[12] B.Liu, Y. Zhang, D. He and Y.Li, "Identification of Apple Leaf Diseases Based on Deep Convolutional Neural Networks", Symmetry, Vol.10, No.1, 2017, pp.11.

[13] M.A.Islam, M.N.R.Shuvo, M.Shamsojjaman, S.Hasan, M.S.Hossain, and T.Khatun, "An Automated Convolutional Neural Network Based Approach for Paddy Leaf Disease Detection", International Journal of Advanced Computer Science and Applications, Vol.12, No.1, 2021.

[14] H.B.Prajapati, J.P.Shah, and V.K.Dabhi, "Detection and Classification of Rice Plant Diseases", 2017.

[15] S. Kumar, K.M.V.V.Prasad, A.Srilekha, T.Suman, B.P.Rao and J.N.V.Krishna, "Leaf Disease Detection and Classification Based on Machine Learning", In 2020 International Conference on Smart Technologies in Computing, Electrical and Electronics (ICSTCEE), IEEE, October, 2020, pp.361-365.

[16] R. Deng, M.Tao, H.Xing, X.Yang, C.Liu, K.Liao and L.Qi, "Automatic Diagnosis of Rice Diseases Using Deep Learning", Frontiers in Plant Science, 1691.2021.

[17] T.Verma and S.Dubey, "Prediction of Diseased Rice Plant Using Video Processing and LSTM-Simple Recurrent Neural Network with

Comparative Study", Multimedia Tools and Applications, 29267-29298, Vol.80, No.19, 2021.

[18] S.B. Jadhav, V.R.Udupi and S.B.Patil, "Identification of Plant Diseases Using Convolutional Neural Networks", International Journal of Information Technology, Vol.13, No.6, 2021, pp.2461-2470.

[19] K. Jayasripriyanka, S. Gaayathri, M.S.Vinmathi and C. Jayashri, "Semi-automatic Leaf Disease Detection and Classification System for Soybean Culture", Int Res J Eng Technology", IRJET, Vol.6, 2019, pp.1721-1724.

[20] G.Jayanthi, K.S.Archana and A.Saritha, "Analysis of Automatic Rice Disease Classification Using Image Processing Techniques", International Journal of Engineering and Advanced Technology, Vol.8, No.3S, 2019.

LINEAR HYDROGEN BOND LIQUID CRYSTAL BINARY SERIES COMPARISON BETWEEN PA+8BAO:PA+9BAO & PA+8BAO:PA+10BAO

P. Rohini
Liquid Crystal Research Laboratory (LCRL)
Bannari Amman Institute of Technology, Sathyamangalam - 638 401, Erode District, Tamil Nadu

Abstract

The existing single hydrogen bond thermotropic liquid crystalline binary series of PA+8BAO & PA+9BAO and PA+8BAO & PA+10BAO are investigated from the synthesized precursors of Palmitic Acid (PA) with p-n-alkyloxy benzoic acid (nBAO) and it comprising of eighteen liquid crystalline complexes. From these two sets, each set provided nine mesogenic complexes and totally eighteen complexes are harvested by varying the molar proportions from 0.1 to 0.9. The attractive phase textures of this binary series are recorded with the assistance of Polarizing Optical Microscope (POM). Thermal analysis is studied with the aid of Differential Scanning Calorimetry (DSC). The intermolecular hydrogen bonding is confirmed through the FTIR analysis. The phase transition temperature values of various phases are compared through POM and DSC analysis. Thermal properties like thermal stability factor, thermal equilibrium, odd-even effect, phase transition temperature, enthalpy estimation and specific heat analysis are compared between these two sets of binary series.

Keywords: *Binary series, Enthalpy and specific heat, Hydrogen bond, Mesogenic complexes, Odd-even effect, Phase textures, Phase transition temperature, Precursors, Thermal stability factor.*

1. INTRODUCTION

Fourth state of matter called liquid crystals that are derived between crystalline solid and isotropic liquid but it exhibited the anisotropic property. These liquid crystals play a vital role in the fabrication of flat panel display devices. Some applications are chromatography, flat window technology, watches, monitors and mesogenic formulations in cosmetics and medicines. The purpose of display devices in this modern world is because of its wide range of viewing angle, high brightness as well as high resolution. But it is sensitive to high temperature and electromagnetic fields. Among the three types of liquid crystal, twisted nematic type is preferable for the display device manufacturing because of its self-assembled molecules as well as lower atomic weight. The complexes chosen for this thermotropic hydrogen bond liquid crystal is the combination of mesogenic and non-mesogenic constituents that is responsible for the maximum efficiency exposed. During the temperature variation, the intermolecular interactions are held, and then the different kinds of mesogenic phases are identified. There are two functional groups available in the HBLC preparation. Due to the intermolecular interaction, the physical and chemical properties of the proposed mesogens are enhanced and it is represented for the application purpose. Paleos and his colleagues investigated several kinds of thermotropic HBLC.

New mesogenic phase is induced or suppressed in the prepared binary series. This is analyzed with the help of different characterization techniques. Two set of linear single bond thermotropic HBLC binary series viz., PA+8BAO: PA+9BAO and PA+8BAO: PA+10BAO are prepared by changing the steps of 0.1 in its molar proportion, then eighteen binary complexes are yielded as the final products. While blended, one complex is taken as X and another complex is taken as Y then its optical, chemical and thermal properties are investigated and compared. Because of the effective ratio of complexes, the enormous phase polymorphism is exposed by these novel series. The well-known mesogenic complex of p-n alkyloxy benzoic acid is synthesized with a non-mesogenic complex of palmitic acid and finally exhibits the conventional mesogenic phases with large transition temperatures. The precursors and its binary series enhanced the structure-property behaviors and it is applicable in the area of optical filters, shutters and modulator.

The projected binary mesogenic complexes possess a large transition with respect to temperature and reveal the nematic phase which is effectively used in the fabrication of display devices. The results of these two binary complexes of PA+8BAO: PA+9BAO and PA+8BAO: PA+10BAO are discussed.

2. REVIEW OF LITERATURE

Chandrasekar et al [1] investigated the double hydrogen bond liquid crystals formed between methyl malonic acid and p-n-alkyloxy benzoic acids are characterized. The molar ratio variation from the precursors of
MM + 8BAO: MM + 11BAO & MM + 8BAO: MM + 12BAO then it revealed rich phase polymorphism and yielded 18 binary mixtures as a result. The molar range varied from 0.1 to 0.9 for the entire 18 binary complexes. Thermal and optical properties are characterized.

Kaushik Pal *et al* [2] established an effort taken to form hydrogen bond between CdS nanostructures and supramolecular mesogens with p–n-alkyloxy benzoic acids (n-OBA). Dielectric relaxation with respect to temperature, measurement of tilt angle, electro-optical switching measurements monitoring the emission of polarization from the semiconductor nanostructures. It exposes electrically tunable interaction may allow for practical engineering applications like electro-optical switch.

Malek Fouzai *et al* [3] derived the linear supra-molecular liquid crystals, 4-(octyloxy) benzoic acid (8OBA) and 4-(octyloxy)-3-fluoro benzoic acid (8OBAF). The chemical analysis was investigated through NMR and FTIR. The phase texture of compounds was studied with polarized optical microscopy (POM), differential scanning calorimetry (DSC) and dielectric spectroscopy. The binary mixtures of complexes are established with high resolution and the phase diagram is plotted for both heating and cooling run.

Sangameswari *et al* [4] established thermotropic double hydrogen bonded ferroelectric liquid crystals with the commbinations of N-carbamyl-L-glutamic acid (CGA) and p-n-alkyloxy benzoic acids (BAO). The projected complexes of CGA + 5BAO, CGA + 6BAO, CGA + 7BAO and CGA + 8BAO were utilized for the preparation of binary series and harvested 27 binary mixtures. From the studies, smectic X* phase is observed in the entire three series. Phase diagrams of these series are constructed from polarizing optical microscope (POM) and differential scanning calorimetry (DSC) examination. Odd–even effect, phase transition, stability factor, thermal equilibrium and tilt angle are also computed.

3. PREPARATION OF BINARY COMPLEXES PA+8BAO: PA+9BAO & PA+8BAO: PA+10BAO

The synthesized complexes of PA+8BAO, PA+9BAO and PA+10BAO are obtained from the well formulated way. In the current work, PA+8BAO is taken as X complex and PA+9BAO /PA+10BAO are taken as Y complex. Eighteen binary complexes are attained as the final product while varying the molar amounts, from 0.1 to 0.9. The optical and thermal properties of these complexes are explained below.

4. DIFFERENT METHODS OF CHARACTERIZATION

Fourier Transform Infrared Spectroscopy (FTIR) analysis is used to confirm the occurrence of intermolecular hydrogen bonding among the binary mixtures of different proportions. ABB Bomem MB 3000 series is the FTIR spectrometer used for taking the spectra of the entire binary complexes with IR range from 4000 cm^{-1} to 400 cm^{-1}.The charming textures of these series are obtained by Polarizing Optical Microscope (POM).Nikon Imaging Software (NIS) is connected with POM to record the various textures of the mesophases. The phase transition temperature is identified through the Instec HCS402-STC 200 temperature controller. The thermal examination was taken through Differential Scanning Calorimetry and recorded thermograms revealed the various thermal properties of the mesogens.

5. POM TEXTURES

The entire binary mesogens melt at the temperature of 60^{o}C. The POM and DSC studies revealed the thermal stability of these binary series.

(a) Droplet nematic at 82.3°C

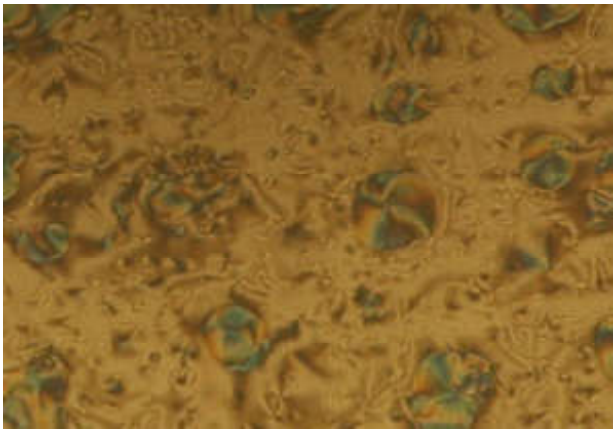

(b) Threaded nematic at 72.7°C

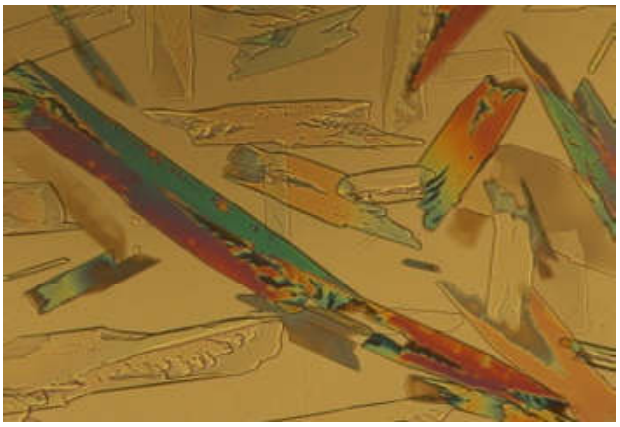

(c) Multi-colored smooth mosaic texture at 58.3°C

Fig.1. PA+8BAO & PA+9BAO (0.6X:0.4Y)

6. PHASE ORDER OF BINARY MIXTURES

The two conventional mesogenic phases are exhibited by this binary series. Nematic phase is denoted in the figure 1(a) & 1(b) and smectic G phase is denoted in the figure 1(c).

In cooling run, the phase transition of binary mixture is denoted below.

Isotropic → N → Sm.G → Crystal

7. CHEMICAL ANALYSIS

7.1 Fourier Transform Infrared Spectroscopy (FTIR)

The existing intermolecular hydrogen bond is confirmed through FTIR mixtures.

7.2 Thermal examination

Thermal examination is done by Differential Scanning Calorimetry (DSC). Phase transition temperature, enthalpy calculation, specific heat computation, stability factor and thermal equilibrium are attained. While cooling runs, from isotropic to crystal changes are observed for the whole binary series. The binary combination is chosen only dependent on the nematic phase suppression as well as exhibition. In the precursors, from (p-n-alkyloxy benzoic acid, nBAO) n=12 to n=8, nematic phase is exposed then from n=7 to n=5 nematic phase is suppressed.

The variation of the nematic phase is analyzed for these binary series. It is denoted in figure 2. This is the essential phase for flat panel display fabrication. The phase variation is dependent on the molar ratio, carbon number in p-n-alkyloxy benzoic acid and non-mesogenic complex (palmitic acid). In the precursor of PA+8BAO, the nematic phase is suppressed but in PA+9BAO that phase is exhibited. The same thing is happening in another binary series of PA+8BAO: PA+10BAO also.

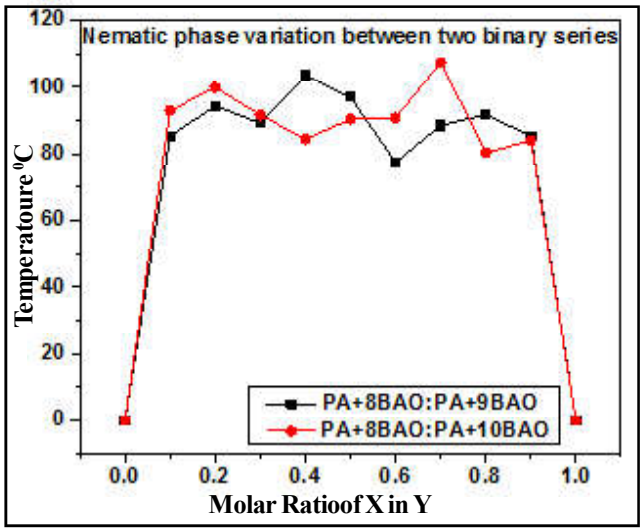

The variation of the smectic G phase is also analyzed for these binary series. It is denoted in figure 3. The phase variation is dependent on the molar ratio, carbon number in p-n-alkyloxy benzoic acid and non-mesogenic complex (palmitic acid). This phase is exhibited by all the series. It is more useful in smart window technology.

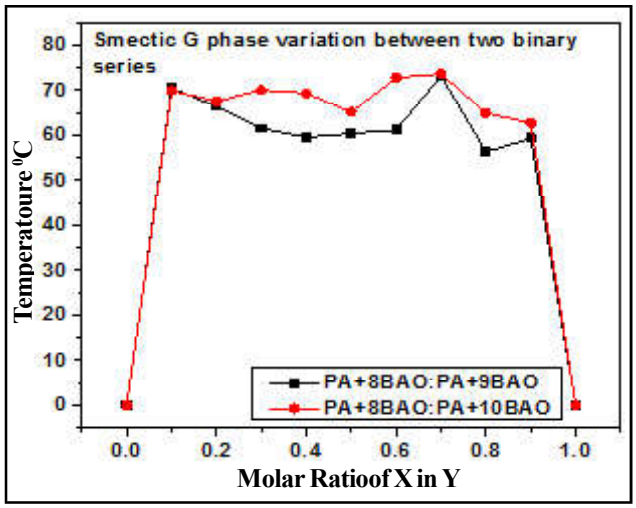

8. CONCLUSION

The noted higher thermal range of both the phases in binary series is utilized for the wide commercial purpose compared to thermal range of the phases in the precursors. Among the various types of liquid crystalline phases, the inducement of nematic phase for these binary series is more favorable for the liquid crystal application.

9. RESULT

9.1 Comparison of Nematic phase temperature between PA+8BAO & PA+9BAO

Molar fraction	Temperature (°C)	Temperature (°C)
0.1	85.37	92.99
0.2	94.42	99.92
0.3	89.2	91.7
0.4	103.48	84.45
0.5	96.98	90.44
0.6	77.52	90.85
0.7	88.53	107.49
0.8	91.84	80.38
0.9	85.29	84.11

9.2 Comparison of Smectic G phase temperature between PA+8BAO & PA+10BAO

Molar fraction	Temperature (°C)	Temperature (°C)
0.1	70.49	69.96
0.2	66.38	67.54
0.3	61.52	70.13
0.4	59.58	69.36
0.5	60.39	65.17
0.6	61.15	72.83
0.7	72.27	73.68
0.8	56.3	64.96
0.9	59.32	62.71

REFERENCES

[1] G. Chandrasekar, N. Pongali Sathya Prabu and M. L. N. Madhu Mohan, "Calorimetric Investigations of Hydrogen-Bonded Liquid Crystal Binary Mixtures", Journal of Thermal Analysis and Calorimetry, Vol.134, 2018, pp. 1799-1822,

[2] K.Pa0, T. Sabu and M. L. N. Madhu Mohan, Evaluation of Versatile CdS Nanomaterials Based Liquid Crystals Switchable Device", Journal of Nanoscience and Nanotechnology, Vol.17, No.4, 2017, pp. 2401-2412,

[3] Malek Fouzai, Ridha Hamdi, Saad Ghrab, Taoufik Soltani, Andreea Ionescu, Tahar Othman, "Properties of Binary Mixtures Derived From Hydrogen Bonded Liquid Crystals", Journal of Molecular Liquids, Vol. 249, 2018, pp. 1279-1286.

[4] G. Sangameswari, N. Pongali Sathya Prabu, M. L. N. Madhu Mohan, "Study and Characterization

of the Smectic X* Phase in Binary Mixtures of Thermotropic Double Hydrogen Bonded Ferroelectric Liquid Crystals", Phase Transitions, Vol. 88, Issue 9, 2015, pp. 907-928.

[5] Denis Andrienko, "Introduction to Liquid Crystals", Journal of Molecular Liquids, Vol.267, 2018, pp. 520-541.

[6] Nagham Mahmood Aljamali, Wijdan Al-qraawy, Manar Ghyath Abd Almutalib Almosawy, "Review on Liquid Crystals and their Chemical Applications", International Journal of Cheminformatics Research, Vol. 7, No. 1, 2021.

[7] J. W. Goodby, P. J. Collings, T. Kato, C. Tschierske, H. Gleeson, P. Raynes (Eds), "Handbook of Liquid Crystals", 2nd edition, Wiley-VCH, Weinheim, 2014.

[8] Irina Carlescu, "Introductory Chapter: Nematic Liquid Crystals", Liquid Crystals and Display Technology, 2020.

[9] Ghassan Q. Ali and Ivan Hameed R Tomi, "Synthesis and Characterization of New Mesogenic Esters Derived from1,2,4-Oxadiazole and Study the Effect of Alkoxy Chain Length in their Liquid Crystalline Properties", Liquid Crystals, Vol. 45, No. 3, 2018, pp. 421-430.

[10] Jana Jensen, Stephan C. Grundy, Stacey Lowery Bretz, and C. Scott Hartley, "Synthesis and Characterization of Self-Assembled Liquid Crystals: p-Alkoxybenzoic Acids", Journals of Chem. Educ., Vol.88, No.8, 2011, pp. 1133-1136.

[11] Omaima A. Alhaddad, Hoda A. Ahmed, Mohamed Hagar, Gamal R. Saad, Khulood A. Abu Al-Ola and Magdi M. Naoum, "Thermal and Photophysical Studies of Binary Mixtures of Liquid Crystal with Different Geometrical Mesogens", Crystals, Vol.10, No.3, 2020, pp. 223.

[12] Rua B. Alnoman, Mohamed Hagar, Hoda A. Ahmed, Magdi M. Naoum, Hanefah A. Sobaih, Jawaher S. Almshaly, Mawadh M. Haddad, Rana A. Alhaisoni and Tahani A. Alsobhi, "Binary Liquid Crystal Mixtures Based on Schiff Base Derivatives with Oriented Lateral Substituents", Crystals, Vol. 10, No. 4, 2020, pp. 319.

[13] H. A. Ahmed, Eman Mansour and Mohamed Hagar, "Mesomorphic Study and DFT Simulation of Calamitic Schiff Base Liquid Crystals with Electronically Different Terminal Groups and their Binary Mixtures", Liquid Crystals, Vol. 47, No.14-15, 2020, pp. 2292-2304.

[14] G. Chandrasekar, N. Pongali Sathya Prabu and M. L. N. Madhu Mohan, "Optical and Thermal Characterization of Double Hydrogen Bonded Liquid Crystals: Binary Mixtures", Ferroelectrics, Vol. 524, No.1, 2018, pp. 102-137.

[15] Thamilarasan Ranjeeth Kumar, Sankaran Sundaram, Thangaiyan Chitravel, Ramasamy Jayaprakasam and Vellalapalayam Nallagounder Vijayakumar, "Design, Synthesis and Characterization of Hydrogen Bonded Binary Liquid Crystal Complex from 4-Methoxycinnamic Acid and 4-Hexyloxybenzoic Acid (4MCA:6OBA)", Zeitschrift för Physikalische Chemie, Vol. 231, No.11-12, 2017.

[16] Mustafa Okumus, "Synthesis and Characterization of Hydrogen Bonded Liquid Crystal Complexes by 4-Octyloxy Benzoic Acid and Some Dicarboxylic Acids", Journal of Molecular Liquids, Vol. 266, 2018, pp. 529-534.

[17] M. Muniprasad, M. Srinivasulu, P. V. Chalapathi and D.M.Potukuchi, "Influence of Chemical Moieties and the Flexible Chain for the Tilted Smectic Phases in Linear Hydrogen Bonded Liquid Crystals with Schiff Based Pyridene Derivatives", Journal of Molecular Structure, Vol. 1015, 2012, pp.181-191.

[18] G. Chandrasekar and N. Pongali Sathya Prabu, "Binary Mixtures Formed between Methyl Malonic Acid and Alkyloxy Benzoic Acids: Optical and Thermal Investigations", Ferroelectrics, Vol. 606, No.1, 2023, pp.146-160.

[19] N. Pongali Sathya Prabu, "Optical and Thermal Applicational Utility of Hydrogen Bond Liquid Crystals", Molecular Crystals and Liquid Crystals, https://doi.org/10.1080/15421406.2023.2195763, 2023.

[20] G. Chandrasekar, N. Pongali Sathya Prabu and M. L. N. Madhu Mohan, "Binary Mixtures of Double Hydrogen Bond Liquid Crystals: Chemical, Optical, Thermal Investigations", Molecular Crystals and Liquid Crystals, https://doi.org/10.1080/15421406.2023.2175966, 2023.

[21] Michael Hird, "Ferroelectricity in Liquid Crystals-Materials, Properties and Applications", Liquid Crystals, Vol. 38, Issue 11-12, pp. 1467-1493, 2011.

[22] S. Chandrasekhar, Liquid Crystals, 2nd edition. (University Press,Cambridge.), 1992.

[23] Constantinos M. Paleos and Dimitris Tsiourvas, "Supramolecular Hydrogen-bonded Liquid Crystals", Liquid Crystals, Vol. 28, No.8, 2001, pp.1127-1161.

[24] D. Demus, J.Goodby, G.W.Gray, H.W.Spiess, and V. Vill, "Handbook of Liquid Crystals", Vol.1-3, (Wiley-VCH.), 1998.

THEORETICAL INSIGHT OF SPECTROSCOPIC INVESTIGATION (H^1 AND C^{13} NMR) AND VIBRATIONAL ASSIGNMENTS OF KAEMPFEROL GLYCOSIDES

V. Deepha[1], R. Praveena [2] and T. Kumaresan[3]
[1&2]Quantum Computing and Phytochemistry Research Laboratory, CRF.
[3]Department of Artificial Intelligence and Data Science
Bannari Amman Institute of Technology, Sathyamangalam-638401, Erode District, Tamil Nadu
E-mail: vdeepha85@gmail.com

Abstract

In this work, we investigated the molecular structure of kaempferol glycosides by using B3LYP/6-311G++(d,p) level of theory. The performance of the quantum chemical methods for predicting theoretical characterization of H^1 and C^{13} NMR spectra is evaluated for afzelin and juglanin using same level of theory as well as standard double-zeta and triple-zeta quality basis sets. In order to determine the appropriate structure and functional groups for the title compounds are elucidated by IR vibrational assignments based on its absorbance and transmittance spectra. From the above observations, DFT method provides suitable platform to design and synthesis of new derivatives with ease of characterization of chemical structure through simulated spectral analysis.

Keywords: *Afzelin, C^{13}-NMR, DFT, H^1-NMR, IR, Juglanin*

1. INTRODUCTION

Flavonoids obtained from natural sources gains prominent towards the antioxidant property. About 8000 compounds with ыavonoids are identified from various parts of plant sources which include ыowers, fruits and leaves [1]. Existence of constituents attached to structure are common to most of the ыavonoids include basic ыavonoid skeleton and various combination of multiple hydroxyl and methoxyl group substituents [2].

Currently, elucidation of structure of secondary metabolites from natural sources through theoretical methods advances over the experimental one. It is due to the fact that availability of compounds is very small in amount and hence not enough to examine to all characterisation process [3]. In this sense, theoretical methods are adopted to determine the various activities based on the basic skeleton and constituents present in it.

The scope of nuclear magnetic resonance (NMR) spectroscopy incorporates both the structure and dynamics for the validation of materials for various fields [4,5].

Among them, the characterization of natural products devises major problems such as i) molecules possess a large and complex molecular backbone, ii) molecules possess many conformations due to its flexible nature and need of much effort to sort out, iii) their spectral assignment of proton (^{1}H) and carbon (^{13}C) NMR spectra with most signals are very crowded at specific regions for each functional groups, iv) ^{1}H chemical shifts are mostly lying to solvent effects [6,7].

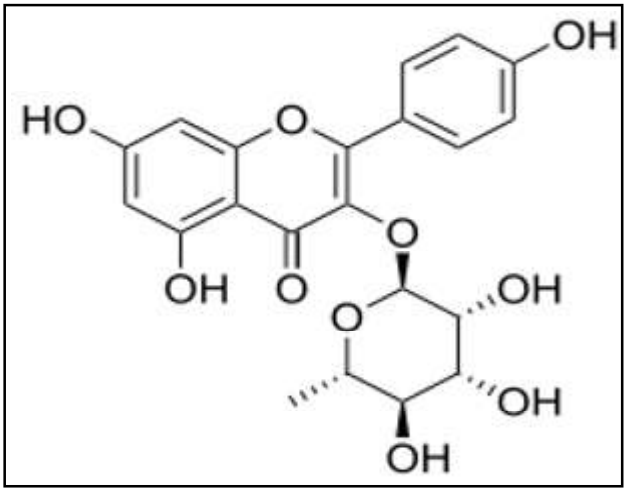

Afzelin

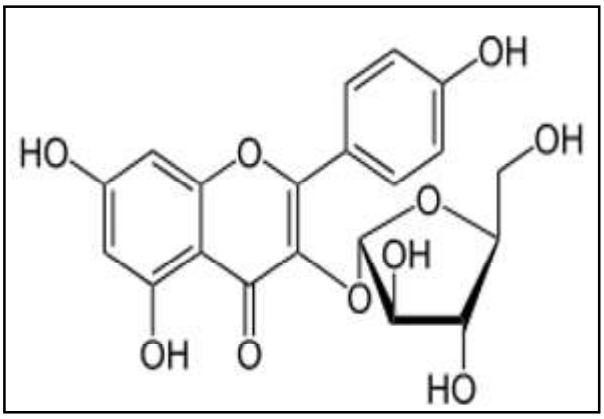

Juglanin

Fig.1 Chemical structure of Afzelin and Juglanin

Hence, it is of interest to study the structural characterisation through theoretical simulation studies using density functional theory (DFT) for kaempferol glycosides, afzelin and juglanin as shown in Fig.1. Owing to the presence of functional groups and glycosidic linkages, its vibrational modes corresponding to them are analysed with the help of infra-red (IR) spectroscopic analysis. Detailed investigation regarding chemical environment and the structure is successfully carried out for afzelin and juglanin compounds with the help of H^1 and C^{13} NMR characterization done through gauge-independent atomic orbital (GIAO) method.

2. COMPUTATIONAL METHODOLOGY

In the present work, cartesian co-ordinates of afzelin and juglanin are considered for ground state geometry optimization. DFT is adapted to perform simulations under the level of theory B3LYP (Beckes-three parameter reformulated by Lee Yang and Parr) using the triple zeta valence basis set 6-311G(d,p) and polarization functions ++ are also been considered, since the system is highly delocalized one[8]. Entire simulations were computed by the quantum chemical software Gaussian 09 and visualizations by both Gauss view 5.0 and chemcraft software. Optimization of structure has been achieved through most stable geometry by applying same level of theory [Fig.2].

For afzelin, the structural optimization took 9 hours 28 minutes 58.0 seconds involving and for juglanin, the structural optimization took 16 hours 59 minutes 34.0 seconds involving 30 optimization steps. Additional feature, an intramolecular hydrogen bond of length 1.699 A is found for afzelin compound with ground state minimum energy of -1564.8771034 Hartrees and for juglanin, it is -1525.5879351Hartrees respectively. The optimized geometry is adopted for frequency simulation to obtain IR and NMR spectral assignments to validate the structure of afzelin and juglanin [5].

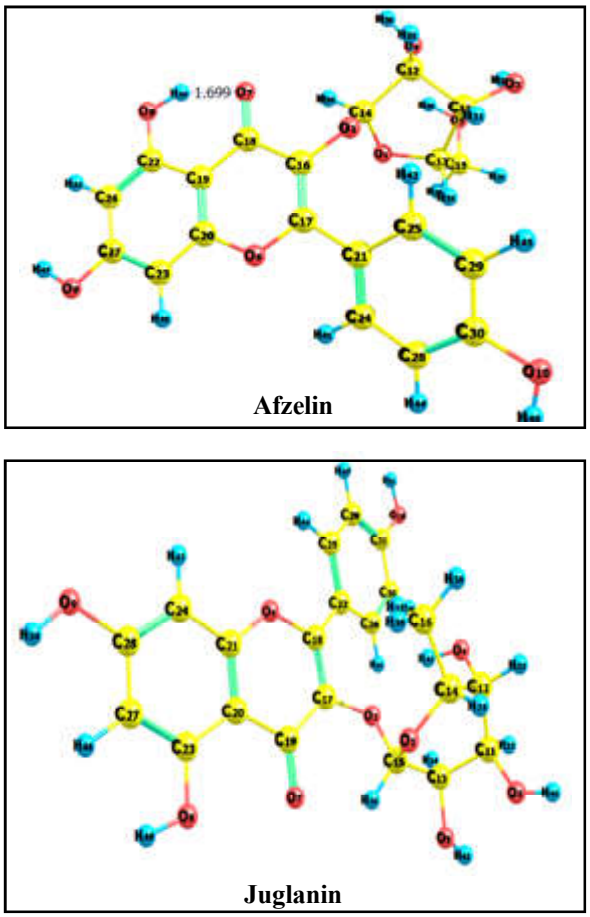

Fig.2 Optimized structures of Afzelin and Juglanin

3. RESULT AND DISCUSSIONS

3.1 Spectroscopy Analysis

3.1.1 Afzelin -C^{13} NMR Analysis:

C^{13} NMR spectroscopy is having chemical shift value is twenty times as that of H^1 spectroscopy due to the low abundance nature of C^{13} isotope are given in Figure 3.

The chemical shift value is increased by the presence of the oxygen and double bond [9]. The oxygen is removing its electron density and double bond generating ring current which makes the deshielding effect. In C-16, high chemical shift value of

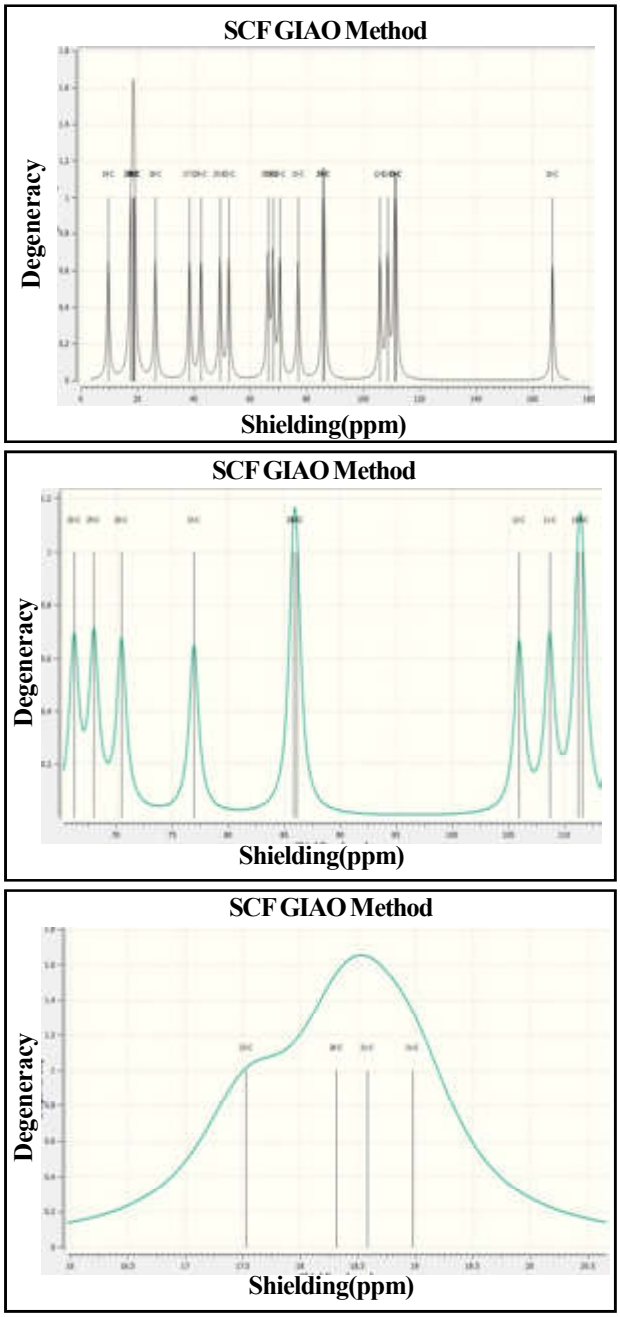

Fig. 3 C^{13} NMR spectra of afzelin simulated by B3LYP/6-311G++ (d,p)level of theory

166.5ppm is obtained due to the presence of oxygen fused in pyranose ring. Consequently, C-14 and C-13 atoms possess chemical shift value of 111.5 ppm owing to ring closure effect of oxygen. The C-11 and C-12 atoms having chemical shift values of 109ppm and 106 ppm in line for the presence of the electronegativity nature of oxygen are displayed in Figure 1.

In the case of C-24 and C-27 atoms, chemical shift values 85 ppm and 86ppm for the presence of double bond. The C-15 and C-20 atoms shows the chemical shift value of 77ppm and 70.5ppm for existence of oxygen and double bond. The C-29 and C-30 are having chemical shift values of 68ppm and 66 ppm shows the presence of a double bond. The C-17, C-31 and C-18 gives chemical shift values are 38ppm, 26ppm. of 19ppm respectively. The C-19, C-23, C-28 and C-21 atoms are having chemical shift values of 9.5ppm,17.2ppm, 18.2ppm, and 18.5ppm. From the various range of chemical shift values, the structure of Afzelin compound is validated and displayed in the Fig.1.

3.1.2 Afzelin- H^1 NMR Analysis

The H^1 NMR spectroscopy is more precession than the C^{13} NMR spectroscopy, because the structure is more accurately identified. The splitting pattern depends upon the principle of spin -spin splitting, but here the identification is based upon the theoretical way [10, 11]. It is based upon the absorption of the radio frequency at higher or lower region due to chemical environment. From the Fig.4, chemical shift values of H-38 and H-37 atoms are 32ppm and 31.8ppm depicts the presence of oxygen atom at the same side having high electronegativity to makes high chemical shift value. Similarly, H-40, H-41, and H-42 positions having chemical shift values of 31ppm, 31.5ppm and 29.5ppm respectively, because of hydrogen is bonded to an alcoholic -OH group. Low chemical shift values for H-39 atom than H-38 and H-37 atoms are due to the less action of oxygen atom which it is fused as a pyranose form. In the case of H-36, H-44 and H-45 hydrogen having low chemical shift value of 24.5ppm, 24ppm and 23ppm, because it is not affected by the double bond and oxygen atom. The H-43, H-47 and H-48 atoms are having higher chemical shift values than the previous case due to their effect of the double bond. The attachment of the oxygen atom is verified by H-33, H-50 and H-51 atoms exhibiting chemical shift values of 27.5ppm, 28ppm and 28.6ppm. The 32and 46 hydrogen having chemical shift value of 26.5ppm and 27ppm due to the oxygen atom and the double bond attachment. Hence from the above H^1 NMR data, the structure of afzelin found to be as displayed in Figure1.

3.1.3 Juglanin -C^{13} NMR Analysis

In juglanin molecule, the observed chemical shift value of 106ppm for C-11 represents the electronegativity nature of oxygen is bonded in the form of -OH group as shown in fig.5. For C-12 and C-13 atoms, the chemical shift values 102.5ppm and 98ppm shows the presence

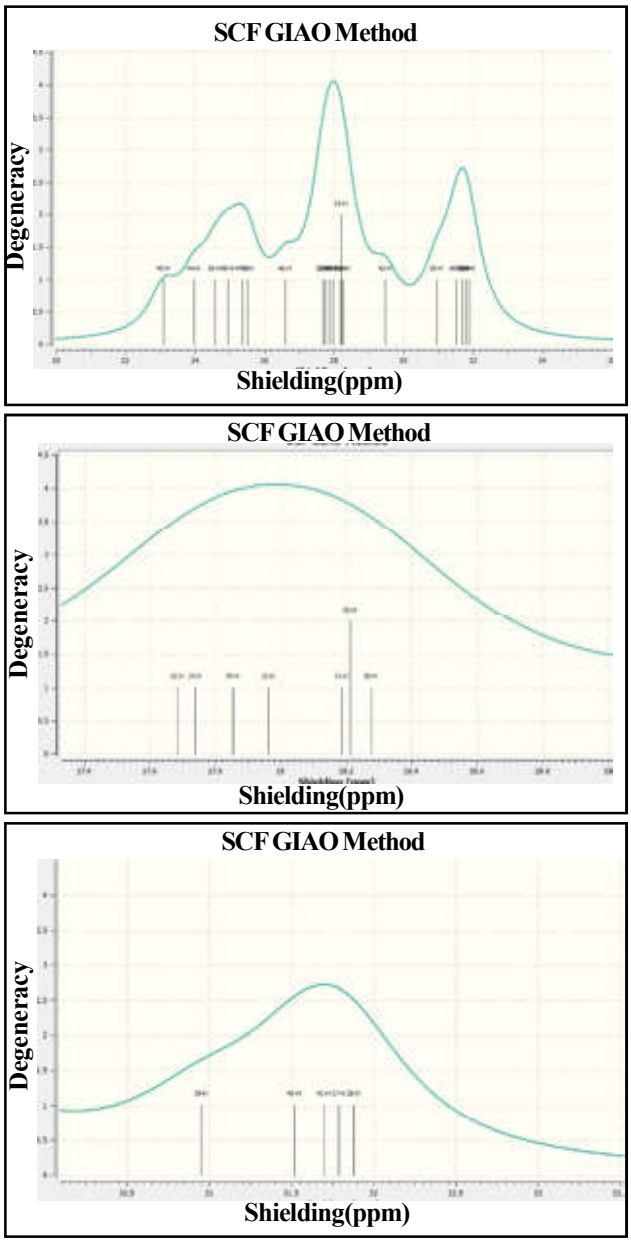

Fig. 4 H^1 NMR spectra of afzelin simulated under B3LYP/6-311G (d,p) level of theory

of -OH group and the furanose ring closure of oxygen. The C-14 having chemical shift of 75ppm which is less than the C-15 of 118ppm owing to the presence of -OH group is attached to the C-15 it makes downfield shift [12]. The C-16 having higher chemical shift value of 42ppm than the C-17 (20ppm), due to the presence of oxygen (electronegative moiety) and the double bond. The C-18 (2ppm) having lower chemical shift value than the C-19 (75ppm), due to the C-18 containing oxygen is makes intramolecular hydrogen bonding.it makes upfield shift. The C-21(54ppm) having higher chemical shift value than the C-20 (21ppm), due to the presence of double bond makes a downfield shift. The C-23 (88ppm) having

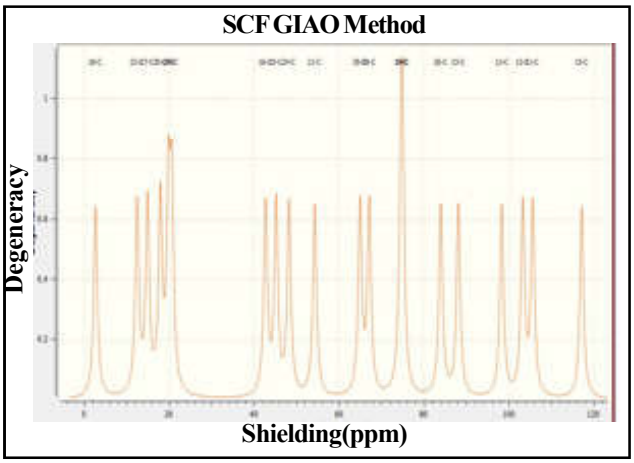

Fig.5 C^{13} NMR spectra of Juglanin simulated under B3LYP/6-311G (d,p) level of theory

higher chemical shift value than the C-22 (12ppm), presence of -OH group is shows intra-molecular hydrogen bonded with C-18 containing oxygen. The C-24 and C-25 carbon having chemical shift values are 48ppm and 45ppm, due to the presence of double bond makes a downfield shift. The C-26 (84ppm) having higher chemical shift value than the C-27 (14ppm), due to the presence of double bond, makes downfield shift. The C-28 and C-29 carbon having chemical shift value of 66.5ppm and 64.5ppm, due to the presence of double bond, makes downfield shift.

3.1.4 Juglanin- H^1 NMR Analysis

The H-31 and H-32 exhibit the chemical shift value of 27.3ppm and 27.6ppm .due to electronegativity character of oxygen (in the form of OH group is attached) to the same carbon atom. The H-33 show chemical shift value of 28.6ppm due to the H-33 is bonded to the carbon is furanose ring closure of neighboring oxygen. The H-34 shows chemical shift of 25.8ppm due to the oxygen is not affected by the hydrogen [13]. The H-35and H-36 gives chemical shift value of the 28.5ppm and 28.3ppm due to the oxygen is bonded to the same carbon. The 37, 38 and 39 positions of hydrogen having chemical shift value of 28.6 ppm, 30.6ppm and 30.0ppm due to the hydrogen is bonded to the oxygen. At H-40, owing to chemical shift value of 25.6ppm for double bond.

The H-41 and H-42 hydrogen having chemical shift value of 24ppm and 23.8 ppm, it is due to the presence of anisotropic nature of double bond creating ring current. At H-43, chemical shift value of 26.1ppm for the presence of double bond. Similarly, for 44 and 45 hydrogen having chemical shift value of 25.1ppm and

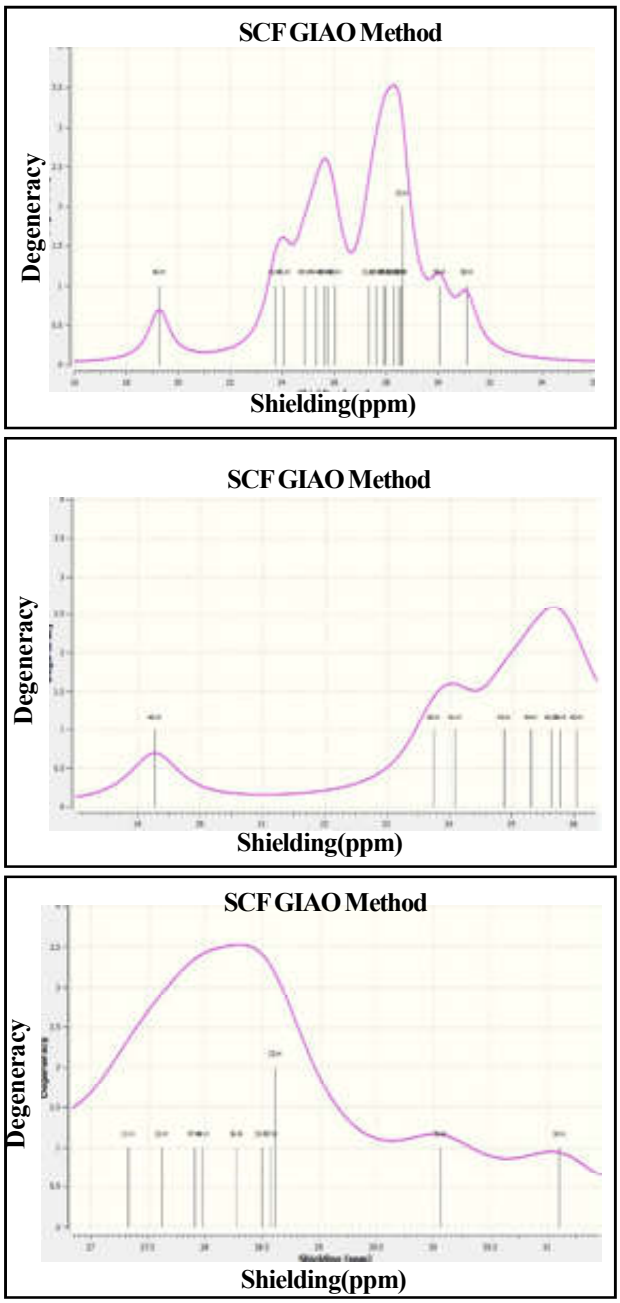

Fig. 6 H^1 NMR spectrograph of Juglanin simulated under B3LYP/6-311G (d,p) level of theory

24.9 ppm. At H-46, chemical shift value of 19.2ppm confirms the presence of intramolecular hydrogen bonding.

3.2 IR Spectroscopy Analyses

IR spectroscopic technique is commonly used for analysing samples with covalent bonds. Simple spectra are obtained from samples with few IR active bonds and high levels of purity. More complex molecular structures lead to more absorption bands and more complex spectra. In the present study IR spectra simulated using density functional theory are presented in absorption and transmittance mode.

3.2.1 Observed Vibrational Assignments for Afzelin

IR spectrum of afzelin is displayed in Fig.7, provides the following observations. The absorbance peak appeared near the region of 1660cm-1 confirms the presence of carbonyl (-C=O) group [14, 15]. The absorption band of C-O stretching is found between 1350-1000 cm-1 confirms the presence of alcoholic (-OH) group. Particularly, for primary alcohols show the absorption band at 1350-1260cm-1 and for secondary alcohols appeared at 1350-1160 cm-1. The absorption bands at regions are 1367cm-1, 1292cm-1 and 1196cm-1 which confirms existence of the secondary alcoholic group. The absorption band of C-H stretching in the region of 969cm-1 confirmed the presence of substituted trans alkene. For C-H stretching, absorption peak in the region of 917 cm-1 is confirmed the presence of monosubstituted alkene systems. The absorption band of C-H in the region of 824cm-1 is confirmed the presence of substituted aromatic hydrocarbons [16].

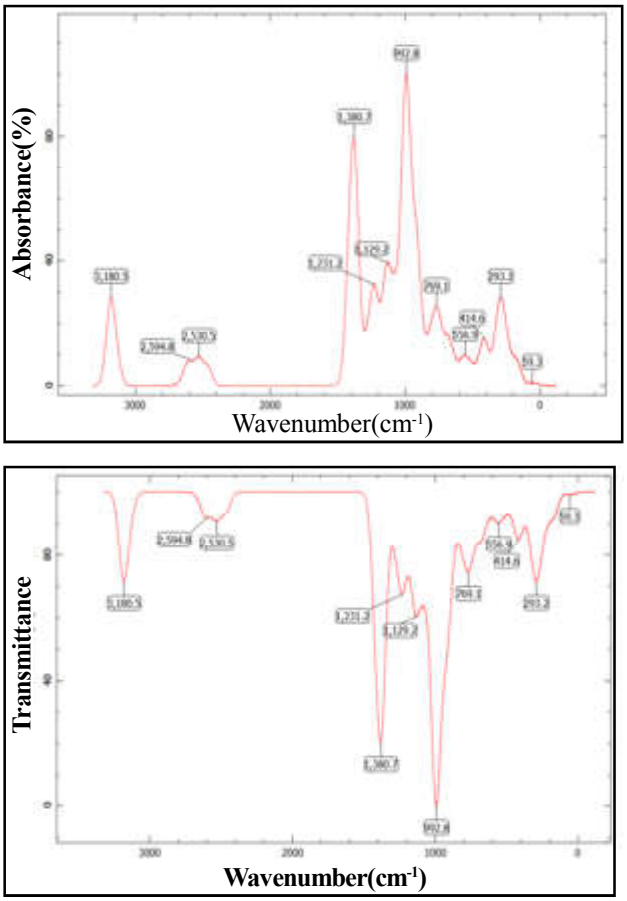

Fig. 7 Observed IR assignments for afzelin - absorbance and transmittance mode

3.2.2 Observed Vibrational Assignments of Juglanin

For juglanin, the vibrational assignments of free -OH group is found in the region of the 3705cm^{-1} is displayed in fig.8. The intramolecular hydrogen bonding of O-H stretching between 5-OH and C=O in C-ring is witnessed in the region of 3267cm^{-1}[14]. The wavenumber corresponds to the 3093 cm^{-1} refers the alkenes groups which occurs as =C-H stretching. The absorption band of -C-O stretching corresponds to the region 1642cm^{-1} confirms the presence of –C=O group[15].

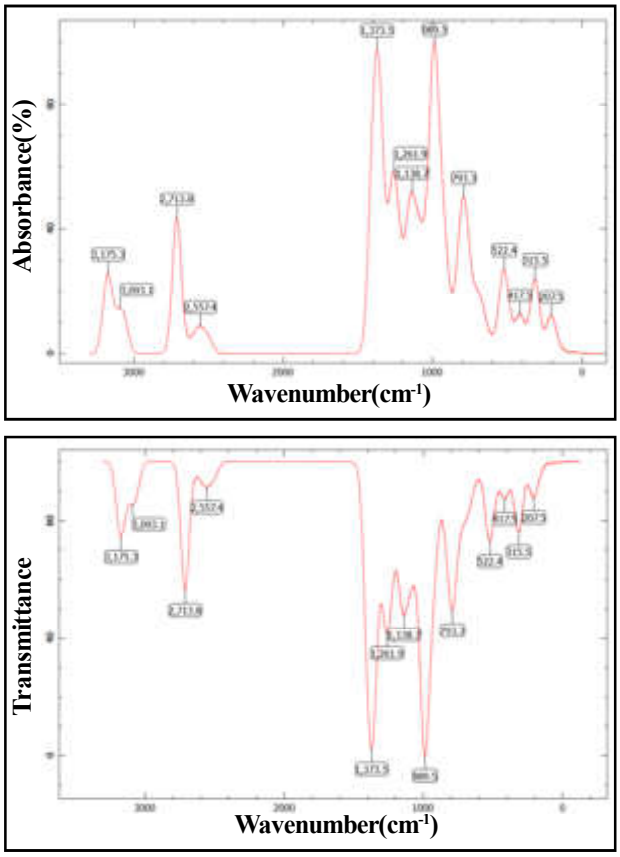

Fig. 8 Observed IR assignments for Juglanin - absorbance and transmittance mode

Consequently, absorption band of C=C stretching in the region of the 1536cm^{-1} confirms the presence of aromatic hydrocarbon systems. The presence of cis-trans alkene ring system is verified at the region of 952cm^{-1}.

4. CONCLUSION

In the present work, structural pattern and the position of functional groups of kaempefrol glycosides which includes afzelin and juglanin through theoretical mode with the aid of DFT has been carried out. Molecular geometry (bond length, bond angle, dihedral angle and minimum ground state energy conformer) are achieved with the help of exchange correlation functional B3LYP and triple zeta valence basis set 6-311G (d,p) is adopted in the present investigation. From the results, it is observed that spectroscopic investigation regarding chemical environment and the structure is successfully carried out for the title compounds with the aid of H^1 and C^{13} NMR methods adopted for characterization has accomplished through GIAO method. In this connection, the existence of the functional groups and its vibrational modes corresponding to them are analyzed with the help of IR spectroscopic analysis.

REFERENCES

[1] K Anbazhakan, R Praveena and K Sadasivam, “Theoretical Insight on Antioxidant Potency of Kanzakiflavone-2 and its Derivatives”, Structural Chemistry, Vol. 32, No.4, 2021, pp. 1451-1458.

[2] J. S.Park, H.S.Rho, D.E.Kim and I.S. Chang, “Enzymatic Preparation of Kaempferol from Green Tea Seed and its Antioxidant Activity”, Journal of Agriculture and Food Chemistry, Vol.54, 2006, pp. 2951-2956.

[3] E.Ruiz, E.Padilla, S.Redondo, A.Gordillo-Moscoso and T.Tejerina, “Kaempferol Inhibits Apoptosis in Vascular Smooth Muscle Induced by a Component of Oxidized LDL”, European Journal of Pharmacology, Vol.529, 2006, pp.79-83.

[4] K.Anbazhakan, R.Praveena, K.Sadasivam, G.Salgado and W. Cardona, “Theoretical Insight on Structural Activities and Targets of Kaempferol Glycosides”, Afinidad, Vol.78, 2020, pp. 236-239.

[5] J.M. Calderσn-Montaρo, E. Burgos-Morσn, C. Pιrez-Guerrero and M. Lσpez-Lαzaro, “A Review on the Dietary Flavonoid Kaempferol”, Mini-Reviews in Medicinal Chemistry, Vol.11, 2011, pp. 298-344.

[6] R.G.Parr and W.Yang, “Density-Functional Theory of Atoms and Molecules”, OUP, Oxford, 1989.

[7] V.Deepha, R.Praveena, R.Sivakumar and K.Sadasivam, “Experimental and Theoretical Investigations on the Antioxidant Activity of Isoorientin from Crotalaria Globosa”, Spectrochimica Acta Part A: Molecular and Biomolecular Spectroscopy, Vol.121, 2014, pp.737-745.

[8] R.Praveena, A.Balasankar, K.Aruchamy, T.Oh and V.Polisetti, “Structural Activity and HAD Inhibition Efficiency of Pelargonidin and its Glucoside-A Theoretical Approach”, Molecules, Vol. 27, No.22, 2016.

[9] Brian C. Smith, "Infrared Spectral Interpretation: A Systematic Approach", 1st Edition, ISBN: 0849324637.

[10] B.Cowan, "Nuclear Magnetic Resonance and Relaxation", Cambridge Univeristy Press, 1997.

[11] C.Banwell and E.M.McCash, "Fundamentals of Molecular Spectroscopy", 4th Edition, McGraw Hill, 1994.

[12] William Kemp, "Organic Spectroscopy", Palgrave MacMillan, 1991.

[13] Dallas L Rabenstein, "NMR Spectroscopy: Past and Present", Analytical Chemistry, Vol. 73, 2001, pp. 214A-223A.

[14] R.J. Abraham, J.Fisher and P.Loftus, "Introduction to NMR spectroscopy", John Wiley and Sons, 1992.

[15] D.C.Harris, M.D.Bertolucci, "Symmetry and Spectroscopy: An Introduction to Vibrational and Electronic Spectroscopy", New York. Dover Publications, INC.

[16] D. Jeevitha, K.Sadasivam, R.Praveena and R.Jayaprakasam, "DFT Study of Glycosyl Group Reactivity in Quercetin Derivatives", Journal of Molecular Structure, Vol.120, 2016, pp.15-24.

DNN CLASSIFICATION USING THREE LEVEL DETECTION OF AUTOMATED ULTRASOUND THYROID IMAGE APPLICATION

K.P. Sampoornam, K. Dhayanithi Devi, J.Sashmitha and S. Sree Harini
Department of Electronics and Communication Engineering,
Bannari Amman Institute of Technology, Sathyamangalam- 638 401, Erode District, Tamil Nadu
E-mail: sampoornam@bitsathy.ac.in , dhayanithidevi.co21@bitsathy.ac.in

Abstract

The most prevalent hormone imbalance in India is hypothyroidism, which affects 42 million individuals. One in ten Indians nationwide suffer from this serious medical condition. The precise use of ultrasound image characteristics is the root of the issue. In this work, we describe a method for differentiating between benign and malignant thyroid nodules that is based on merging traditional ultrasound and deep neural infrastructure ultrasound elasticity pictures. evaluating small sample sizes and determining depth characteristics. To produce a hybrid feature space, the depth information from ordinary ultrasound pictures and images of ultrasonic elasticity are integrated. The experimental results show that the suggested method, with an accuracy rating of 0.9829, outperforms contemporary single information procedures under identical conditions.

Keywords: *DNN, Elasticity photographs, GLCM, RMSE, Ultrasonography*

1. INTRODUCTION

Thyroid dysfunction is a significant matter in the medical field nowadays, particularly for women in their middle years. Thyroid problems are illnesses that prevent your thyroid from producing the right amount of hormones. Your thyroid typically produces the hormones needed to keep your body operating normally. Your body utilizes its resources too rapidly when the thyroid produces inadequate amounts of the hormone thyroid.

Image understanding, image analysis, and computer vision employ electrical (digital, in this context) techniques of observing and analysing pictures. This paradigm is used to forecast the consequences of human vision. Enhancing visual information for human interpretation and processing scene data for unsupervised machine perception are the two main goals of digital image processing.

If thyroid autoimmune infection is suspected, blood samples can be taken then tested for anti-thyroid autoantibodies. The diagnosis of a nodule may be assisted by technologies such as ultrasound, biopsy, radioiodine imaging, and uptake testing. The rate of thyroid nodule and carcinoma identification has decreased due to the widespread use of ultrasonography (US), the major approach for the diagnosis and risk assessment of thyroid nodules as well as for providing recommendations for their evaluation and non-invasive treatment.

2. MATERIALS AND METHODS

2.1. Existing System

One of the most common hormonal carcinomas are thyroid nodules. Global epidemiology statistics show that thyroid cancer becomes increasingly common. Ultrasonography is the most used technique for identifying and tracking thyroid cancer. The accurate localization of thyroid masses, the characterization of echogenic properties inside thyroid nodules, and the detection of ring - shaped, argument blood flow signals inside the masses are all made possible by the safe, practical, quasi-repeatable, and repeatable ultrasound diagnostic technology.

Also, it may discover incredibly small lesions and evaluate how smoothly the blood flows through them. Compared to Computed Tomography (CT) and magnetic resonance imaging, ultrasonography is more effective in identifying the pathological features of benign and malignant tumours (MRI).

2.1.1 Training Fine-tuning

The initial notion is the most logical. As images taken using diverse imaging techniques have characteristic distributions other than their own, we anticipate that the network can learn the relationships between two separate feature distributions. We combine ultrasonic

elasticity pictures and standard ultrasound images to provide a single dataset for training. Each batch of data is fed into the pre-trained VGG16 model using Gaussian random sampling. A 4096-grouped-dimension output vector is provided by the model.

2.1.2 Ultrasonic Equipment

Using the most recent real-time SWE capabilities on an L14-5 linear transducer and the Resona 7 diagnostic US system, thyroid nodule evaluations were performed (Mindray Medical International, Shenzhen, China). The stiffness of a margin was determined using the Resona's unique shell analysis technique (0.5–9mm surround the lesion).

2.2 Proposed System

The clinical diagnosis of autoimmune disease requires SPECT imaging since thyroid disease has surpassed diabetes to become the second-most prevalent endocrine condition. The application of SPECT pictures in computer-aided thyroid disease detection based on machine learning algorithms has, however, been given relatively little attention. A convolutional neural network with optimization-based computer aid is developed to recognize thyroid disease using SPECT images. The three parameters taken into account are subacute thyroiditis, Graves disease, and Hashimoto disease. The educational process has been improved by employing modified convolutional neural network community dense internet structure.

The usage of a neural network improves the training program. The creation of the trainable weight parameters upgrades each skip link in the Dense Net. The learning rate optimization of the flower pollination method is added to the network teaching model. Studies have demonstrated that when used to identify thyroid problems in SPECT images, the recommended convolutional neural network method performs better than prior CNN algorithms. CNN may ascertain the thyroid stage. Conclusions When it comes to correctly predicting thyroid cancer in US consumers, CNN's practicality and quality transcend those of trained radiologists.

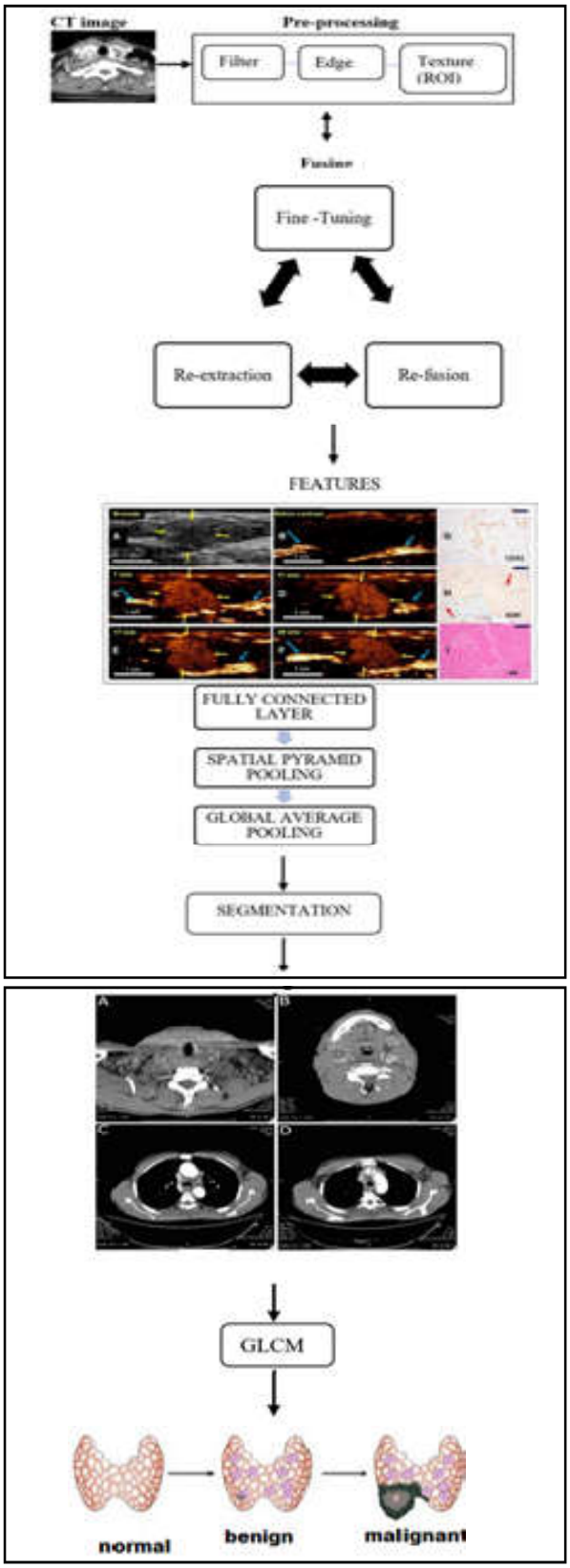

Fig.1 Block Diagram for Characteristics Identification Using Deep Learning

As per Figure 1, many thyroid nodules are inadvertently found, it is crucial to distinguish between benign and malignant nodules during Fine Needle Aspiration (FNA) biopsies and therapies. Since many thyroid nodules are discovered unintentionally, it's essential to distinguish between benign and cancerous nodules. the method of identifying characteristics in thyroid ultrasound images using deep learning.

Ultrasound pictures are pre-processed to normalise their scaling and remove any undesired artefacts. The pre-processed image samples are then used to improve the already trained Google Net model, increasing feature extraction. The features uncovered by thyroid computed tomography is used to separate the data into "malignant" and "benign" incidences using a Cost-sensitive Random Forest classifier. With classification results, sensitivity, and specificity of 96.34%, 86.6%, and 99% for images in our local health region database and 98.29%, 99.10%, and 99.90% for images in an open access database.

Table 1 Experimental Results Comparison

Method	Accuracy (%)	Sensitivity (%)	Specificity (%)
Cost-sensitive Random Forest Classifier	96.34	86.6	99
DNN Classifier	98.29	99.10	99.90

The experimental results given in Table 1 shows that the proposed Google Net model generates exceptional classification performance even before it is properly tuned.

2.2.1 Need of DNN?

Regardless of whether there is a linear or nonlinear relationship between the input and the output, the DNN selects the most appropriate mathematical operation to transform the input into the output. As the network progresses through the layers, the probability of each output is determined. A DNN that has been taught to recognize dog breeds, for example, may look at the image supplied and assess the chance that the dog in the image belongs to a certain breed. While seeing the results, the user may input the recommended label and choose which probabilities the network should represent (those that are larger than a specific threshold, etc.).

2.2.2 Data and Evaluation Indexes

Clinical pathology supported the thyroid ultrasound imaging results that Huiying Medical Technology (Beijing) Co, Ltd. provided for the study. The ultrasonic pervasive by Implorer provided the experimental data, and the detector's frequency ranged from 10 to 14 MHz. The tests included 1156 sonograms of the pulmonary nodules in 233 patients. 539 benign photos and 617 malignant images were captured throughout 578 longitudinal and cross-sectional images. Before extraction, the ROI region of each nodule picture underwent a colour channel modification. Moreover, using the radiologist's annotation data, we individually obtained the conventional ultrasound and ultrasonic elasticity data components of each photograph during the pre-processing step.

3. RESULTS AND DISCUSSION

The results of our provided code for the subsequent thyroid segmentation and extraction are described in the findings shown below. Fig.2(a) demonstrates the network layer graph, which is created between the x and y axes and between the T and A. The differences in selecting the best course of action are represented by the dots that are interconnected.

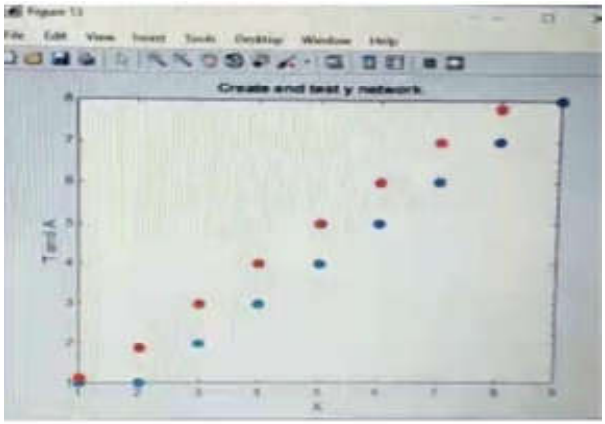

Fig.2 (a)Create and test network

Fig.2 (b)Maximum Pooling

The area afflicted by the thyroid may be seen in the highest swimming photograph in Figure 2(b). Considering this, Figure 2(c) muddled appearance of the thyroid affected region. The above-mentioned graphic provides details on the histogram equalized image of the thyroid area affected that is handed the grey image of the segmented section of the image, and then the linear Figure 2(d) procedure contrasts that in an interesting manner.

Fig.2 (c) Convoluted Image

Fig.2 (d) Linear contrast stretched image

After the segmentation based on the neural network that the segmented are of the normal image and the convoluted grey scale image if given for the calculation in the neural network, and the values are being given in the figure 2(e).

6. CONCLUSION

In this research, we present research and a method for discerning between benign and malignant thyroid nodules leveraging feature extraction and feature fusion using conventional ultrasound and ultrasonic elasticity images. After considering the clinical use of ultrasound imaging, we employed two separate data sources-ultrasound and ultrasound elasticity images-to distinguish

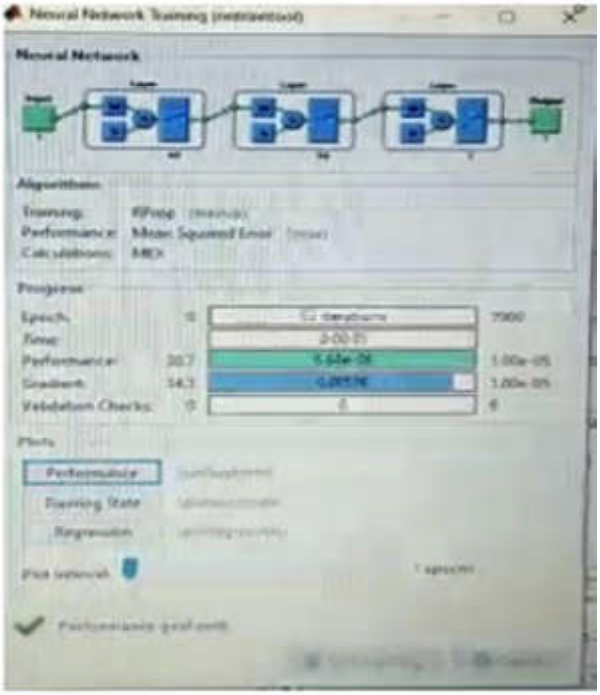

Fig.2 (e) Neural Network

between malignant and benign thyroid nodules. Moreover, the feature extraction method ensures that different feature extractors are independent, that the target data domain's data distribution is classified, that conventional ultrasounds have heightened awareness, and that representations of ultrasound elasticity have higher specificity.

REFERENCES

[1] T. Liu, S. Xie, J. Yu, L. Niu and W. Sun, "Classification of Thyroid Nodules in Ultrasound Images Using Deep Model-Based Transfer Learning and Hybrid Features", IEEE International Conference on Acoustics, Speech and Signal Processing, 2017, pp. 919-923.

[2] J. Hu, R. Ji, S. Zhang, X. Sun, Q. Ye, C.W. Lin and Q. Tian, "Information Competing Process for Learning Diversified Representations", arXiv preprint arXiv:1906.01288, 2019.

[3] J. Chi, E. Walia, P. Babyn, J. Wang, G. Groot and M. Eramian, "Thyroid Nodule Classification in Ultrasound Images By Fine-Tuning Deep Convolutional Neural Network", Journal of Digital Imaging, Vol. 30, No. 4, pp. 477-486.

[4] J. Wang, S. Li, W. Song, H. Qin, B. Zhang and A. Hao, "Learning from Weakly-Labelled Clinical Data for Automatic Thyroid Nodule Classification in Ultrasound Images", in 25th IEEE International Conference on Image Processing, 2018, pp. 3114-3118.

[5] J. Ma, F. Wu, T. Jiang, J. Zhu and D. Kong, "Cascade Convolutional Neural Networks for Automatic Detection of Thyroid Nodules in Ultrasound Images", Med. Phys., Vol.44, No.5, 2017, pp. 1678-1691.

[6] Y. Zhu, Z. Fu and J. Fei, "An Image Augmentation Method Using Convolutional Network for Thyroid Nodule Classification by Transfer Learning", in Computer and Communications (ICCC), 2017 3rd IEEE International Conference on IEEE, 2017, pp. 1819-1823.

[7] K. He, X. Zhang, S. Ren and J. Sun, "Deep Residual Learning for Image Recognition", in Proceedings of the IEEE Conference on Computer Vision and Pattern Recognition, 2016, pp.770-778.

[8] C.Y.Chang, S.J. Chen and M.F.Tsai, "Application of Support- Vector-Machine-Based Method for Features Election and Classification of Thyroid Nodules in Ultrasound Images", Pattern Recognition, Vol.43, No.10, pp.3494-3506.

[9] U.R. Acharya, G. Swapna, S.V. Sree, F. Molinari, S. Gupta, R.H. Bardales, A. Witkowska and J.S. Suri, "A Review on Ultrasound-Based Thyroid Cancer Tissue Characterization and Automated Classification", Technology in Cancer Research & Treatment, Vol.13, No.4, 2014, pp.289-301.

QUANTUM CHEMICAL BEHAVIOR OF HBLC COMPLEX: HPA+12OBA

S.Sundaram[1], V.N.Vijayakumar[2] and V.Balasubramanian[3]
[1&2]Department of Physics,
Condensed Matter Research Laboratory (CMRL), Research Park,
Bannari Amman Institute of Technology, Sathyamangalam - 638 401, Erode District, Tamil Nadu
[3]Department of Physics,
Sona College of Technology, Salem - 636 005, Tamil Nadu
E-mail: sundaram0024@gmail.com

Abstract

Density functional theory (DFT) is the most popular theoretical method for investigating the electronic properties of soft matter. DFT calculation is employed to optimize a new hydrogen bond liquid crystal complex (HBLC). In this DFT approach, the HBLC complex was designed, and the intermolecular hydrogen bonding between liquid crystalline 4-(Dodecyloxy) benzoic acid and non-liquid crystalline homophthalic acid (HPA) was justified using theoretical IR spectrum. Extensive DFT studies was performed on the electronic properties of the HPA+12OBA HBLC complex and its chemical reactivity descriptors were discussed. MEP analysis (Molecular Electrostatic Potential) is engaged to explore the chemical properties and active sites of the HPA+12OBA HBLC complex. By using Natural Bond Orbital (NBO) analysis, the stabilization energy and charge transfer between the HPA and 12OBA moiety was reported. Mulliken population analysis was employed to estimate the atomic charges and electronic charge distribution of the HPA+12OBA HBLC complex. The theoretical (DFT) predictions, like reactivity parameters, frontier molecular orbital study explains the liquid crystalline characteristics of the HPA+12OBA HBLC complex and its stability.

Keywords: *DFT method, HBLC complex, MEP, NBO method, Reactivity descriptors*

1. INTRODUCTION

At Present, dynamic research era in liquid crystal scientists is intermolecular interaction [1, 3]. LCs were used in technological applications through H-bonding because of their self-assembling characteristics [4-7]. 4-n-alkyloxy benzoic acid based liquid crystals (LCs) have fascinated a distinctive attention in the designing of hydrogen bond liquid crystal complex due to its anisotropic nature [8]. Presence of maximum chain length in the HBLC complex, induces mesomorphic nature [9], also enhanced thermal stability of smectic behaviour was reported [10]. As a result, higher homologues of HBLC complex is used in optical modulator [11], optical shutter and filter [12, 13].

The addition of 12OBA compound into a non-mesogenic materials results drastic change in molecular properties of HBLC complex including an increase in thermal span width, thermal stability, induced smectic behaviour along with decreasing melting point [14] and significant influence on the LC properties [15, 16]. While increasing alkyloxy chain length in the HBLC complex, enhances the mesogenic range by providing improved smectic layered arrangement which is also favour of decreasing clearing point [17].

Exploring the reactivity of LC molecules via intermolecular H-bonding, the DFT approach is the most effective tool [18]. In the designing of HBLC complex, rigid core and flexible core units play vital role in thermotropic LCs. The carboxylic acid group (-COOH) having strong polarity and rigidity [19]. The effect of flexible and rigid core unit on the HBLC complex via intermolecular H-bonding shows significant variations in mesomorphic properties [20]. K.D. Katariya et al studied that higher chain length LC compound exhibit more ordered smectic behaviour of DFT calculation [21]. Deepak Gupta et al explained the molecular dynamics, charge distribution and NLO properties of LCs by DFT method [22]. H. A. Ahmed et al studied the LC phase stability and mesophase dependent alkyloxy chain length by theoretical method [23]. The novelty of HPA+12OBA HBLC complex as follows: The increment of alkyloxy chain length results tuneable mesogenic behaviour in the HBLC complex. As compared to lower homologues of HPA+nOBA (n=6-8) HBLC complex, higher homologues (HPA+12OBA) HBLC shows four brush

texture of nematic phase, broken focal conic texture of smectic C phase along with smectic F phase (Checkardboard texture) respectively.

As compared to lower homologues of HPA+nOBA (n=6-8) HBLC complex, HPA+12OBA HBLC shows tilted smectic ordering phase which is more beneficial in optical modulator, optical shutter and optical filter. As increment of carbon number in the HPA+nOBA (n=6 to 12) HBLC complex, HPA+12OBA HBLC complex shows optimal thermal width for tiled smectic C phase. The thermal stability of smectic C phase was found to be very high compared to its lower homologues series which is apt material for optoelectronic devices. In the present study, newly designed HBLC complex is studied using DFT calculations. Further, the structural parameter, chemical reactivity, global reactivity descriptor (GRD), diploe moment and intermolecular charge transfer of optimized HPA+12OBA HBLC complex were extensively studied. Finally, atomic charges and active sites of HPA+12OBA HBLC complex were discussed.

2. COMPUTATIONAL (DFT) METHOD

DFT/B3LYP theory model is used to calculate the molecular geometry of the HPA+12OBA HBLC complex with a basis set of 6-311G. (d, p) [24-27]. Gaussian 09 software is used to calculate the molecular modelling of the HPA+12OBA HBLC complex using the DFT approach [28]. Chemcraft and Gauss view 52 software is utilized to display the optimised geometry, frontier molecular orbitals (HOMO-LUMO), and active sites of the HPA+12OBA HBLC complex [29]. NBO (NBO 3.1 software) analysis is used to calculate the charge transfer from the lone pair or -electrons to the antibonding atoms, the stabilisation energy and the intermolecular hydrogen bonding of the HPA+12OBA HBLC complex [30]. Figure 1 represent the optimized geometry of HPA+12OBA HBLC complex, corresponding H-bond length/angles were shown in figure 2.

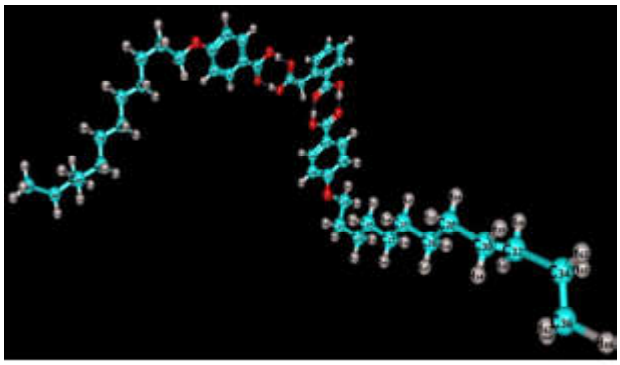

Fig.1 The molecular geometry of HPA+12OBA HBLC

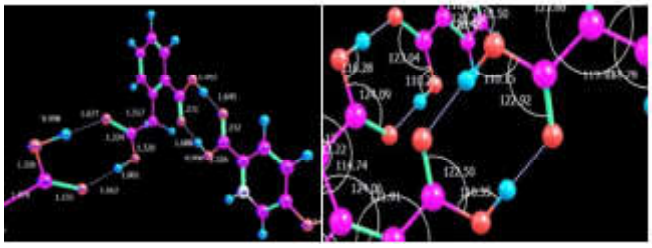

Fig.2. a) HB length b) HB angle of HPA+12OBA HBLC complex

3. RESULT AND DISCUSSION

3.1Global reactivity descriptors

The molecular structural parameters of HPA+12OBA HBLC complex are calculated using formula [31] and given in Table 1. The HPA+12OBA HBLC complex shows higher electrophilicity index (3.5845) which confirms the higher electronic transition [32]. The HPA+12OBA HBLC complex shows low global hardness and increasing global softness compared to lower homologues [33]. This is an evidence to the optical polarizability, improved chemical stability and induced mesomorphic behaviour.

Table 1 Physicochemical properties of HPA+12OBA HBLC complex

HPA+12OBA HBLC Complex	Molecular Properties
Molecular Weight (g/mol)	793.037
Chemical formula	$C_{47}H_{68}O_{10}$
Dipole moment (D)	1.776
No of atoms	125
No of bonds	125
LUMO energy (eV)	-1.7507
HOMO energy (eV)	-6.5101
Band gap energy (eV)	4.7593
Nucleophilicity index (N)	0.2789
Chemical potential (μ)	-4.1304
Global hardness (η)	2.3797
Global softness (S)	0.2101
Global electrophicity index(ω)	3.5845
Maximum electronic charge (ΔN_{max})	1.7356

3.2 Theoretical Vibrational Assignments of HPA+12OBA HBLC Complex

The vibrational assignment of HPA+12OBA HBLC complex computed plays remarkable role to analyse functional group of LCs using theoretical DFT calculation [33]. Fourier transform infrared (FT-IR) spectra of HPA+12OBA HBLC complex was recorded in the range of 3500–500 cm^{-1} and it is presented in figure 3.

HPA+12OBA HBLC complex shows red shift of 28 cm^{-1} and 120 cm^{-1} for C=O and O-H stretching respectively while compared to 12OBA. Similarly, red shift of 52 cm^{-1} and 40 cm^{-1} is observed for C=O and O-H stretching respectively while compared to HPA compound. The experimentally observed vibrational assignment (figure 3a) shows C=O stretching as 1628 cm^{-1} and O-H stretching is identified as 2870 cm^{-1}.

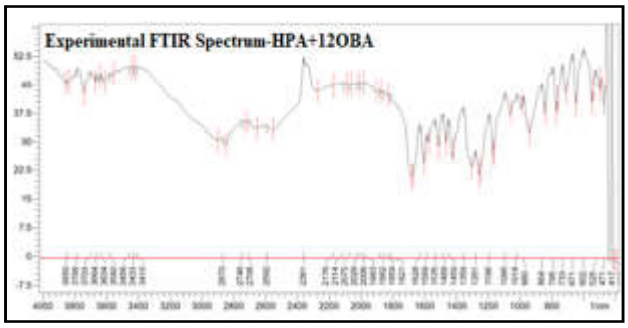

Fig.3 a) Experimental FTIR spectrum of HPA+12OBA HBLC complex

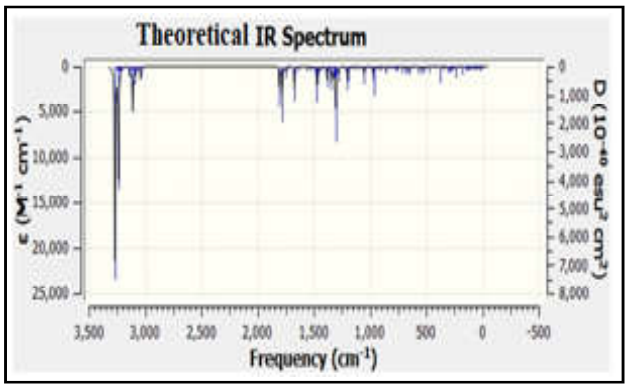

Fig.3 b) Theoretical FTIR spectrum of HPA+12OBA HBLC complex

Symmetric vibration of benzene ring of 12OBA is identified at 514, 1630, 1671 cm^{-1}. The alkyloxy carbon stretching is observed between 538-1529, 3021cm^{-1}. Asymmetric stretching of benzene ring of HPA is observed at 1636cm^{-1}. The symmetric carbonyl stretching (C=O) is identified at 1734, 1746, 1779, 1805 cm^{-1} respectively. The O-H stretching is theoretically observed at 3093, 3109, 3135cm^{-1}. The symmetric hydroxyl stretching (O…H) is observed as 3268cm^{-1}, which confirms the existence of intermolecular hydrogen bonding in between HPA and 12OBA which induces smectic phases in HPA+12OBA HBLC complex (Figure 3b). This is confirmed by the HOMO-LUMO analysis. The stimulated IR spectrum of HPA+12OBA HBLC complex validated with the experimental result [33].

3.3. HOMO-LUMO Analysis

HOMO-LUMO analysis is a significant method to govern the chemical stability of LCs [34]. The frontier molecular structure of HPA+12OBA HBLC complex is shown in figure 4. 12OBA act as an electron donor (HOMO) whereas HPA acts as an electron acceptor (LUMO). In HPA+12OBA HBLC complex, HOMO confined with mesogenic 12OBA while the LUMO spreads over non-mesogenic HPA moiety.

Band gap energy, E_g (eV) = E_{LUMO} - E_{HOMO}… (1)

In the HPA+12OBA HBLC complex, E_{HOMO}= -6.5101 eV whereas E_{LUMO}= -1.7507 eV. Using above formula, the band gap energy of HPA+12OBA HBLC complex is calculated as 4.7594 eV. This band gap energy value is lower than the reported HBLC complex [33].

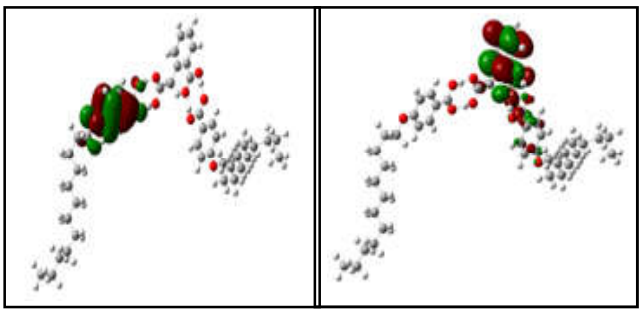

(a) (b)

Fig. 4 a) HOMO and b) LUMO plot of HPA+12OBA HBLC complex

3.4. Molecular Electrostatic Potential (MEP) Analysis

Electrostatic potential surface in 3D colour of HPA+12OBA HBLC complex is represented in figure 5 (predicted by DFT calculation). MEP is used to study the active atomic sites of LCs [35]. The negative electrostatic potential surface of HPA+12OBA HBLC complex is distributed in the red region (flexible core).

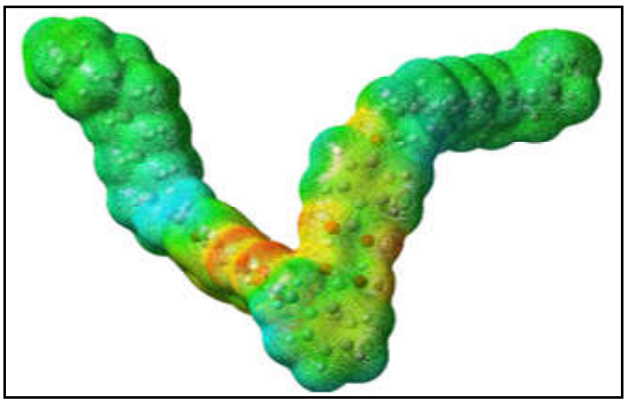

Fig. 5 3D MEP map of HPA+12OBA HBLC complex

The blue region (Rigid core) indicates the positive electrostatic potential surface of HPA+12OBA HBLC complex. The stimulated MEP charge distribution of HPA+12OBA HBLC complex shows the superior mesogenic behaviour. The electrophilic sites locate over oxygen atom of HPA+12OBA HBLC complex whereas, the nucleophilic sites spread over H-atom of benzene ring of HPA+12OBA HBLC complex. Followed by, the neutral electrostatic potential surface (green colour region) spread over alkyloxy chain of HPA+12OBA HBLC complex. Due to charge transfer between non-mesogenic HPA and mesogenic 12OBA, the MEP surface of HPA+12OBA HBLC complex changed which evidences the existence of intermolecular H-bonding.

3.5 Natural Bonding Orbital (NBO) Analysis

NBO analysis is powerful tool for the stabilization of LC molecular fragments [33]. In HBLC complex contain lone pair (LP) of H-bond acceptor and H-bond donor. The corresponding stabilization energy of HPA+12OBA HBLC complex is calculated using second order perturbation theory of Fock Matrix method. Intermolecular H-bonding ($O_3 \ldots H_{125}$) ($O_4 \ldots H_{73}$) ($O_{24} \ldots H_{21}$) ($O_{76} \ldots H_{20}$) along with its stabilization energy is listed in Table 2.

From the table 2, lone pair orbital of LP (2) O_{24} to antibonding orbital of π^* (O_2-H_{21}) transition shows strong interaction with highest stabilization energy (23.51 kcal/mol). A noteworthy observation is that H- atom and O-atom of carboxyl groups of HPA+12OBA HBLC complex contribute hyper conjugate interaction in the HBLC complex. The NBO study is a good agreement with Mulliken atomic charge distribution analysis of HPA+12OBA HBLC complex.

Table 2 Charge Transfer Mechanism of HPA+12OBA HBLC Complex

Donor (i)	Acceptor (j)	E (2) Kcal/mol	E (j)-E (i) a.u	F (i,j) a.u
from unit 1 to unit 2				
LP(1) O_4	π^* (O_{23}-H_{73})	7.93	1.08	0.083
LP(2) O_4	π^* (O_{23}-H_{73})	18.49	0.71	0.104
from unit 1 to unit 3				
LP(1) O_3	π^* (O_{75}-H_{125})	7.68	1.07	0.081
LP(2) O_3	π^* (O_{75}-H_{125})	20.33	0.71	0.109
from unit 2 to unit 1				
LP(1) O_{24}	π^* (O_2-H_{21})	8.56	1.06	0.086
LP(2) O_{24}	π^* (O_2-H_{21})	23.51	0.71	0.117
from unit 3 to unit 1				
LP(1) O_{76}	π^* (O_1-H_{20})	8.29	1.06	0.084
LP(2) O_{76}	π^* (O_1-H_{20})	21.55	0.70	0.112

3.6 Mulliken Charge Distribution Study

Mulliken atomic charge distribution techniques is a versatile theoretical calculation to analyze the molecular behaviour of LCs [34]. In general, reactivity, dipole moment, and the IR spectrum are governed on atomic charges [36]. Mulliken atomic charge distribution of HPA+12OBA HBLC complex is shown in figure 6.

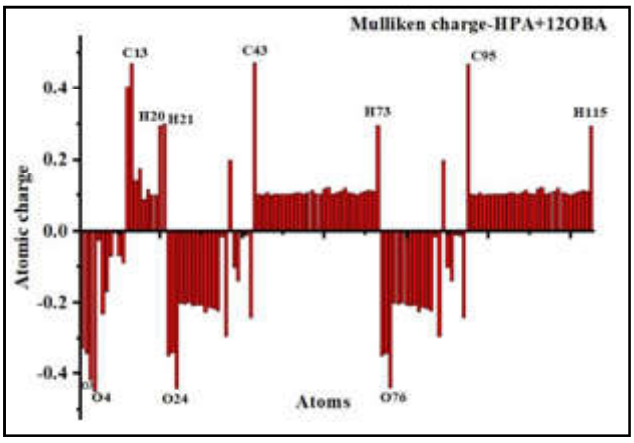

Fig. 6 Mulliken charge distribution of HPA+12OBA HBLC complex

It is observed that all the H-atoms in the HPA+12OBA HBLC complex shows positive charge whereas, O-atoms are negative charge. The maximum value of negative charges are identified for O_3, O_4, O_{24} and O76 (-0.2761e, -0.3412e, -0.3777e and -0.2791e) while the maximum value of positive charges are observed for H_{20}, H_{21}, H_{73} and H_{125} (0.4334e, 0.5780e, 0.5595e and 0.5311e). Here the noteworthy observation is that the charge exchange between oxygen and H atom significantly influence the electronic properties of LCs. During HBLC complex formation, $O_3 \ldots H_{125}$, $O_4 \ldots H_{73}$, $O_{24} \ldots H_{21}$ and $O_{76} \ldots H_{20}$ confirms the intermolecular H-bonding which implies that rich phase polymorphism in LCs.

4. CONCLUSION

The theoretically calculated IR spectrum of HPA+12OBA HBLC complex is good agreement with the experimental data. Global reactivity descriptors of HPA+12OBA HBLC complex is discussed. The calculated HOMO–LUMO energy gap values proved that the HPA+12OBA HBLC complex is optically more reactive complex. The electrophilic and nucleophilic sites of HPA+12OBA HBLC complex studied through MEP analysis. NBO and Mulliken charge distribution supported intermolecular charge transfer in the HPA+12OBA HBLC complex.

REFERENCES

[1] M.K. Sonali, P. Bhagavath, M. Srinivasulu, R. K. Sinha and K. Swamynathan, "Induced Mesomorphism In Supramolecular Structures of H-Bonded Binary Mixtures Containing Fluoro and Chloro Substituted Benzoic Acids", Journal of Fluorine Chemistry, Vol. 259-260, 2022, pp. 110002.

[2] M.S.Fedorov, N.I. Giricheva, S.A. Syrbu, E.A. Belova, I.A. Filippov and M.R. Kiselev, "New Supramolecular Hydrogen-Bonded Liquid Crystals based on 4-alkylbenzenesulfonic acids and 4-pyridyl 42 -alkyloxybenzoates: Quantum Chemical modeling and Mesomorphic Properties", Journal of Molecular Structure, Vol. 1244, 2021, pp.130890.

[3] M.Okumus, "Synthesis and Characterization of Hydrogen Bonded Liquid Crystal Complexes by 4-Octyloxy Benzoic Acid and Some Dicarboxylic Acids", Journal of Molecular Liquids, Vol.266, 2018, pp.529-534.

[4] M.L.N. Madhu Mohan, "Diversified Applications of Hydrogen Bond Liquid Crystals", IOP Conference Series: Materials Science and Engineering, Vol.1084, 2021, pp.012089.

[5] A.J.Thote and R.B.Gupta, "Hydrogen-Bonding Effects in Liquid Crystals for Application to LCDs", Industrial & Engineering Chemistry Research, Vol. 42, No.6, 2003, pp. 1129-1136.

[6] M.L.N. Madhu Mohan, N. Pongali Sathya Prabu and Kaushik Pal, "Phase-segregated Hydrogen Bonded Thermotropic Liquid Crystal's Optical Shuttering Response and Electro-Optical Sensor Application", Materials Letters, Vol. 305, 2021, pp. 130821.

[7] M.L.N. Madhu Mohan and Kaushik Pal, "Camphoric Acid Based Ferroelectric Hydrogen Bonded Liquid Crystalline Materials Integration Further Dielectric Relaxations and Novel Applications", Journal of Molecular Structure, Vol. 1232, 2021, pp.130022.

[8] T.Mahalingam, T.Venkatachalam, R.Jayaprakasam and V. N. Vijayakumar, "Structural and Thermo-Optic Studies on Linear Double Hydrogen Bonded Ferroelectric Liquid Crystal Homologous Series", Molecular Crystals and Liquid Crystals, Vol. 641, No.1, 2016, pp. 10-24.

[9] S.Sundaram, P.Subhasri, T.R.Rajasekaran, R. Jayaprakasam, T. S. Senthil and V. N. Vijayakumar, "Induced Smectic X Phase Through Intermolecular Hydrogen-Bonded Liquid Crystals Formed Between Citric Acid and p-n-(Octyloxy)Benzoic Acid", Brazilian Journal of Physics, Vol.47, 2017, pp.382-392.

[10] R. Rajanandkumar, N. Pongali Sathya Prabu and M. L. N. Madhu Mohan, "Analysis of Optical and Thermal Properties of Double Hydrogen Bonded Liquid Crystal Binary Mixtures", Molecular Crystals and Liquid Crystals, Vol.652, No.1, 2017, pp. 111-125.

[11] V. N. Vijayakumar and M. L. N. Madhu Mohan, "Double Hydrogen Bonded Liquid Crystals: A Study of Light Modulation and Field Induced Transition (FiT)", Molecular Crystals and Liquid Crystals, Vol.517, No.1, 2010, pp. 113-126.

[12] V.N. Vijayakumar and M.L.N. Madhu Mohan, "Thermally Controlled Optical Shutter in an Inter-Molecular Hydrogen Bonded Liquid Crystal", Physica B: Condensed Matter, Vol. 406, No. 21, 2011, pp. 4139-4144.

[13] N. Pongali Sathya Prabu and M.L.N. Madhu Mohan, "Optical Shuttering and Filtering Action in

Nematogens of Supra Molecular Hydrogen-Bonded Liquid Crystals", Molecular Crystals and Liquid Crystals, Vol.557, No.1, 2012, pp.190-205.

[14] G. Chandrasekar, N. Pongali Sathya Prabu and M.L.N. Madhu Mohan, "Design, Synthesis and Characterization of Hydrogen Bonded Liquid Crystals Formed Between Methyl Malonic Acid and p-n-alkyloxy/alkyl Benzoic Acids", Molecular Crystals and Liquid Crystals, Vol.652, No.1, 2017, pp.23-40.

[15] A.V.S.N. Krishna Murthy, M. Srinivasulu, M.L.N. Madhumohan, M. Muni Prasad and Y. V. Rao, *et al.,* "Influence of Molecular Architecture, Hydrogen Bonding, Chemical Moieties and Flexible Chain for Smectic Polymorphism in (4) EoBD(3)AmBA:nOBAs", Molecular Crystals and Liquid Crystals, Vol.715, No.1, 2021, pp.1-36.

[16] M. Surekha, A.V.N. Ashok Kumar, P.V. Chalapathy, M. Muniprasad and D.M. Potukuchi, "Synthesis and Phase Transition Characterization by Polarized Optical Microscopy and Differential Scanning Calorimetry in Hydrogen Bonded Chiral Liquid Crystal Series:M*SA:nOBAs", Molecular Crystals and Liquid Crystals, Vol.668, No.1, 2018, pp.1-28.

[17] V.Balasubramanian, V.N. Vijayakumar and T.Vasanthi, "Photonic Applications of Linear Double Hydrogen Bond Ferroelectric Liquid Crystal Mixture: Optical Modulators", Brazilian Journal of Physics, Vol.53, No.36, 2023.

[18] S. Sundaram, R. Jayaprakasam, M. Dhandapani, T.S. Senthil and V.N. Vijayakumar, "Theoretical (DFT) and Experimental Studies on Multiple Hydrogen Bonded Liquid Crystals Comprising Between Aliphatic and Aromatic Acids", Journal of Molecular Liquids, Vol. 243, 2017, pp.14-21.

[19] A.V.N. Ashok Kumar, P.V. Chalapathi, M. Srinivasulu, M. Muniprasad and D.M. Potukuchi, "Influence of Spacer Moiety and Length of End Chain for the Phase Stability in Complementary, Double Hydrogen Bonded Liquid Crystals, MA:nOBAs", Journal of Molecular Structure, Vol. 1079, 2015, pp. 94-110.

[20] P. Bhagavath, S. Mahabaleshwara, S.G. Bhat, D.M. Potukuchi, P. Shetty and M.Srinivasulu, "Influence of Polar Substituents and Flexible Chain Length on Mesomorphism in Non-Mesogenic Linear Hydrogen Bonded Complexes", Journal of Molecular Liquids, Vol. 336, 2021, pp.116313.

[21] K. D. Katariya, K. J. Nakum and M. Hagar, "New Thiophene Chalcones with Ester and Schiff Base Mesogenic Cores: Synthesis, Mesomorphic Behaviour and DFT Investigation", Journal of Molecular Liquids, Vol. 359, 2022, pp.119296.

[22] D. Gupta, P. Kalita and A. Bhattacharjee, "Observation of New Mesophases and Detailed QM Analysis of Terephthalylidene-bis-[4-n-decylaniline] Liquid Crystal Molecule", Journal of Molecular Structure, Vol. 1269, 2022, pp.133815.

[23] H. A. Ahmed, M. Hagar and G.R. Saad, "Impact of the Proportionation of Dialkoxy Chain Length on the Mesophase Behaviour of Schiff base/ester Liquid Crystals; Experimental and Theoretical Study", Liquid Crystals, Vol.46, No.11, 2019, pp.1611-1620.

[24] A.D.Becke, "Density-functional Exchange-Energy Approximation with Correct Asymptotic Behavior", Physical Review A, Vol.38, pp.3098–3100, 1988.

[25] K.Anbazhakan, K.Sadasivam and R.Praveena, *et al.,* "Target Prediction and Antioxidant Analysis on Isoflavones of Demethyltexasin: A DFT Study", Journal of Molecular Modelling, Vol.25, No.169, 2019.

[26] A.G. Baboul, L.A. Curtiss and P.C. Redfern, *et al.,* "Gaussian-3 Theory Using Density Functional Geometries and Zero-Point Energies", The Journal of Chemical Physics, Vol.110, No.16, 1999, pp.7650–7657.

[27] R.G. Parr and W.Yang, "Density Functional Theory of Atoms and Molecular Orbital Theory", Oxford University Press, New York, 1998.

[28] M.J.Frisch, G.W. Trucks and H.B.Schlegel, *et al.,* Gaussian 09, Revision C. 02, Gaussian Inc., Wallingford CT, 2010.

[29] R. Dennington, T. Keith and J.Millam, GaussView, Version 5, Semichem Inc., Shawnee Mission, KS, 2009.

[30] E. D. Glendening, A. E. Reed and J. E. Carpenter, *et al.,* NBO version 3.1, Theoretical Chemistry Institute and Department of Chemistry, University of Wisconsin, Madison, 1998.

[31] S.Sundaram, P. Subhasri, R. Jayaprakasam and V.N. Vijayakumar, "Thermal and Optical Characterization of Multiple Hydrogen Bonded Liquid Crystals Derived From Mesogenic and Non-Mesogenic Compounds: Experimental and Theoretical (DFT) Studies", Canadian Journal of Physics, Vol.98, No.5, 2019, pp.413-424.

[32] G. Vijayakumari, N. Iyandurai, M. Raja, V. Vetrivelan, A. Thamarai, Saleem Javed and S. Muthu, "Chemical Reactivity, Solvent Effects, Spectroscopic (FTIR, Raman, SERS, UV–Visible), Hirshfeld Analyses and Antimalarial Investigation

of 3-Acetylbenzoic Acid", Chemical Physics Impact, Vol.6, 2023, pp.100190.

[33] S.Sundaram, V.N.Vijayakumar, V.Balasubramanian and S.Balamuralikrishnan "Experimental and Computational (DFT) Methods: Exploration of Thermochromisim in Homophthalic Acid and 4-N-Alkyloxybenzoic Acid Comprised Hydrogen Bond Liquid Crystals", Molecular Crystal and Liquid Crystal, Vol.740, No.1, 2022, pp. 85-103, 2022.

[34] R. Praveena, K. Sadasivam, V. Deepha and Raman Sivakumar, "Antioxidant Potential of Orientin: A Combined Experimental and DFT Approach", Journal of Molecular Structure, Vol. 1061, 2014, pp.114-123.

[35] S.Z. Mohammady, D.M. Aldhayan and M.Hagar, "Pyridine-Based Three-Ring Bent-Shape Supramolecular Hydrogen Bond-Induced Liquid Crystalline Complexes: Preparation and Density Functional Theory Investigation" Crystals, Vol.11, 2021, pp.628.

[36] R.Carbo-Dorca and P.Bultinck, "Quantum Mechanical Basis for Mulliken Population Analysis", Journal of Mathematical Chemistry, Vol.36, 2004, pp.231-239.

An Experimental and Theoretical Studies on Benzimidazo Oxyquinoline Derivative (AVMPDO) as Aqueous Soluble Fluorescent Receptor For pH and Metal Ion Sensing

M. Malathi[1], I Manikandan[2] and C.K.Venil[3]
[1&2]Department of Chemistry,
Bannari Amman Institute of Technology, Sathyamangalam - 638 401, Erode District, Tamil Nadu
[3]Department of Biotechnology,
Anna University, Regional Campus, Coimbatore- 641 046, Tamil Nadu
E-mail: bharathia@bitsathy.ac.in,rsr026@gmail.com

Abstract

3-(6-methyl-1H-benzo[d]imidazol-2- yl)quinoline-2(1H)-one (AVMPDO) is prepared and characterized by FT-IR and NMR spectral studies. The optical properties of the synthesized compound are analyzed using absorption and emission studies. In application part pH titration and metal binding are carried out and notable sensing property is identified in aqueous medium. Theoretical studies are also performed using Differential functional theory and Auto dock studies.

Keywords: *Absorption, Auto dock study, Benzimidazole, Differential functional theory, Emission, Fluorescence, Metal binding, pH sensor, Quinolines*

1. INTRODUCTION

Fluorescence chemosensors play a vital role in various fields, including analytical chemistry, biology, environmental monitoring, and materials science[1]. The following list details the key reasons for the importance of the fluorescence compounds: (1) Sensitivity and Selectivity for detecting specific analytes which play a crucial in applications such as detecting pollutants, monitoring biological processes, and identifying trace amounts of substances in complex samples; (2) Real-time Monitoring of analytes which provides immediate feedback and continuous data acquisition, making them valuable tools in various dynamic processes for example study cellular processes, or monitor environmental parameters like pH, temperature, and ion concentrations; (3) Fluorescence-based sensing techniques are often non-invasive, minimizing the need for sample preparation or destruction; (4) Imaging and Visualization- By modifying the sensor's structure and chemical properties, researchers can tailor its characteristics to suit specific applications, expanding the versatility of fluorescence-based sensing platforms[2,3]. All listed applications are very limited and there are enormous applications are observed [4]. Accordingly, continued research and development in this field hold promise for addressing various analytical challenges and advancing to understand the complex systems[5].

Consequently, the synthesis and characterization of new fluorescent probes have emerged as a vibrant area of research in the field of supramolecular chemistry [6,7]. Many of the reported fluorescent probes exhibit dual functionality as dyes for cell imaging studies and molecular sensors for specific species, including metal ions and anionic species [8]. Moreover, they have proven to be crucial for sensing molecular-level environmental factors such as pH and solvent polarity [9]. Recently, there has been a growing aspiration to develop single probe systems capable of detecting multiple species simultaneously, driven by the diverse needs in various fields and the demand for cost-effective application [10,11]. Based on this context, 3-(6-methyl-1H-benzo[d]imidazol-2-yl)quinoline-2(1H)-one was synthesized, followed by a comprehensive analysis of its characterization and application studies.

2. EXPERIMENTAL PART

Dehalogenation reaction of Benzimidazo quinoline AVMPDA [12] results benzimidazo oxyquinoline AVMPDO compound. The synthetic procedures of the dehalogenation process are as follows. 5 mmol (1.5 g) of compound AVMPDA in 100 ml round bottom flask was dissolved in 30 ml of acetic acid. To this mixture 5 mmol (0.42 g) of sodium acetate was added and stirred for 10 min.

The resulting mixture was refluxed in an oil bath with the duration of about 3 hrs. Completion of the reaction was confirmed by thin layer chromatography (TLC) using chloroform and methanol mixture as eluent.

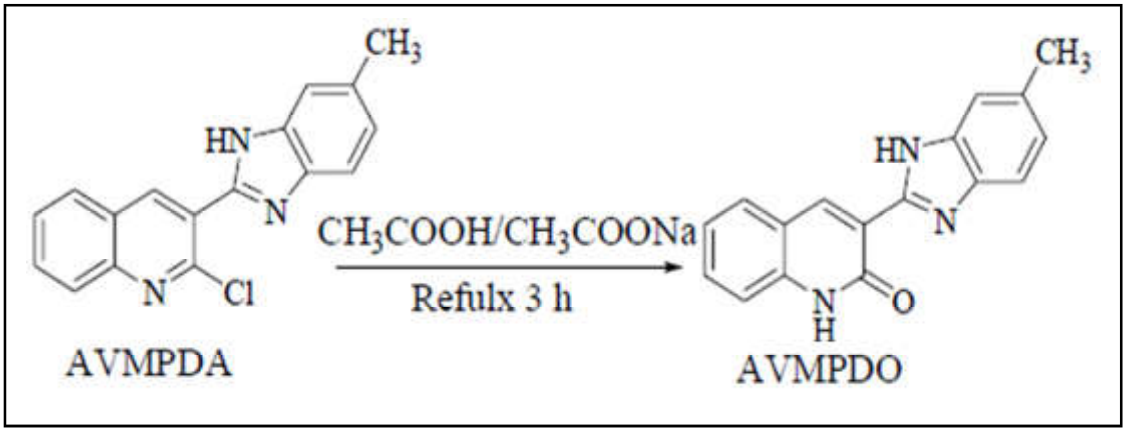

Fig. 1 Preparation of AVMPDO

Finally, the mixture was poured into the crushed ice taken in 500 ml beaker and the solution was neutralized using 0.1 N NaOH and HCl. The resulting product was filtered and dried. The pure AVMPDO compound was isolated by column chromatography using 10 % of chloroform and methanol solvent medium as eluent (volume ratio of methanol: chloroform) medium. Yield 83.32 %; Melting point 298 °C

3. RESULTS AND DISCUSSION

3.1 Spectral Characterization

The FTIR spectrum of the synthesized compound AVMPDO is done and the functional groups absorption band at 3554, 3323, 1652, and 1565 cm^{-1} reveals the presence of quinoline cyclic amide N-H, imidazole N-H, carbonyl quinoline and imidazole -C=N groups respectively [13].

The ^{1}H and ^{13}C-NMR spectrum of the synthesized (AVMPDO) in $CDCl_3$ is performed and the results following data. ^{1}H-NMR Spectral data: ($CDCl_3$, TMS): $ä_H$ 2.50 (s, 3H, IM-C6-CH3-H), 7.10 to 7.75 (m, 7H, IM-C4-H, C5-H, C7-H, Q-C9-H, C10-H, C11-H, C12-H), 9.16 (s, 1H, Q-C8-H), 11.28 (s, 1H, Q-N-H), 11.91 (s, 1H, IM-N-H).

In ^{13}C NMR Spectrum, Carbon atoms in the molecules are appeared at $ä_C$; 26.48, 119.22, 119.43, 119.87, 119.92, 120.59, 124.22, 124.28, 127.73, 129.13, 133.38, 136.22, 136.29, 137.19, 143.51, 152.93, 166.60.All spectral results confirmed the target compound AVMPDO [14].

The absorption and emission spectrum of AVMPDO is presented in the Fig. 2. Both Absorption and emission are examined in ethanol solvent medium. In the UV-Vis absorption spectra, the compound shows the absorbance spectra near to the visible region at the wavelength of 377 nm. This is due to the n-đ* electronic transitions. The compound AVMPDO shows a strong fluorescence band in the emission spectra at the wavelength of 435 nm by the absorbing energy at 377 nm. The Stokes shift is calculated using the absorption and emission $ë_{max}$ of AVMPDO with 58 nm.

3.2 Photophysical Studies

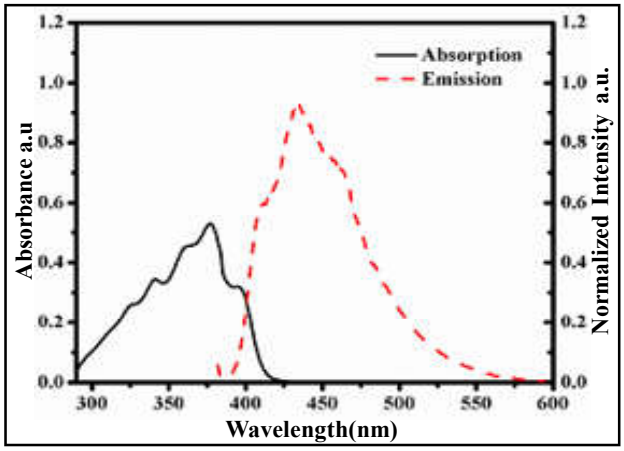

Fig.2 Absorption and emission spectrum of AVMPDO

3.3 Solvent Polarity Studies

The term "solvent polarity" lacks a precise definition, but it is generally understood as the intermolecular interaction behavior of solvent molecules towards solutes. Solvent polarity significantly impacts the molecular

polarity of the solute, thereby affecting the photochemical properties of compounds. In the context of fluorophores, the emission characteristics are particularly influenced by the molecular polarity and the specific type of solvent used.

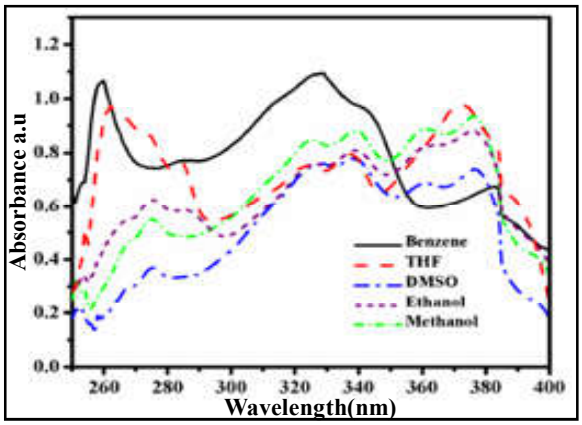

Fig.3 Absorption spectra of AVMPDO in different solvent medium

The photo physical behavior of the compound AVMPDO with respect to solvent polarity is studied by UV-visible absorbance and emission studies using different solvents such as benzene, ethanol, methanol, THF, dimethyl sulphoxide. In this study, $20x10^{-5}$ M concentration of compound AVMPDO is taken. In absorption spectrum of the molecule AVMPDO shows p-p* and n- p* type of electronic transitions (Fig. 3).

The absorption peak of the compound AVMPDO was noted at лmax 328 nm in benzene a least polar solvent medium, which is changed to $л_{max}$ 382 nm in higher solvent polarity. Thus the compound exhibits red shift or bathochromic shift.

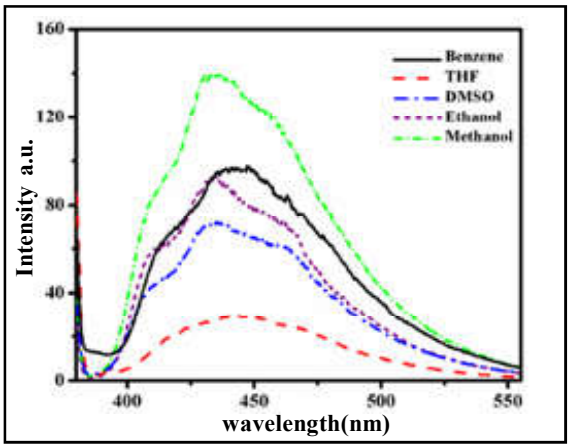

Fig.4 Emission spectra of AVMPDO in different solvent medium

The solutions of compound AVMPDO in different solvents used in the absorbance studies are again used in the emission spectral studies by using respective absorbance wavelength as the excitation wavelength. The compound exhibits the emission wavelength at 445 nm for low polar solvent like benzene and it is shifted to successively to lower wavelengths up to 426 nm with respect to solvent polarity.

Table 1 Photo-physical Characteristics of AVMPDO

Solvents	λabs (nm)	λemi (nm)	Stokes shift (nm)	ϕf
Benzene	328	445	117	0.0348
THF	371	441	70	0.0102
DMSO	375	436	61	0.0352
Ethanol	378	431	53	0.0278
Methanol	382	426	44	0.0395

Thus the compound exhibits a slight blue shift with respect to the solvent polarity. The difference in the emission wavelength from lower to higher polar solvents was found to be H" 5 nm. Additionally an increase in fluorescence intensity of this compound AVMPDO in methanol solvent medium is observed.

3.4 pH Response Study

Absorption spectra of AVMPDO solution (20 мM) in different pH are recorded at room temperature and present in Fig. 5. At low pH values AVMPDDG showed a strong absorption peak at 335 nm which decreased gradually for the subsequent increase in pH. Base induced deprotonation of nitrogen atoms in the compound AVMPDO leads a charge transfer between the quinoline and benzimidazole ring.

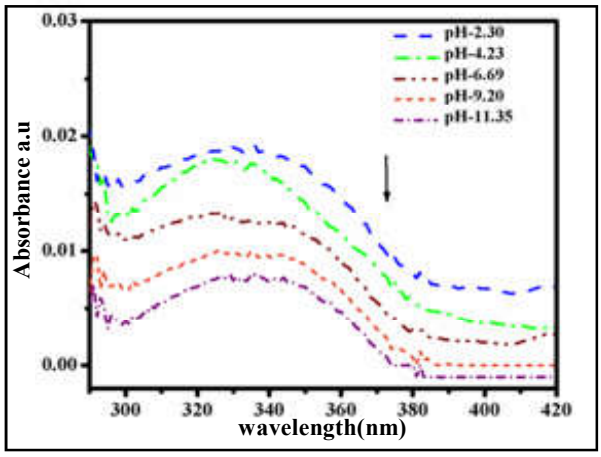

Fig. 5 Absorption spectra of AVMPDO at various pH

The emission pH titration for the compound AVMPDO is presented in Fig. 6. At acidic condition the compound AVMPDO shows an emission peak at 416 nm. The intensity of the emission has varied slightly up to the pH 5. Above that, an enhancement in the emission intensity is noted with red shift from 416 to 445 nm and the intensity has continuously increased with subsequent increase in the pH. However a strong reduction in the emission intensity has been observed after pH 10. The further increase of pH leads to nonradiative molecular relaxation which is responsible for the fluorescence quenching.

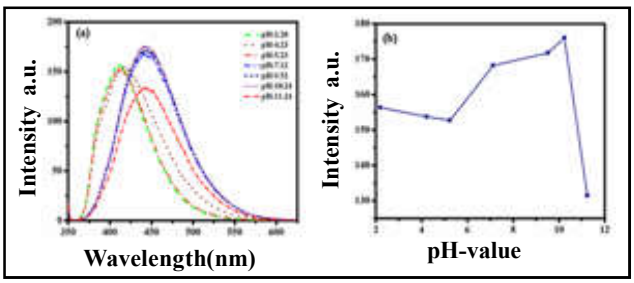

Fig.6 Emission spectra of AVMPDO at various pH

3.5 Metal Sensing Studies

The combined absorption spectra of AVMPDO (20 мM) with metal ions Cd^{2+}, Co^{2+}, Fe^{3+}, Zn^{2+}, Hg^{2+}, Pb^{2+}, Ni^{2+} and Mg^{2+} ($1x10^{-4}$ M) in HEPES buffer medium is presented in the Fig. 7. An intensive absorption band of AVMPDO is found at 327 nm. In the presence of Fe^{3+} ion alone, AVMPDO give a signal through a notable absorption enhancement without any shift in the absorption wavelength. However the other metal ion does not influence the absorption spectrum of the binding receptor. The observed spectral changes indicates the interaction of the AVMPDA with Fe^{3+} ion and revealed the strong metal chelating property of AVMPDA with Fe^{3+} ion.

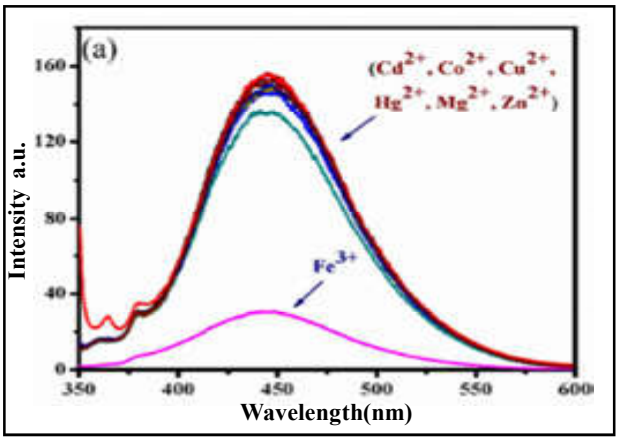

Fig.7(a) Metal binding fluorescence titration of AVMPDO

To have a better understanding of the fluorescence spectral response of AVMPDO to Fe^{3+} ion, fluorescence titration is performed with increasing concentration of Fe^{3+} ion from 10 μM to 100 μM and the combined spectral reports are presented in the Fig. 8. The titration study shows a gradual decrease in the fluorescence intensity with the increasing concentrations of Fe^{3+} ion. The quenching result reveals the existence of excitation energy transfer from the receptor to metal ion and chelating property of the receptor AVMPDO.

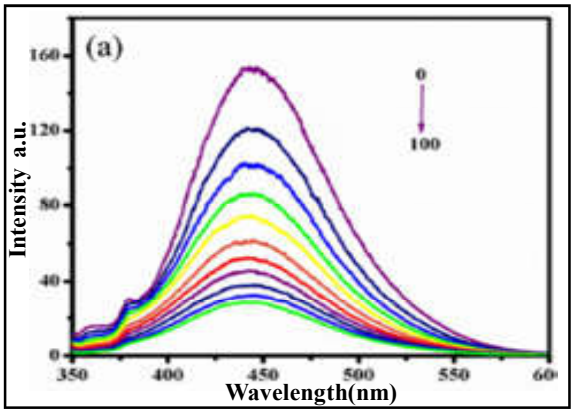

Fig.8 Fe^{3+} ion binding fluorescence titration of AVMPDO

3.6 DFT Optimization

Theoretical calculations are performed at the RB3LYP level of theory using Gaussian-09 series of program based on the 6-31G (d,p) basis set. The main objective of the theoretical studies of the receptor is to understand the molecular charge distribution, active site for binding and feasibility mode. The optimized structure of the compound is given in Fig. 9 with minimum energy -1195.1858 and Dipole moment in 5.4115 Debye.

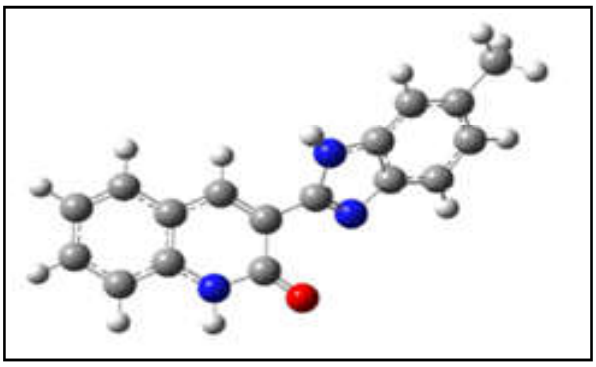

Fig. 9(a) Metal binding fluorescence titration of AVMPDO

3.7 Molecular Docking

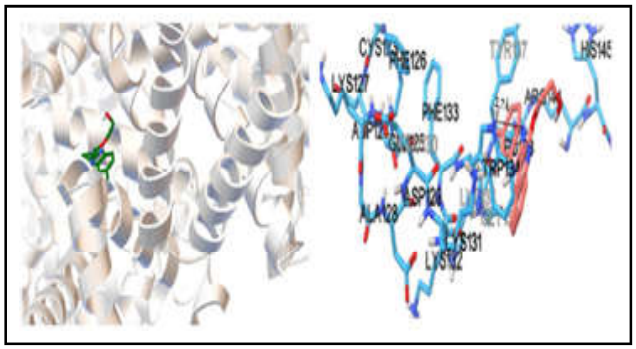

Fig. 10 Docking study of AVMPDO with BSA

The compound AVMPDO is docked to protein Bovine serum albumin (BSA) and the resulting docked view of the ligand-protein complex is presented in the Fig. 10. The minimum binding energy for the AVMPDO-BSA complex is found to be -6.9KJ/mol at 298k. In complex structure, the compound AVMPDO is surrounded by the hydrophobic residues of the BSA proteins i.e., PHE133, PHE126 and GLY135. The BSA protein's polar residues of TYR137, TRP134 and HIS145 are also found to be involved a strong interaction with the compound AVMPDO. Among all, polar residue tryptophane 134 formed hydrogen bonding with the compound AVMPDO i.e., Ligand imidazole ring azide C=N with NH of tryptophan with the observed bond distance of 2.7Å. Hence the formation of H-bonding between the compound AVMPDO and the tryptophan residue should result a polarity change around the chromophore of BSA. In corresponds, protein docking studies illustrate and evident the experimental results observed in the fluorescence titration studies.

4. CONCLUSION

In the current paper, the compound 2-chloro-3-(6-methyl-1H-benzol-2-yl)quinoline (AVMPDO) is successfully synthesized and characterized by spectroscopy techniques using IR and NMR [^{1}H and ^{13}C]. The photo-physical properties of the synthesized compound are analyzed using spectrophtometer and spectrofluorometer by varying the environmental factors such as solvent polarity. In all studies the compound exhibits specific optical response with respect to the subjected environmental factors. As a part of applications, all the synthesized compound are subjected to metal binding studies. In metal binding studies, AVMPDO exhibits optical response to ferric ion. Based on titration plot the compound AVPDO is defunded as best metal sensor among the studied compounds by having highest quenching percentage. DFT calculations using Gaussian-09 series are performed and interpreted with experimental results. In addition Auto Dock study depicted the binding affinity of the compound specifically through the lowest binding energy and hydrogen bonding distances.

REFERENCES

[1] V. Arun, S. Mathew, P.P Robinson, M. Jose, Nampoori, and Yusuff, KKM 2010, "The Tautomerism, Solvatochromism and Nonlinear Optical Properties of Fluorescent 3-Hydroxyquinoxaline-2-Carboxalidine-4-Aminoantipyrine", Dyes and Pigments, Vol. 87, No. 2, pp. 149-157.

[2] Au, W, Pathak, S, Collie, CJ & Hsu, TC 1978, 'Cytogenetic toxicity of gentian violet and crystal violet on mammalian cells in vitro', Mutation Research/Genetic Toxicology, vol. 58, no. 2-3, pp. 269-276.

[3] Banjoko, V, Xu, Y, Mintz, E & Pang, Y 2009, 'Synthesis of terpyridine-functionalized poly (phenylenevinylene) s: the role of meta-phenylene linkage on the Cu^{2+} and Zn^{2+} chemosensors', Polymer, vol. 50, no. 9, pp. 2001-2009.

[4] Becke, AD 1988, 'Density-functional exchange-energy approximation with correct asymptotic behavior', Physical review A, vol. 38, no. 6, pp. 3098.

[5] Bhalla, V, Kumar, R, Kumar, M & Dhir, A 2007, 'Bifunctional fluorescent thiacalix [4] arene based chemosensor for Cu^{2+} and F> ions', Tetrahedron, vol. 63, no. 45, pp. 11153-11159.

[6] Biyiklioglu, Z, Durmus, M & Kantekin, H 2010, 'Synthesis, photophysical and photochemical properties of quinoline substituted zinc (II) phthalocyanines and their quaternized derivatives',

Journal of Photochemistry and Photobiology A: Chemistry, vol. 21, no. 1, pp. 32-41.

[7] Bricks, JL, Kovalchuk, A, Trieflinger, C, Nofz, M, Büschel, M,Tolmachev, AI & Rurack, K 2005, 'On the development of sensor molecules that display FeIII-amplified fluorescence', Journal of the American Chemical Society, vol. 127, no. 39, pp. 13522-13529.

[8] Cao, H & Liu, Q 2009, 'Effects of temperature and common ions on binding of puerarin to BSA', Journal of solution chemistry, vol. 38, no. 8, pp. 1071-1077. 198.

[9] Cao, Y, Yang, M, Wang, Y, Zhou, H, Zheng, J, Zhang, X & Wu, Z 2014, 'Aggregation-induced and crystallization-enhanced emissions with time-dependence of a new Schiff-base family based on benzimidazole', Journal of Materials Chemistry C, vol. 2, no. 19, pp. 3686-3694.

[10] Chakraborty, B, Roy, AS, Dasgupta, S & Basu, S 2010, 'Magnetic Field Effect Corroborated with Docking Study to Explore Photoinduced Electron Transfer in Drug-Protein Interaction', 12 The Journal of Physical Chemistry A, vol. 114, no. 51, pp. 13313-13325.

[11] Shen, Z, Burrows, PE, Bulovic, V, Forrest, SR & Thompson, ME 1997, 'Three-color, tunable, organic light-emitting devices', Science, vol. 276, no. 5321, pp. 2009-2011.

[12] Chakraborty, B, Roy, AS, Dasgupta, S & Basu, S 2010, 'Magnetic Field Effect Corroborated with Docking Study to Explore Photoinduced Electron Transfer in Drug-Protein Interaction', 12 The Journal of Physical Chemistry A, vol. 114, no. 51, pp. 13313-13325.

[13] Shen, Z, Burrows, PE, Bulovic, V, Forrest, SR & Thompson, ME 1997, 'Three-color, tunable, organic light-emitting devices', Science, vol. 276, no. 5321, pp. 2009-2011.

[14] Singh, P & Kumar, S 2006, 'Three different fluorescent responses to transition metal ions using receptors based on 1, 2-bis-and 1, 2, 4,5- tetrakis-(8-hydroxyquinolinoxymethyl) benzene', Tetrahedron, vol. 62, no. 26, pp. 6379-6387.

COMPARISON OF THE ACTIVITY OF VASICOL AND GALLIC ACID - A THEORETICAL APPROACH

R. Praveena[1], V. Deepha[2] and K. Anbazhakan[3]
[1&2]QCPRL-CRF
Bannari Amman Institute of Technology, Sathyamangalam - 638 401, Erode District, Tamil Nadu
[3]Department of Physics
Gobi Arts and Science College, Gobichettipalayam - 638 476, Erode District, Tamil Nadu

Abstract

Alkaloids, are compounds found widely in plant parts, consumed by humans and helps in reducing oxidative stress. Studies related to exploration of pharmacological activity of alkaloids is limited which paved a way to analyse vasicol, an alkaloid derived from Justicia adhatoda, a common plant found in India, The current investigation compares the structure-activity of vasicol and gallic acid using quantum chemical calculations of density functional theory. The structures are initially optimised for its ground state followed by analysis of electron donating capability through frontier molecular orbital analysis, molecular electrostatic potential mapping, molecular descriptor analysis and target prediction analysis. The results show that both the compounds vasicol and gallic acid contribute equally as an electron donor, also as the biovailability of gallic acid is limited, vasicol acts as a better target compared to gallic acid.

Keywords: *Density functional theory, Gallic acid, Molecular electrostatic potential and Target prediction, Vasicol*

1. INTRODUCTION

Naturally occurring compounds isolated from plant or animal sources play a vital role in drug discovery for several diseases caused due to oxidative stress [1]. Synthetic drugs derived based on slight modifications in structure from the entities of compounds from natural products is found to exhibit short term and long term destructive health effects on humans [2]. Hence over the past few decades' researchers/scientists explored the activity of known compounds to find potential drugs that act as antioxidants. Gallic acid - 3,4,5-trihydroxybenzoic acid found in higher plants occur in free state as well as ester derivatives. Gallic acid including its derivatives are extracted from bark, leaves, flowers and fruits of edible plants. Humans have the capacity to adsorb more than 65 % gallic acid and convert it to 4-O-methylgallic acid. The compound is an eminent antioxidant that exhibits various neuroprotective actions and remedy for oxidative stress[3]. Regulation of diabetes mellitus, a result of oxidative stress is studied by Yu Xu et al and they stated that ingestion of Gallic acid at proportionate levels may be effective against diabetes[4]. In this study gallic acid which is less studied in DFT is taken as standard against a rare compound vasicol.

Vasicol is an alkaloid initially isolated from the roots of *Adhatoda vasica* [5], a plant species used against diabetes in traditional medicine. Its structural formula is given as 1,2,3,4,9,11 hexahydro pyrrolo (2,1-b) quinazolin-3,11 diol. The compound was also isolated from *P. harmala* seeds using chromatographic techniques. Recently the alkaloid is found to be used as tablet for pain in legs [6].

In this article, a comparison study of the structure activity relationship of the two compounds gallic acid and vasicol is made through density functional theory analysis. Molecular descriptive parameters, frontier molecular orbital , molecular electrostatic potential and target prediction analysis for the specified compounds are made using Gaussian 09.

2. COMPUTATION DETAIL

In order to study the molecular properties of two flavonoids considered here it is necessary to know their ground state energies for which optimization of their structural features is been carried out. Here structural optimization is carried out using density functional theory[7]. The triple zeta valences basis set 6-311G(d,p) along with the exchange correlation functional B3LYP is been adopted here, since the considered molecules

are highly delocalized. The simulations are supported by Gaussian 09 program[8]. The visualization of the computed properties are made through Gauss view 05 and Chemcraft software. Docking analysis is supported by Auto Dock Vina using Lamarckian genetic algorithm and the visualizations are made using UCF Chimera molecular visualizer[9].

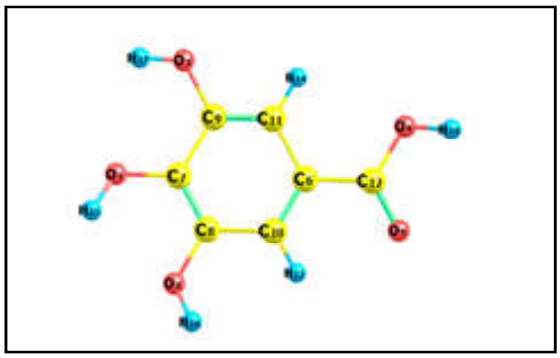

(a) Gallic acid

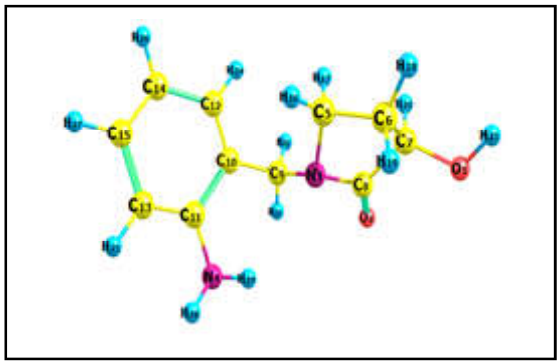

(b) Vasicol

Fig.1 Optimized structures of (a) Gallic acid and (b) Vasicol

3.2 Frontier Molecular Orbitals

HOMO

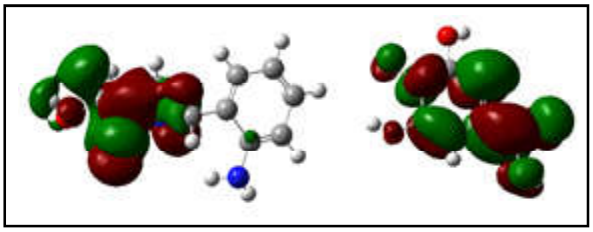

LUMO

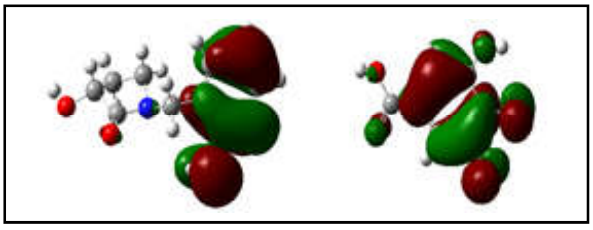

Vasicol Gallic acid

Fig.2 Frontier Molecular Orbitals of Vasicol and Gallic acid

Frontier molecular orbitals(FMOs) play a crucial role in a wide range of chemical reactions determining the reactivity of biocompounds by explaining their charge distribution[11]. The electron donating ability of a molecule is characterized by ð electron delocalization in a compound. The highest occupied molecular orbital (HOMO) is the orbital of highest energy that is still occupied, so energetically it is easier to remove electrons from this orbital. From the Figure 2 for both vasicol and gallic acid it is observed that lowest unoccupied molecular orbitals are found to be spread over hydroxypyrrolidin unit with lower intensity.

Whereas the occupied molecular orbitals are found to be spread over the hydroxyl units for both the compounds which makes the sense that they possess highest electron density and it is the highest reactive site for both the compounds. The energy gap between the occupied energy levels and unoccupied energy levels of vasicol and gallic acid found to be 1.648 eV and 1.738 eV which is of same order with minor variation. Therefore, from this analysis it can be concluded that while considering reactivity both the molecules tend to project same kind of reactivity since both of them occupy same energy level.

3.3 Molecular Electrostatic Potential (MEP) Analysis

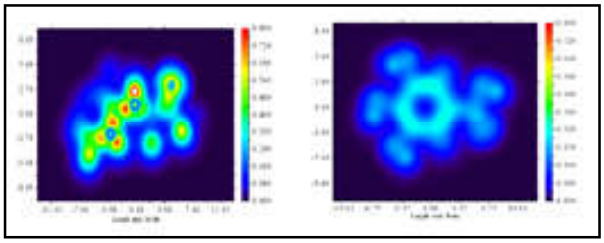

Vasicol **Gallic acid**

Fig.3 MEP visualization for (a) Vasicol and (b) Gallic acid

MEP analysis is one of the successful tool to analyze the ability of biomolecules to donate or gain electrons by visualizing the electronegative and electropositive regions around the molecular surface. From the Fig.3 it is evident that, for both of the compounds the electropositive region is highly concentrated over –OH units which indicates their readiness in donating the electron. Whereas oxygen atom attached to carbonyl atom in both the compounds projects electronegative region, representing their readiness for accepting electrons. Further the visualizations depict that both the compounds possess highly intense and majorly spread electropositive nature around them which makes them to be better electron donors rather than electron acceptors.

3.4 Global Reactivity Parameters

Table 1 Molecular Descriptive Parameters for Vasicol and Gallic acid

Molecular Descriptors	E_v (eV) of Vasicol	E_v(eV) of Gallic acid
IP (eV)	5.7634	6.6774
EA (eV)	0.5654	1.9306
ω(eV)	2.5989	2.3733
S(eV)	0.1923	0.2106
X(eV)	3.1644	4.3040
η(eV)	1.9264	3.9026

Molecular descriptors for Vasicol and Gallic acid are displayed in Table 1. From the table it is evident that electron removal ability for vasicol is slightly higher when compared with gallic acid with an energy difference of 0.9140eV. Electron affinity of both compounds seems to be varied one denoting that there will be energy change during removal of atom from the compound and here the difference is 1.3652eV. Here hardness of Vasicol is slightly higher when compared to that of Gallic acid with the difference of 0.2255eV and softness of difference 0.0182eV indicating higher higher degree of flexibility in terms of reaction for Gallic acid. Both compounds have electronegativity here with the difference is **0eV**, projecting the idea that they easily attract the invading radicals and scavenge them.

Electrophilicity index of two compounds doesn't show any major change reflecting a result that the two compounds act as donors rather than acceptors, which is a much essential quality of the antioxidant compounds.

3.5 Molecular Target Prediction Analysis

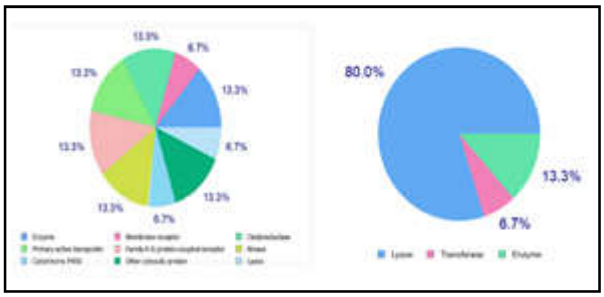

Vasicol **Gallic acid**

Fig.4 Target prediction analysis

Screening of suitable targets is an important step in the process of drug designing. Since, the studied compounds vasicol and gallic acid act as valid antioxidants, targets of their interest is essential here[12].

Hence target prediction analysis was done via SwissAdme online database which selected numerous targets for both the compounds where top 9 targets are selected here for interpretation(Fig.4). Vasicol prefers 9 targets out of 9 and gallic acid prefers 3 targets of out of 9. The above observed difference is making vasicol to be superior antioxidant than gallic acid in terms of target preference.

4. CONCLUSION

In today's medicine, study related to drugs derived from natural products has gained importance to explore their activity through theoretical analysis, followed by experimental investigation invitro/invivo. This method provides a platform to identify new potential drugs and revisit the activity of existing drugs against new targets. In this study a known antioxidant gallic acid is compared with vasicol, an alkaloid for its radical scavenging behaviour. Through FMO analysis, the energy gap between the occupied energy levels and unoccupied energy levels of vasicol and gallic acid found to be 1.648 eV and 1.738 eV which is of same order with minor variation. MEP analysis revealed that for both of the compounds the electropositive region is highly concentrated over –OH units which indicates their readiness in donating the electron. evident that electron removal ability for vasicol is slightly higher when compared with gallic acid with an energy difference of 0.9140eV. Target prediction analysis showed that vasicol prefers 9 targets out of 9 and gallic acid prefers 3 targets of out of 9. Theoretical studies indicate vasicol to be a better radical scavenger than gallic acid. Experimental investigation for the same is to be carried out to confirm the activity.

REFERENCES

[1] Veronique Seidel, "Plant-Derived Chemicals: A Source of Inspiration for New Drugs", Plants, Vol. 9, No.11, pp.1562.

[2] K Anbazhakan, R Praveena, K Sadasivam, Guillermo Salgado, Wilson Cardona, Lorena Gerli, Leonor Alvarado-Soto and Rodrigo Ramirez-Tagle, "Theoretical Insight on Structural Activities and Targets of Kaempferol Glycosides", Afnidad, Vol.78, No 594, 2021, pp.236-239.

[3] Jinrong Bai, Yunsen Zhang, Ce Tang, Ya Hou, Xiaopeng Ai, Xiaorui Chen, Yi Zhang, Xiaobo Wang and Xianli Meng, "Gallic acid: Pharmacological Activities and Molecular Mechanisms Involved in

Inflammation-related Diseases", Biomedicine & Pharmacotherapy, Vol.133, 2021, pp.110985.

[4] Yu Xu, Guoyi Tang, Cheng Zhang, Ning Wang and Yibin Feng, "Gallic Acid and Diabetes Mellitus: Its Association with Oxidative Stress", Molecules, Vol. 26, No.23, 2021, pp.7115.

[5] K.L. Dhar, M.P. Jain, S.K. Koul and C.K. Atal, " Vasicol, a New Alkaloid from Adhatoda Vasica", Phytochemistry, Vol .20, No.2, 1981, pp.319-321.

[6] Xin Fang , Hai-Yang Yu , Li-Feng Han and Xu Pang, " N-containing Compounds from Seeds of Paganum Harmala", National Library of Medicine, Vol. 44, No.8, pp.1601-1606.

[7] K Anbazhakan, R Praveena and K.Sadasivam, "Theoretical Insight on Antioxidant Potency of Eanzakiflavone-2 and its Derivatives", Structural Chemistry, Vol.32, 2021, pp.1451-1458.

[8] M. J. Frisch, G. W. Trucks, H. B. Schlegel, G. E. Scuseria, M. A. Robb, J. R. Cheeseman, G. Scalmani, V. Barone, G. A. Petersson, H. Nakatsuji, X. Li, M. Caricato, A. Marenich, J. Bloino, B. G. Janesko, R. Gomperts, B. Mennucci, H. P. Hratchian, Cossi, J. M. Millam, M. Klene, C. Adamo, R. Cammi, J. W. Ochterski, R. L. Martin, K. Morokuma, O. Farkas, J. B. Foresman, and D. J. Fox, Gaussian, Inc., Wallingford CT, 2016.

[9] R Praveena, K Anbazhakan, Lorena Gerli Candia, Daniel Glossman-Mitnik, Wilson Cardona, K Sadasivam and Guillermo Salgado," Theoretical Assessment of Antioxidant Property of Polyproponoid and its Derivatives", Structural Chemistry, Vol.31, 2020, pp.1089-1094.

[10] C. Lee, W. Yang, R.G. Parr, "Local Density Component of the Lee–Yang–Parr Correlation Energy Functional", The Journal of Chemical Physics, Vol.100, 1994.

[11] V. Deepha, R. Praveena and K. Sadasivam," DFT Studies on Antioxidant Mechanisms, Electronic Properties, Spectroscopic (FT-IR and UV) and NBO Analysis of C-glycosyl Flavone, An Isoorientin" , Journal of Molecular Structure, Vol.1082, 2015, pp.131-142.

[12] Rangasamy Praveena, Athinarayanan Balasankar, Kanakaraj Aruchamy, Taehwan Oh, Veerababu Polisetti, Subramaniyan Ramasundaram and Kandasamy Anbazhakan, "Structural Activity and HAD Inhibition Efficiency of Pelargonidin and Its Glucoside-A Theoretical Approach", Vol.27, No.22, 2022, pp.8016.

SIMULATION STUDY ON DESIGN OF SPACE JUNK COLLECTOR MECHANISM WITH CUBE-SATELLITE FOR ACTIVE DEBRIS REMOVAL IN LOW EARTH ORBIT (LEO)

M.S. Prasath, G. Sivaraj, D.Lakshmanan and P. Vadivelu
Department of Aeronautical Engineering,
Bannari Amman Institute of Technology, Sathyamangalam - 638 401, Erode District, Tamil Nadu
E-mail: prasathms@bitsathy.ac.in, sivarajg@bitsathy.ac.in

Abstract

Space debris is the man-made or natural debris developed in space as a consequence of satellite collision, human space activities, and many more. The growth of this debris around the planet is significantly increasing over the years and many research works are going on for space debris removal techniques as well as in the mitigation field. This paper will capitalize on the existing debris removal technologies and bring forth the idea of developing a systematic space debris collector for active space debris removal in the Low Earth Orbit (LEO). The fundamental objective of this research work is to develop a systematic space junk collector with a 1U CubeSat configuration for tracking and capturing the orbital debris. In this research work, CubeSat has been designed according to the 1U standard configuration and its details are also presented in this paper. The objective of this work is to collect the space debris after slowing them down with any of the feasible technologies such as laser ablation or gunshot technology and drop that captured debris into either the International Space Station (ISS) or orbital storage tank for recycling. From the deploying stage of the collector in the orbit to the dropping stage of the captured debris for the proposed model are discussed in this paper. The proposed model in this research could be very effective shortly for collecting and re-cycling the space junk.

Keywords: *CubeSat, Debris removal, Low Earth Orbit (LEO), Capture, P-POD and Ejection..*

1. INTRODUCTION

In the evolution of mankind, the Sputnik satellite launch was indeed a historical achievement. It was the first-ever man-made satellite that paved the path for space-age and human space activities. After the grand success of this Sputnik mission, space industries started to grow and expand quickly to accomplish many milestones and for the greater good of our planet[1]. Now in the modern world, satellite and space technology have a significant purpose by providing vital information and use such as worldwide communications, Weather forecasting, Defense and Military communications, Deep space exploration, and so on. With this immense development, there was a threatening aftermath that emerged and it is the development of space junk. Space debris is the man-made or natural detritus developed in space as a consequence of satellite collision, human space activities, and many more[11]. Now you may wonder what is this natural debris are and how it is formed[9]. These natural detritus can either be Metroid or Micro Metroid Orbital Debris (MMOD). The Micro-Metroid is the fragments or broken parts of an actual asteroid that will be originated inside our solar system. Micro Metroid Orbital Debris (MMOD) and the artificial space junk make the space-exposed parts of ISS, satellites, and spacecraft vulnerable.

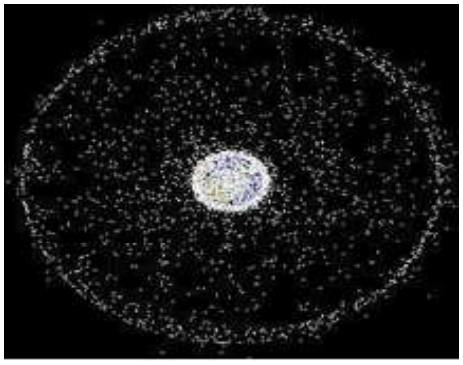

Fig.1 Space Debris Population From Outside The Geosynchronous Orbit Published By NASA

The International Space Station (ISS) in LEO periodically performing evasive maneuvers to get rid of orbiting space junk. When the orbital debris strikes the

subsystems of ISS such as solar arrays it will cause overheating damage to the entire subsystem[10]. The space debris population from outside the geosynchronous orbit published NASA is presented in Fig.1[3].

These threatening space junks are orbiting the planet at speed of around 18000 mph in vacuum space. And these space junk speeds will be comparatively lower in Low Earth Orbit (LEO) due to the effect of air drag force. The density of air in the Low Earth Orbit (LEO) is lower compared to sea level but it can make a huge impact on the dynamics of orbiting satellites and decrease its decay rate. Even for the astronauts the gloves and torso parts in the Extravehicular Mobility Unit (EMU), the space junk, and MMOD cause serious damage. From these data, we can clearly say that these space junk are very dangerous for satellites, spacecraft, astronauts, and ISS orbiting around the earth.

There are various ways to remove space debris, including active and passive approaches. Active approaches require the spacecraft's energy input to remove space junk. Passive approaches do not necessitate the spacecraft's energy input [20]. Departure from a functional orbit using its own propulsion system, braking, and deorbiting via the procedures listed below: Some of the active ways include capture and drag by other spacecraft, remote energy impact (laser or ion flow), and full or partial recycling [16]. Direct capture methods are classified as rigid or flexible. Several methods for flexible direct capture have been proposed, including nets, harpoons, and tentacles [17]. Significant progress has been made in proving many concepts related to approaches such as the collective method, laser-based method, IBS-based method, and tether-based method [18]. The most effective strategy is still under investigation. Recent ground and space tests of systems such as robot manipulators, harpoons, docking devices, electromagnetic capture, tether nets, and tether grippers have demonstrated their effectiveness and potential in space trash removal [19].

2. MODELLING THE CUBE-SAT DESIGN

In the digital era, the development of technology is at its peak. Our smart phones are way faster than the 1960s Apollo mission computer system.

In modern space applications, CubeSat plays a major role when it comes to focused objectives or missions [2]. Their construction cost and the miniature design have made them more useful for telecommunications and remote sensing. The CubeSat generally falls in the classification between Pico-satellite (< 1 Kg) and Nano-satellite 1kg to 10 kg) [12]. Our CubeSat design comes under one-unit standard 1U category specifying its dimensions as 10*10*10 cm, weight 1.33 kg, and volume 10 cm^3. This CubeSat design has represented in below the diagram along with its stand-off design. To fit in the subsystems inside this cube- satellite, the framework has also been designed.

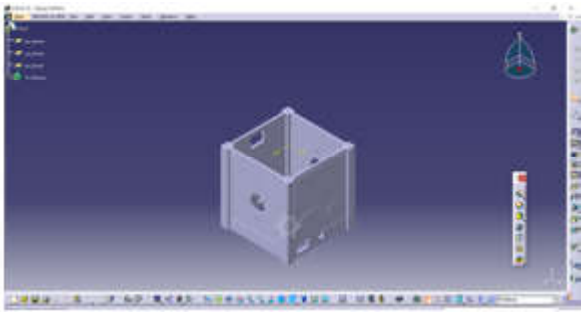

Fig.2 View of CubeSat Model

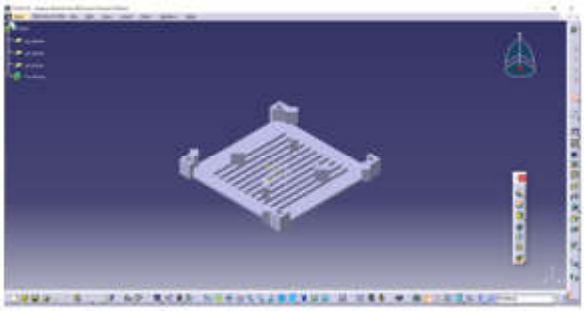

Fig.3 Front Plate - CubeSat

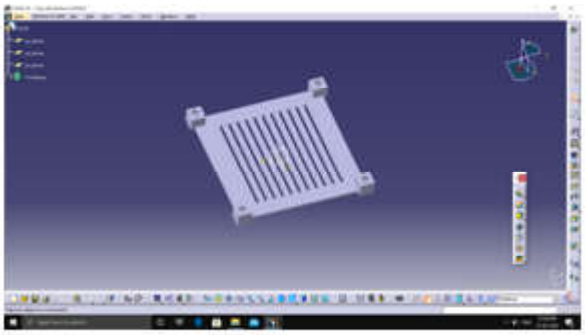

Fig. 4 Back Plate – CubeSat

3. MECHANISM OF DEPLOYMENT WITH COLLECTOR

Everyone will wonder how the cube satellite or Pico satellite can be deployed in the actual orbit. It can be deployed by using Poly-Pico Satellite orbital Deployer (P-POD) which isolates it from the primary vehicle and also act as an interface between the cube satellites and launch vehicle. It is a block of aluminum container which

is designed specifically to launch and deploy different configurations of cube satellites. The length and width (Square) of this P-POD are 40.64 and 12.7 cm respectively.

According to data published by United Launch Alliance (ULA), Cube-satellites can be deployed after the primary payload deployment (spacecraft separation) in the orbit. Initially, P-POD will be positioned inside the aft end of Centaur upper stage of the launch vehicle and with the help of the Aft-Bulkhead Carrier (ABC) plate, P-POD will come out of the launcher.

After this the launch vehicle sends an electrical signal to the P-POD which will, in turn, causes its door to open, and following that cube satellites will be ejected into the orbit.

3.1 Programming with IDE Platform

After the design module, the programming and calibration module for servos and other subsystems of the satellite was completed in the IDE platform. Embedded C language has been used in this platform. Before starting programming, the library function should be installed and pins should be connected to the apt ports. Initially, it was calibrated for a single sensor and a single servo, and then it was done by integrating all the subsystems of the systematic machine.

Final Code:

```
#include <ESP32Servo.h>
/* Comment this out to disable prints and save space */
#define BLYNK PRINT Serial
#include <WiFi.h>
#include <WiFiClient.h>
#include <BlynkSimpleEsp32.h>
#include<Ultrasonic.h>
int aO = 39;
int measurePin = 36;
int ledPower = 25;
int sensorValue;
int sensorValue;
unsigned int samplingTime = 280;
unsigned int deltaTime = 40;
unsigned int sleepTime = 9680;
float voMeasured = 0;
float calcVoltage = 0;
float dustDensity = 0;
ULtrasonie ultrasonic (18: 1.9) ;
int d;
char auth[] =
“lvJ4T15Fxmv3fklGcgr_ TOwelnYotELv”;
char ssid[] = “vivo 1818”;
char pass[] = “1234567890”;

Servo servol;
Servo servo2;
Servo servo3;
Servo servo4;
void setup ()
{
        Serial.begin(9600);
        Blynk.begin(auth, ssid, pass);
        pinMode (a0, OUTPUT) ;
        servol.attach(13);
        servo2.attach(12);
        servo3.attach(14);
        servo4.attach(15);
}
BLYNK_ WRITE (V1)
{ servol.write (param.asInt());}
BLYNK WRITE (V2)
{ servo2.write(param.asInt());}
BLYNK WRITE (V3)
```

```
{ servo3.write(param.asInt());}
BLYNK WRITE (V4)
{ servo4.write(param.asInt());}

void loop ()
{
Blynk.run();
d = ultrasonic.read();
Serial.print("Debris is at ");
Serial.print(d);
Serial.print(" cm distance");
Serial.printlin();
Blynk.virtualWrite(V5,qd) ;
int AQ = analogRead(a0);
Serial.print("Air Quality = ");
Serial.print (AQ);
Serial.printlin();
Blynk.virtualWrite(V6,AQ) ;
pinMode (ledPower, OUTPUT) ;
digitalWrite(ledPower, LOW) ;
delayMicroseconds (samplingTime) ;
voMeasured = analogRead(measurePin) ;
delayMicroseconds (deltaTime) ;
digitalWrite(ledPower, HIGH) ;
delayMicroseconds (sleepTime) ;
calcVoltage = voMeasured*(5.0/1024);

dustDensity = 0.17*calcVoltage-0.1;
if ( dustDensity < 0)
{
dustDensity = 0.00;
}
Serial.println("Raw Signal Value
(0-1023):");
Serial.println(voMeasured) ;
Serial.println("Voltage:");
Serial.println(calcVoltage) ;
Serial.println("Dust Density:");
Serial.printin(dustDensity) ;
delay(1000);
Blynk.virtualWrite (V7, voMeasured) ;
Blynk.virtualWrite(V8,calcVoltage) ;
Blynk.virtualWrite(V9,dustDensity) ;
Serial.println();
}
```

3.2 CUBE-SAT with 3D Printing Technology

The CAD models were fabricated using 3D printing technology. The Repetier-Host a 3D printing application and WOL 3D ender 3 models have been used for 3D printing. In the Repetier application import the model (Designed model saved as an STP file) by using the load option. The designed model will be imported and by using the object placement tool we can change the axis of the model in which it should be printed.

Fig. 5 Main body and frame structure of the cubesat

Fig.6 Front and back plate of the CubeSat

The parameters like the adhesion type, quality, support type, and infill density from the slicer option were assigned. At last, Cura engine option was used to get the details of the printing models such as printing time, axis, thickness, etc. Then the g-code file was saved to SD card, which will be inserted in the 3D printing.

4. DEVELOPMENT PROCESS OF SPACE DEBRIES COLLECTOR

Stage 1: Ejection into the orbit
Stage 2: Collector's arms open after the ejection stage
Stage 3: Targeting space debris
Stage 4: Moving closer to the targeted debris
Stage 5: Debris capture
Stage 6: Dropping the captured debris to ISS or storage tanks

Stage 1: Ejection into the Orbit

CubeSat is generally deployed by P-POD. This P-POD will be positioned inside the Aft-Bulkhead Carrier (ABC) system. For some launch vehicles, ABC uses the volume of Centaur aft bulkhead which was no longer in use after its propulsion tank. These ABCs will be placed at the aft end of Centaur's upper stage of the launch vehicle. With the help of a telescope and RADAR system, the movement of space junk can be predicted[6]. After predicting the suitable position and the orbit, the collector will be intended to deploy.

To deploy the collector safely, the launch vehicle sends an electrical signal to the P-POD which will in turn causes its door to open, and following that collector will be ejected into the orbit safely[7][8].

Fig.7 Ejection into the LEO

Stage 2: Collector's arms open after the ejection stage

Initially, the four arms of the collector will be closed to fit into the P-POD. Once the collector is ejected from the P-POD, the arms will be opened to predict the distance between the orbital debris and the collector through the Ultrasonic sensor in Low Earth Orbit[5]. Additional technologies such as the NanoFeep propulsion system can be incorporated into our collector to capture the debris sequentially[14].

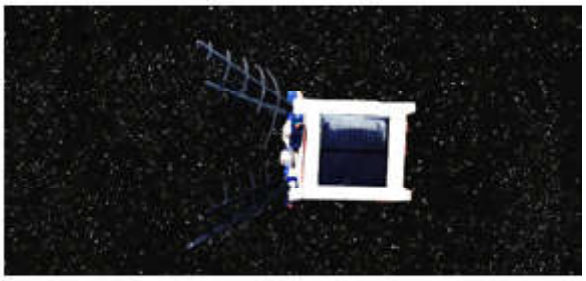

Fig.8 Collector's arms opening after deployment

Stage 3: Targeting Space Debris

The collector will attain the moment of debris from the telescope or RADAR system. In this case, to slow down the debris, laser ablation or gunshot technology can be utilized [3]. After that, with the help of an ultrasonic sensor and other subsystems of the collector, it could obtain the distance between the space debris from the collector and other parameters of the orbit. Subsequently, the debris near or around the storage tank or ISS will be targeted first [4].

Stage 4: Moving Closer to the Targeted Debris

In this stage, the collector will get aligned to the targeted debris and moves closer to it.

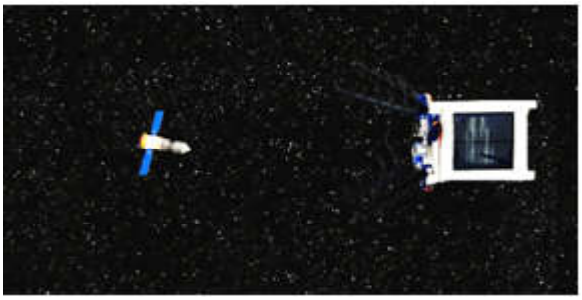

Fig. 9 Moving closer to the targeted debris

Stage 5: Debris Capture

After moving closer to the target, the collector will make the final approach to capture it[13]. When the debris enters the arms region, all the arms of the collector will be deflected at an instant to capture it. The number of targeted debris at one deflection depends on the orbital moment of space junk and its size [1].

Stage 6: Dropping the Captured Debris to ISS or Storage Tanks

After capturing the debris, it will be dropped either in an orbital storage tank or in International Space Station (ISS) for recycling. It can either be recycled for re-usable metal or as a raw material for 3D printing in ISS[15].

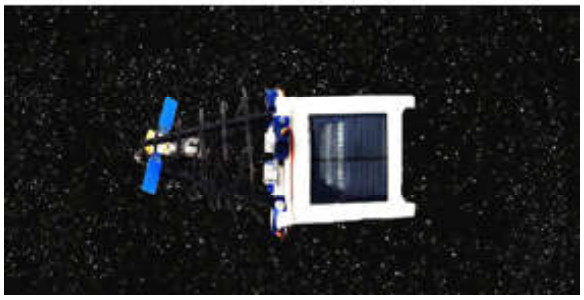

Fig.10 Debris capture

5. CONCLUSION

In this research work, a theoretical concept and the actual ground test was conducted for the developed space debris collector system. The deflecting arms were very effective and efficient in capturing space debris and they can collect the debris between two to ten centimeters in the Low Earth Orbit (LEO). There is an ample number of techniques proposed to remove the debris while re-entering the earth's atmosphere. In this paper, it is proposed to collect the orbital space junks and drop them into ISS or orbital storage tanks for recycling. After re-cycling, it can be used to develop the parts of satellites, subsystems of ISS, and space shuttle which in turn reduces the necessity of extracting the materials and also the cost of fabricating it. This developed debris collector can be upgraded and capitalized with existing techniques to remove the space debris from the planet and to prevent the Kessler Syndrome.

In conclusion, Space debris is a rising concern that endangers space missions and satellites. There are various methods for eliminating space debris, both active and passive. Recent ground and space tests of systems such as robot manipulators, harpoons, docking devices, electromagnetic capture, tether nets, and tether grippers have demonstrated their effectiveness and potential in space trash removal. The most effective strategy, however, is currently being investigated.

Future research should concentrate on establishing more efficient and cost-effective ways of space debris removal. Collaboration between governments, space agencies, and private enterprises will be required to create new technologies and tactics for clearing space debris. Because launching a satellite would costs more for an individual and it would be better if the cube-sat with the debris removal system can be collaborated with any of the above suggested organizations.

REFERENCES

[1] James L.Hyde, Eric L.Christiansen and Dana M .Lear, "Observations of MMOD Impact Damage to the ISS", International Orbital Debris Conference.

[2] T.A Aadithya, "Review Paper on Orbital Debris Mitigation and Removal and a New Model Insight", International Journal Of Electrical Electronics and Data communications.

[3] Shankar Bhattarai and Jie-Rou Shang, "Space Debris Removal Mechanism Using CubeSat With Gun Shot Facilities", American Journal Of Applied Science

[4] Sang H. Chol and Richard S.Pappa, "Assessment Study of Small Size space Debris Removal by Orbit-stationed Laser Satellites", Recent Patents on Space Technology.

[5] R.Lucken, N.Hubert and D. Giolito, "Systematic Space Debris Collection using CubeSat Constellation", 7th European Conference for Aeronautics and Aerospace Sciences (EUCASS).

[6] Christopher P.Clark, Dun Y.Tan, Patricia Arnal Luna, Daniel E. Hastings, Rebecca A. Masterson and Michael J. Richard, "Effectiveness of CubeSat-based Architectures for Active Removal of on-orbit Rocket Bodies", Accelerating Space Commerce, Exploration, and New Discovery Conference.

[7] Sherif A.M. Kamal, Ahmed Gaber and Farouk El-Baz, "An Integrated Design for Collecting and Recycling of Space Debris", Journal paper.

[8] Gaurav Kumar, "Removing and Tracking Orbital Debris with LASER", Removal and Tracking of Orbital Debris using Laser.

[9] Susan Samwel, "Effect of Air Drag Force on Low Earth Orbit Satellites during Maximum and Minimum Solar Activity", Space Research journal

[10] C. Pirat *et al.*, "Mission Design and GNC for in-orbit Demonstration of Active Debris Removal Technologies with Cubesats".

[11] Takahashi, Kazunori, *et al.* "Demonstrating a New Technology for Space Debris Removal Using A Bi-directional Plasma Thruster", Scientific Reports, Vol.8, No.1, 2018, pp. 14417.

[12] Zhang, Fan, *et al.,* "Dynamics Modeling and Model Selection of Space Debris Removal via the Tethered

Space Robot", Proceedings of the Institution of Mechanical Engineers, Part G: Journal of Aerospace Engineering, Vol. 231, No.10, 2017, pp. 1873-1897.

[13] Singh, Prabhat & Chand, Dharmahinder & Pal, Sourav & Mishra, Aadya. (2021). Study of Current Scenario & Removal Methods of Space Debris, Vol.10, pp.223-236.

[14] G. Feng, C. Zhang, H.Zhang and W.Li, "Theoretical and Experimental Investigation of Geomagnetic Energy Effect for LEO Debris Deorbiting", https://doi.org/10.3390/aerospace9090511, Aerospace, Vol.9 No.9, 2022, pp.511.

[15] P. Zhao, J. Liu and C.Wu, "Survey on Research and Development of On-orbit Active Debris Removal Methods", Sci. China Technol. Sci. Vol.63, 2020, pp.2188-2210.

[16] https://orbitaltoday.com/2022/03/30/space-debris-removal-importance-todays-methods-innovative-spacecrafts

[17] Zhao, Pengyuan & Liu, Jinguo & Wu and Chenchen, "Survey on Research and Development of On-orbit Active Debris Removal Methods", Science China Technological Sciences, Vol.63, 2020.

[18] C. Priyant Mark and Surekha Kamath, "Review of Active Space Debris Removal Methods", Space Policy, ISSN 0265-9646. Vol.47, 2019, pp.194-206.

[19] Hirohisa Kojima, Sajjad Keshtkar, Fumika Baba, Yuma Kato, Haruma Suzuki, Kaito Kosuge and Pavel M. Trivailo, "Design, Development, and Experiments of Novel Tether-Net Release Mechanism", Advances in Space Research, Vol.71, No.8, 2023, pp.3203-3221.

[20] Alexander S. Ledkov and Vladimir S. Aslanov, "Active Space Debris Removal by Ion Multi-Beam Shepherd Spacecraft", Acta Astronautica, Vol.205, 2023, pp.247-257.

INCREASING THE ROAD VISIBILITY OF AUTOMOBILE DRIVERS USING SMART HEAD LIGHT TECHNOLOGY

V. Vadivelvivek[1], T.C.R. Dinesh[2], T.S. Rakesh[3], M.C. Pravin[4], C. Boopathi[5] and K. Kamalakkannan[6]

[1,4&5]Bannari Amman Institute of Technology, Sathyamangalam - 638401, Erode District, Tamil Nadu

[2]Vellalar College of Engineering and Technology, Erode - 638012, Erode District, Tamil Nadu

[3]Nirmala Institute of Technology, Thrissur - 680311, Kerala

[6]Surya Engineering College, Erode - 638107, Erode District, Tamil Nadu

E-mail: vadivel.vivek@gmail.com

Abstract

The main objective of this study is to prevent accidents that occur at night due to poor lighting conditions. Around 63% of accidents happening at night are due to pedestrians, animals and improper road conditions. This study aims to improve the visibility at night time by developing a simple, smart headlight system that is linked to headlight arrangement. The main components used in this study are LDR (light dependent resistors) sensor, ultrasonic sensor, LED (light emitting diode), voltage protection module. The major function of LDR sensor is to observe the external lights from the vehicle and environment. The opposite vehicle is detected by the ultrasonic sensor and it sends the signal to microcontroller which processes the signal and reduces the intensity of the LED light automatically, because of that visibility of the automobile driver will increase. This mechanism is connected to an automobile's headlight in turn the vehicle's headlight intensity is controlled, which eliminates manual headlight switching and replaces it with automatic headlight switching. Using the external environment light conditions the intensity of the light will be adjusted. It is economical to implement this work in all type of vehicles and the operation is simple with no maintenance.

Keywords: *Accidents, Automobiles, Headlights, LDR sensor, LED lights, Visibility*

1. INTRODUCTION

The traditional headlight system is not suitable for present traffic and road conditions. Hence there is a requirement to develop a system which automatically controls the intensity of the head light. Recent literature also shows that developing an automatic headlight system is possible and it will increases the visibility of drivers during night time.

The Aslam Musthafa R *et al* (2018) developed a self-adjusting headlight beam controller. It observe the opposite vehicle light intensity, according to light intensity and it will switch the light into low beam to avoid the glare in mirror to drive safely in night, so automatic switches are provided here for controlling the high beam of the light to low beam to avoid the accidents [1].

Abdul Kader Riyaz M *et al* (2016) manufactured a new type of LED with graphene coat that is used for street light. The advantage of this light is that the heat produced by the light will decrease automatically. The graphene coated light is used as a street light because the street light is producing high intensity output. For increasing the life span of the light, the heat of light need to be reduced. So they have controlled the light using arduino. They have developed an LED capable for a head sink using arduino micro controller to automatically control the light [2].

Pablo Fernandez *et al.* made a system that employs a camera to detect a vehicle approaching from the opposite side at night. They have used a self-adjusting headlight beam controller, it will observe the opposite vehicles light intensity, according to that light intensity it will switch the light into low beam to avoid the glare in mirror to drive safely at night. To avoid glares, it will also modulate the headlight between low and high brightness [3].

N Keerthi *et al.* presented an economical, electricity automated headlight regulator for the traffic density on the roadways. According to their study, halogen bulbs are used in automobiles which is integrated with manual switches. It consumes more power but gives less output and also it does not focus on the road so it difficult to

drive. Low beam and high beam lights are utilized for different situations that affects the driving on the road [4].

C K Chan *et al.* used the simulation model to evaluate the function of various sections of the advanced headlight system, before developing a physical model. Because this sensor is light-dependent, the primary function of the LDR sensor is to examine the external lights from the vehicle and the surroundings. The ultrasonic sensor detects the opposing car and provides a signal to the microprocessor, which interprets the signal and automatically adjusts the intensity of the LED light, allowing the driver to see more clearly [5].

Padmavathi. S *et al.* reviewed the traffic surveillance systems, the primary idea of their work is to prevent night time accidents caused by poor lighting [6].

Mohamed taha *et al.* provided a robust and adaptable detection technique using automatic thresholding approach. The proposed system has the capability to track the vehicles by detecting the vehicles head lights and/or rear lights and it functions well in night light conditions [7].

Hyungiun Kim *et al.* employed background extraction and automatic vanishing point detection process for traffic surveillance. They have used a single video camera to operate and detect the vanishing point during day time. [8]

Neelima *et al.* focused on the night time traffic surveillance using available cameras in the road to analyse the traffic and to record the traffic scenes, the developed system is proven to be robust in traffic surveillance [9]. Raja et al focused on reducing the number of accidents by developing a multi beam LED head lamp employing image processing. The brightness of the multi beam LED head lamp is automatically adjusted by detecting the approaching vehicle using image processing technique [10].

The main objective of this study is to build a smart head light technology for better nighttime visibility. An attempt is made to design and create a simple smart headlamp system that is related to headlight arrangement, which uses a gamma correction to mitigate the influence of headlight.

2. MATERIALS AND METHODS

The list of components used in this work are given in the table 1 below

Table 1 List of Components

Sl. No	Component	Specification
1	LDR Sensor	Liner type light emitting diode
2	LED	12V, 900LM
3	LED controller	Adjustable current and voltage
4	Microcontroller	Arduino uno r3
5	Voltage protection module	Dc-dc step down SMPS
6	Ultrasonic sensor	High frequency type

The major components of this work are presented the figure1 below.

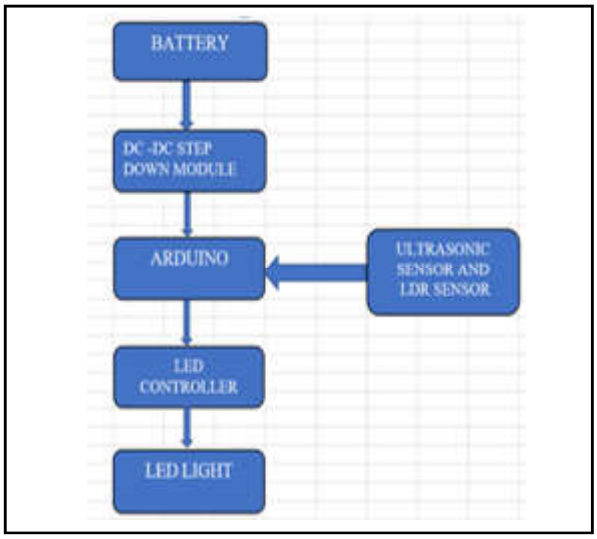

3. COMPONENTS USED

3.1 LDR Sensor

Light dependent resistors (LDR) shown in figure 2, also known as photo resistors are used in electronic circuit to detect the presence or level of light condition, and they also called as photo cell or photoconductor. This kind of sensor works on surround lighting condition. When the surrounding light will decrease the sensor output voltage will increases but the lighting will increase around the LDR sensor, the output voltage automatically decreases. and also, the sensor functions the around voltage between 1volt to 5volt. they provide a significant change in resistance in response to changes in light level.

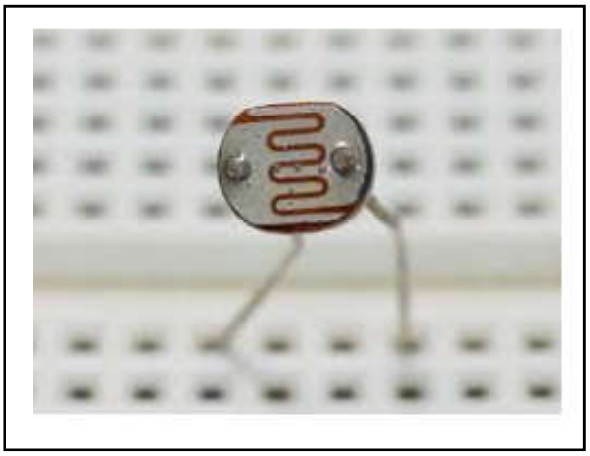

Fig.2 LDR Sensor

3.2 LED

LED (light emitting diode) lighting products produces lighting up to 88% more efficiently and consumes less power compared to halogen bulbs. By varying the voltage, the brightness of the light also increases and decreases, when power supply passes through the LED. The energy is produced in the form of photons in the semiconductor by electrons recombination in electron hole. The color of the light is determined by the amount of energy required by the electrons to pass through the semiconductor band gap. White light is produced by using number of semiconductors or using a light emitting phosphor coating on the semiconductor device.

3.3 LED Controller

Led controller shown in figure 3 is a common type of dimming used to adjust the current in white led driver devices. Controller takes a rectangular waveform with variable positive duty cycle and adjustable led current proportionally.

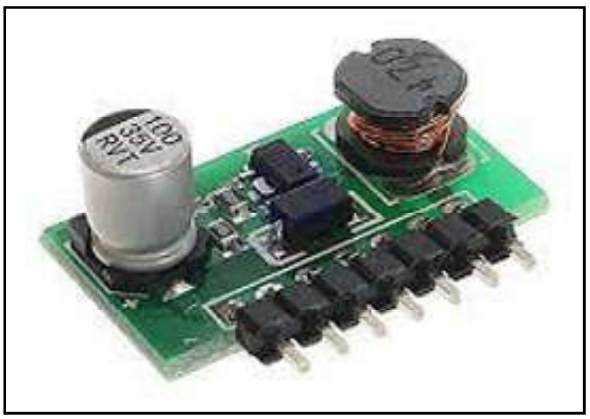

Fig.3 LED controller

3.4 Resistor

A resistor, shown in figure 4 is a device with electrical resistance that is used to safeguard, operate, or control current in an electric circuit.

Fig.4 Resistor

3.5 Arduino

Arduino, shown in figure 5 is a device that can be controlled with an open source programming. In this work atmega2560-16au board is used in order to give i/o lines. Arduino consists of USB connection, 54 digital I/O terminals, 16 analog inputs and a 16 MHz crystal oscillator. It controls all the electronic components depending on the required application.

Fig.5 Arduino

3.6 Voltage Protection Module

Voltage protection module, shown in figure 6 is also known as buck convertor or step-down converter. The power is stored in the battery as light requires less amount of power, in case of using total amount of power for the light, light will bust. Hence we have to reduce the output power supply from the battery with the help of voltage protection module. It converts the step down voltage from its input supply (battery) to its output while drawing required voltage.

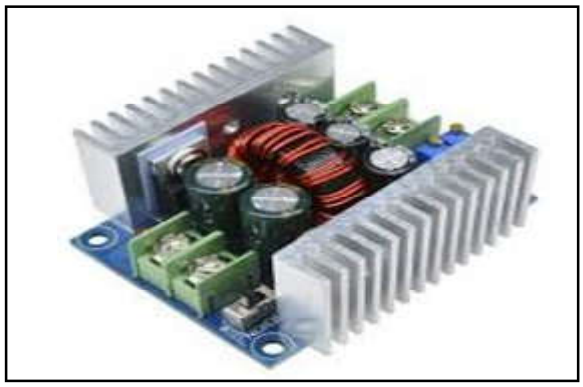

Fig.6 Voltage protection module

3.7 Ultrasonic sensor

Ultrasonic sensor, shown in figure 7 is an object finding sensor. The sensor works using the sound waves above the human hearing range. The microphone acts as the transducer. Optical method may fail but ultrasonic sensors are a trustworthy solution for detecting translucent things.

Fig.7 Ultrasonic sensor

3.8 Zero PCB

A Zero PCB, shown in figure 8 is a general-purpose printed circuit board (PCB), also known as pre board or DOT PCB. It is a thin, inflexible copper sheet with 2.54 mm spacing holes pre-drilled at regular intervals throughout a grid (0.1 inch).

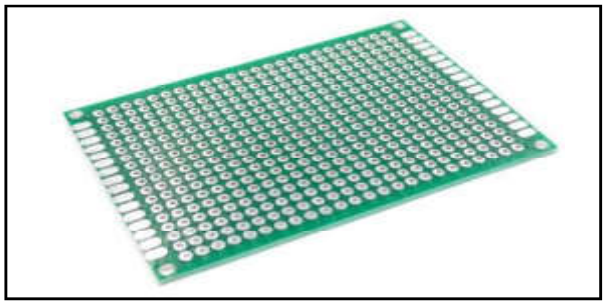

Fig.8 Zero PCB

3.9 Soldering Station

A soldering station, shown in figure8 is a power soldering device that can be used to solder electrical components. The most popular uses for this type of equipment are electronics and electrical engineering.

Fig.9 Soldering station

4. RESULTS AND DISCUSSION

4.1 Source Code and Simulation

The source code and simulation of the developed circuit is shown in the figure 9 below.

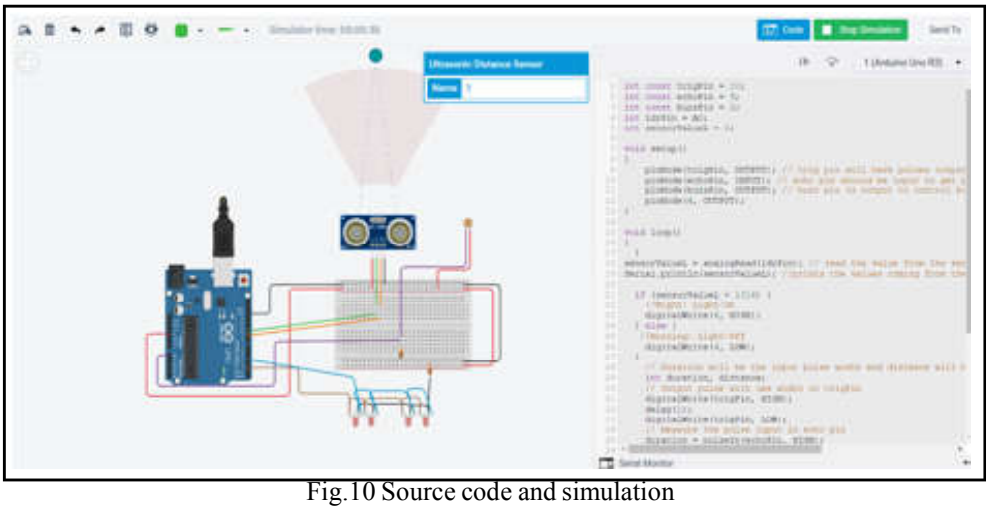

Fig.10 Source code and simulation

The source code used for the developed circuit is given below

```
int const trigPin = 10;
int const echoPin = 9;
int const buzzPin = 2;
int ldrPin = A0;
int sensorValueL = 0;

void setup()
{
        pinMode(trigPin, OUTPUT);
        pinMode(echoPin, INPUT);
        pinMode(buzzPin, OUTPUT);
        pinMode(4, OUTPUT);
}

void loop()
{
 {
sensorValueL = analogRead(ldrPin);
Serial.println(sensorValueL);

 if (sensorValueL < 1014) {
  Night: Light-On
 digitalWrite(4, HIGH);
 } else {
  Morning: Light-Off
  digitalWrite(4, LOW);
 }
```

Duration will be the input pulse width and distance will be the distane to the obstacle in entimeters

```
    int duration, distance;
    Output pulse with 1ms width on trigPin
    digitalWrite(trigPin, HIGH);
    delay(1);
    digitalWrite(trigPin, LOW);
    Measure the pulse input in echo pin
    duration = pulseIn(echoPin, HIGH);
    Distance is half the duration devided by 29.1 (from datasheet)
    distance = (duration/2) / 29.1;
    if distance less than 0.5 meter and more than 0 (0 or less means over range)
if (distance <= 320 && distance >= 0) {
    Buzz
    digitalWrite(buzzPin, HIGH);
} else {
    Don't buzz
    digitalWrite(buzzPin, LOW);
}
Waiting 60 ms won't hurt any one
delay(60);
}
}
```

4.2 Working Principle

The function of LDR sensor is to observe the external light from the vehicle. First the LDR sensor detects the external light and sends the signal to the arduino. Then the arduino process the signal from the LDR and activates the voltage driver, in turn the voltage driver decreases the voltage, as a result the intensity of the LED is reduced. The function of the ultrasonic sensor is to sensing the vehicle nearing and it send the signal to the arduino. The arduino process the received signal and makes the LED dim or bright according to the data received. Ultrasonic sensor also detects the vehicle, pedestrians, etc. and sends the signal to arduino to increase the intensity of the light with the help of LED controller.

5. CONCLUSION

By automatically adjusting the brightness based on exterior lighting changes, we were able to extend the life of the headlight, potentially saving battery life. All difficulties with headlights, whether they occur at night or during adverse weather, will be solved by the suggested model and components. The proposed components are also fairly affordable when compared to existing premium car components. As a result, cars in the economy sector can utilize this. Previous research used a manual headlamp system with an automatic headlight system. We anticipate to see more road vehicles with smart headlight technology in serial production in the future.

REFERENCES

[1] R.Aslam Musthafa, T.Bala Krishnan, N.Seetha Raman, M.Shankar and R.Swathi, "Automatic Headlight Beam Controller", International Journal of Trend in Research and Development (IJTRD) 15th March 2017.

[2] M.Abdul Kader Riyaz, S.ArunJeyakumar, M.AbdulHameedSharik and A.Tamilarasi ,"Graphene Coated LED based Automatic Street Lighting System using Arduino Microcontroller", IEEE Internationl Conference on Power, Control, Signals and Instrumentation Engineering (ICPCSI-2017).

[3] P.F. Alcantarilla, L.M. Bergasa, P. Jiménez, I. Parra, D.F.Llorca, M.A.Sotelo and S.S.Mayoral, "Automatic LightBeam Controller for Driver Assistance", Machine Vision and Applications DOI 10.1007/s00138-011-0327-2011.

[4] N Keerthi, Venkat Ajay Kumar and Deepthi, "Design and Fabrication of Solar Powered Automatic Headlight Brightness Controller", Managers Journal on Mechanical Engineering, Vol.5. No.2, FebruaryApril 2015.

[5] C.K.Chan, K.W.E.Cheng and S.L.Ho, "Development of Packaging and Electrical Interfacing for Electrical Vehicles", Proc PESA '06, Vol.24, Nov.2006. pp.234.

[6] K.Gunasekaran and S.Padmavathi "Night Time Vehicle Tracking for Live Time Traffic Surveillance Systems: A Review", International Journal of Computer Technology & Software Products, Vol.6, 2014.

[7] Mohamed Taha, H. Zayed, T. Nazmy and M. E. Khalifa, "Multi Objects Tracking in Nighttime Traffic Scenes
ICIT 2015, The 7th International Conference on Information Technology, doi:10.15849/icit.2015.0002.2015.

[8] Hyungjun Kim, "Vehicle Detection and Speed Estimation for Automated Traffic Surveillance Systems at Night Time", Technical Gazette, Vol.26, No.1, 2019, pp.87-94.

[9] D.Neelima, Gowtham Mamidisetti, "A Computer Vision Model for Vehicle Detection in Traffic Surveillance", International Journal of Engineering Science & Advanced Technology,Vol.2, No.5, 2012, pp.1203-1209.

[10] Rajas S Pandharkar, Rajiv Sharma, Samruddhi Naik, A. Thomas, U.Tushar Chaudhari, "Smart LED Headlights using IP", International Journal for Research in Engineering Application & Management (IJREAM), Vol.03, No.02, Apr 2017, pp.2454-9150.

REMOVAL OF NICKEL2+ IONS FROM POLLUTED AQUEOUS SYSTEM USING NATURALLY OCCURRING BIO SORBENT

C. Kavitha
Department of Chemistry,
Bannari Amman Institute of Technology, Sathyamangalam - 638 401, Erode District, Tamil Nadu
E-mail:ckaviuvaraja@gmail.com

Abstract

Nickel (II) ions are one among the highly harmful pollutants in quite a few industrial discharges being discharged into the surroundings as industrial wastes, originating serious soil and water pollution. Nickel can exist in more than a few valence states. In aquatic stream, nickel probably complexes with high affinity for soil by organic matter giving soluble and insoluble compounds, which are having ill effects on living organisms. Most probably the part which is not complexed with organic matter exists in soil solutions predominantly as divalent cations. The scope of this work is to observe the removal of nickel ions from water systems by means of cotton seeds. Batch investigational studies were accomplished to assess the optimum conditions for Ni2+ removal by modifying relevant controlling factors such as initial pH of solution and dosage of adsorbent used. The absorbance measurements were carried out on a Systronics UV-Visible spectrophotometer with 1 cm matched quartz cells. The pH of buffer solutions was monitored by using Systronic digital pH meter (India). From the absorbance measurements, the optimum pH for removal of Ni2+ ions are found to be between 4 – 7 at the dosage of 50 mg of cotton seed adsorbent allowed at an equilibration time of 5 hours. At pH 7, the amount of adsorbent is optimized and found to be 50 mg / 100 ml solution containing Ni2+ ions for effective removal up to 90 %. Also, based on the investigational results, it can be concluded that cotton seed has the greater probability of application as a competent adsorbent for the elimination of heavy metals from aqueous solutions. Also the extent of removal can be effectively studied using spectrometer.

Keywords: *Absorbents, Cotton seeds, Nickel (II), Spectrophotometer*

1. INTRODUCTION

Water is the most indispensable component to all forms of life. It also serves as a medium, catalyst and participant in all the chemical reactions occurring in our environment. In nature a number of regulatory mechanism plays an important role in controlling the physic-chemical properties of water as well as the number and types of its biological population. Irrespective of origin, it always contains a complex mixture of organic and inorganic substances, most of which are of natural origin resulting from complex interaction between water, soil and underlying geological strata and from complex biological and micro biological processes occurring in soil and water.

The dissolved inorganics, on the other hand, usually range between 50 – 500 mg /L although in some arid region water containing more than 1500 mg / L is consumed. The dissolved species is mostly the bicarbonates, chlorides and sulphates of calcium and magnesium, normally with lower concentrations of sodium and potassium ions. Other elements constitute the remaining.

Certain distinctions can be made concerning the cationic constituents present in natural waters. Those cations that are abundant in marine or fresh water habitats are required to perform certain key biological functions like ionic strength to the blood and the other body fluids are depositing as the salts for the formation of bones and shells. Among these are Ca^{2+}, Mg^{2+}, Na^{+} and K^{+}. A few ions that are present in trace levels like Mn^{2+}, Co^{2+}, Cu^{2+}, Zn^{2+}, Fe^{2+} etc., are useful to catalyze biochemical reactions and to participate in oxidation-reduction reactions in biological systems. As excess amount of these ions, however can exert some adverse effects. Certain other metal ions like Cd^{2+}, Hg^{2+}, Pb^{2+}, Be^{2+}, Ag^{+} etc., can exert toxic effect even at quite low concentrations, because human beings and other species have little or natural defense against them.

There are several other inorganic constituents of water that have been a subject of concern in recent years.

Endemic fluorosis is prevalent in some parts of the world due to the intake of excess of fluorides present in ground water. An extensive study of this element has been carried out by the World Health Organization (WHO) [1].

Hence it is rarely possible to find a source of water that is completely free from damage of pollution. Industries continue to increase its use of diverse range of potentially hazardous substances. Many of which very often find their way into water body meant for human consumption. The toxic species, when once released into the aquatic system, may continue to cycle between the sediments, water and biota for several years before flushed from the system. For example, it is reported that approximately 5000 years will be required for mercury presently stored in lake St.Clair eco system in United States to effectively flush out by natural process [2]. Similarly, the small amounts of mercury released over three decades of age in to the river system has kept it contaminated to the present time with sediment mercury levels exceeding 240 mg / L in some places [3]. Many examples sufficiently illustrate that decontamination is an impossible task [4-10]. In view of this and the possibility of serious threat to public health arising due to biological amplification, prevention rather than cure is by far the most effective policy in dealing with pollution. Nickel is used most expansively in nickel plating and alloy manufacturing. The current users of nickel include nuclear power plants, gas turbine engine, cryogenic containers and pollution abatement equipment [11, 12] Acute nickel poisoning causes dizziness, headache, nausea and vomiting, chest pain, dry cough and shortness of breath, rapid respiration, cyanosis and extreme weakness [13]. The harmful effects of Ni^{2+} necessitates its removal from wastewater before releasing into the streams.

1.1 Wastewater Treatment Methods

Many waste water treatment practices are available for tackling the problems associated with heavy metals removal. Normally any waste water is first treated in conventional primary and secondary processes to remove most of the settleable solids and the organics. The tertiary treatment is usually a polishing procedure by which pathogens as well as phosphates can be removed.

For heavy metal removal physio-chemical treatment method is usually applied. Almost all industries discharge wastewater at some stage of the manufacturing processes. The range of industrial effluents is very wide. Examples are paper mill, diary waste, tannery waste, vegetable and home tanning, distilleries and oil refineries. Since there are numerous types of industries dealing with various metals and their compounds, a number of specialized processes have been developed for the removal of heavy metals from waste discharge.

Some of the unit operations include chemical precipitation, coagulation or flocculation, ion exchange & solvent extraction, complexation, electro chemical operations, biological methods, adsorption & evaporation etc.,

Adsorption is the accumulation of a substance at the interphase between two substances. In water purification techniques, adsorbents are used to remove organic impurities which are non-biodegradable or organic compounds associated with taste, odour and colour. Even though activated carbon is extensively used for final polishing of the effluents, in recent times it is extensively used as a primary technique to remove soluble organics from waste water.

Many inorganic and organic materials have been applied as commercial adsorbents for wastewater treatment purposes. These commercial adsorbents generally have a large surface area per unit mass. Some of the common industrial adsorbents used for fluids include silica gel, activated alumina, molecular sieves, activated carbon, etc., Among the various solid adsorbents, activated carbon finds a prominent place in water treatment purposes [14]. In industrial applications concerned with waste water treatment both powdered and granular carbons are used.

For inorganics removal, the coal waste activated carbon is normally used. AMCOPX-21 has been successfully applied for the removal of Barium at pH 9.0 in the powdered form and found to remove 70%. However other varieties of carbon such as Darco HDB and Buchar Aqua showed 1% removal only [15]. Experiments with powdered activated carbon AMCOPX-21 and Darco HDB, the removal of Cd from water containing 0.5 mg/L at pH = 9.0, were found to be doubled. Lead removal from river water containing 0.15 mg / L at pH = 7.3 to 7.4 with powdered activated carbon showed 89% removal, when the carbon was 100 mg / L and 98% removal was achieved using 200 mg / L of carbon. Experiments with the use of granular activated carbon, Filtrasorb 200, the removal of Mercury in the concentration range of 0.02 – 0.03 mg / L concluded

that almost 80% of inorganic and organic mercury were removed [16-20].

1.2 Aim and Scope of the Work

Many methods are available for the treatment of heavy metals from aqueous systems. Among the various methods, precipitation by suitable precipitating agents such as lime, NaOH, Na_2CO_3 etc., have been practiced widely. However, enormous volumes of sludge produced by these precipitating agents pose disposal problems. Ion exchange methods using different types of cationic exchangers require critical control of pH and also very expensive in regenerance. Adsorption technique seems to be a less important process in the sense; suitable adsorbents will have to be developed, for the specific removal of metal ions. In this connection, various mineral adsorbents, activated carbons, biosorbents and modified biosorbents had been extensively used for the elimination of heavy metals from aqueous region. In this connection a modified biosorbents is to be tried for the removal of a toxic metal namely Nickel from water / wastewater.

The biosorbents proposed to be used for the given study is Cotton seed. This particular biosorbents is modified by soaking it in a suitable ligand namely urea. The Urea Loaded Cotton Seed (UCS) is used to study the adsorption behavior with respect to the removal of Ni^{2+} from water and wastewater.

2. MATERIALS AND METHOD

2.1 Batch Experiments

Batch experiments were conducted in polythene bottles of 300 mL capacity provided with screw caps. These polythene bottles washed well before and after use. 100 mL of the solution containing 10 mg/L of ions (Ni^{2+}) under investigation were taken in the bottles. After the addition of Urea loaded Cotton Seed (UCS), the bottles were equilibrated for specific periods of time in a horizontal mechanical shaker. At the end of equilibration time, the solutions were decanted and the concentrations of the ions are established by spectrophotometry.

2.2 Analytical Procedure – Determination of Nickel

Appropriate volumes of nickel working solution covering the range up to 100 µg are filled into a series of 50 mL volumetric flasks (or 50 mL Nessler tubes). A 50 mL volumetric flask containing none (Ni^{2+} ion) is used as a blank. A suitable aliquot of the sample containing not more than 100 µg is placed in a 50 mL volumetric flask. If the sample contains organic matter, it must first be destroyed by acid digestion. Then, aliquot of the digested sample has to be neutralized and taken in the volumetric flask. If the sample contains small amounts of iron, manganese and copper, it may be determined directly as they will not interfere. If it contains excessive amounts, a separate procedure has to be adopted.

To the blank, standards and sample add 20 mL of 0.5 n HCl is added. Then the following reagents are added in order with mixing after each addition,

- 10 mL sodium citrate solution
- 2 mL iodine solution
- 4 mL dimethyl glyoxine solution

The solutions are made up to 50 mL using distilled water and allowed to stand for 20 minutes. The colour is compared visually or potentiometrically using a spectrophotometer at 470 nm or filter photometer with a suitable blue filter taking water as reference. A calibration graph is prepared and from the graph mg of nickel equivalent to the observed optical density is found.

2.3 Preparation of Urea loaded Cotton Seed

The cotton seed were procured from M/s Govt. seed farm – Danishpet and are washed quite a lot of times with distilled water to remove any soil impurity and dried. About 100 g of this dried cotton seed was soaked in 1% solution of Urea for 24 hours. At the end of the drenching period, the cotton seeds were washed several times using water to remove urea and finally dried. This Urea loaded Cotton Seeds (UCS) were then used for the experimental conditions.

3. EXPERIMENTAL DETAILS AND RESULTS ON NICKEL (II) REMOVAL

3.1 Batch Studies

Batch experiments are executed to determine various limitations for the elimination of Ni^{2+} from aqueous solution. Trials were conducted with 100 mL solution including 10 mg of Ni^{2+} per litre, attuned to pH range 2-10 contained in300 mL stoppered bottle. After adding requisite amount of Urea loaded Cotton Seed (UCS), the solutions were equilibrated with the help of a mechanical shaker. The equilibrated solutions were filtered using G_3 crucible if necessary and the amount of Ni^{2+} there in the solutions were determined by DMG method using spectrophotometer. From these data Ni^{2+} adsorbed by the UCS were established.

3.2 Effect of Equilibration Time

In order to find out the optimum equilibrium time required for a maximum removal of Ni^{2+} from aqueous solutions, experiments were carried out using 50 mg of UCS and 100 mL of Ni^{2+} solution of 10 mg/ L at pH 6-7. The solutions were equilibrated for various periods of time. Finally, the solutions were investigated and Ni^{2+} removal was recognized. The results are shown in figure 1.

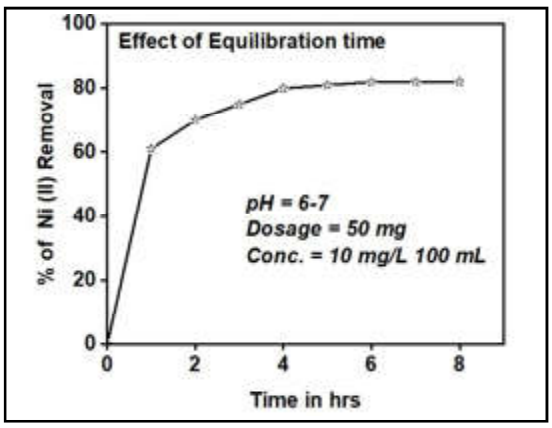

Fig.1 Effect of Equilibration time

It could be seen from the graph that a minimum of 4 hours of equilibration time is required for the utmost removal of 75-80%. However, for practical considerations, it was decisive to continue an equilibration time of 5 hours for subsequent experiments.

3.3 Effect of pH

The optimum pH required for the maximum removal of Ni^{2+} was identified using experiments done with 100 mL of 10 mg of Ni^{2+} per litre, adjusted to various pH conditions ranging from 1.0 to 10.0. About 50 mg of UCS was added into these solutions and equilibrated for 5 hours. Finally, the solutions were analyzed for Ni^{2+} removal under various pH conditions and recorded as figure 2.

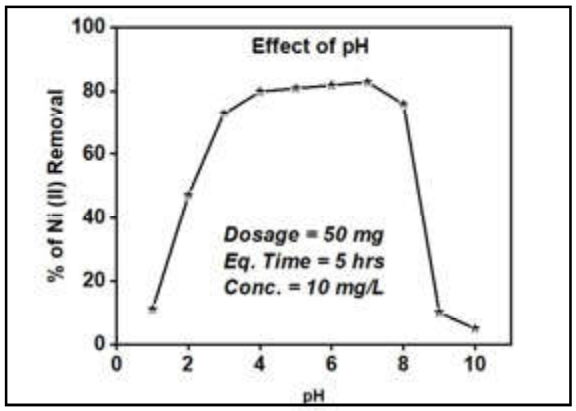

Fig. 2. Effect of pH on % removal of Ni^{2+}

The above figure clearly indicates that over the pH range of 4-8, the average Ni^{2+} removal was found to be 88%.

3.4 Effect of UCS Dosage Under Different pH Conditions

Batch experiments were conducted to obtain the optimum UCS dosage required for maximum percentage removal of Ni^{2+} over the pH range of 2-9. Experiments were conducted with 100 mL of Ni^{2+} solution containing of 10 mg of Ni^{2+} per litre. UCS dosages in the range of 50-400 mg / 100 mL were added to these solutions. Each of these bottles was adjusted with pH conditions ranging from 2.0-9.0 and kept for 5 hours. At the end of the prescribed equilibration time, solutions were investigated for Ni^{2+} content and the same was recorded in figures 3 and 4.

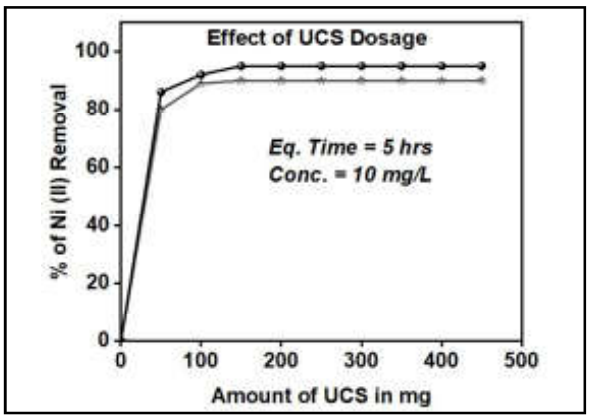

Fig.3 Effect of UCS dosage on % removal of Ni^{2+} at pH 7 and 5

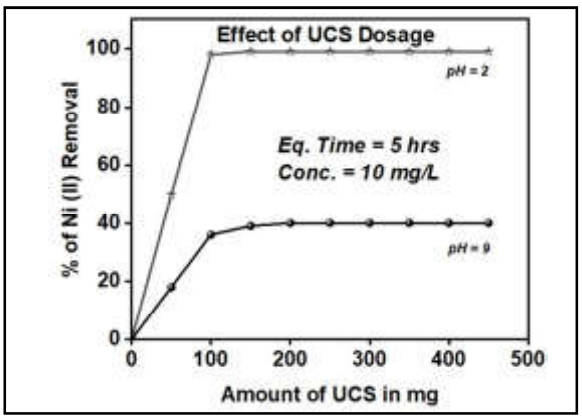

Fig.4. Effect of UCS dosage on % removal of Ni^{2+} at pH 2 and 9

It is clearly evident from the figures 3 and 4 that at pH 2.0, a minimum of 100 mg of UCS was required for the maximum removal of Ni^{2+} viz., 99.9%. However, at pH 5.0 a minimum of 150 mg of UCS was required for 95% removal and at pH 7.0 the same 150 mg of UCS

removed 98-99%. But at pH 9.0, the minimum dosage required boosted up to 200 mg for the maximum removal of only 42-45%.

3.5 Effect of Ni^{2+} Concentration on UCS Dosage

The optimum UCS required under different Ni^{2+} concentrations were also studied. Experiments were done with Ni^{2+} concentrations ranging from 20-50 mg / L, adjusted to a pH of 7.0. UCS dosages were added in the range 50 to 400 mg per 100 mL and the Ni^{2+} containing solutions were kept for a period of 5 hours. At last, the percentage of Ni^{2+} removal was determined and the results were exhibited as figures 5 and 6.

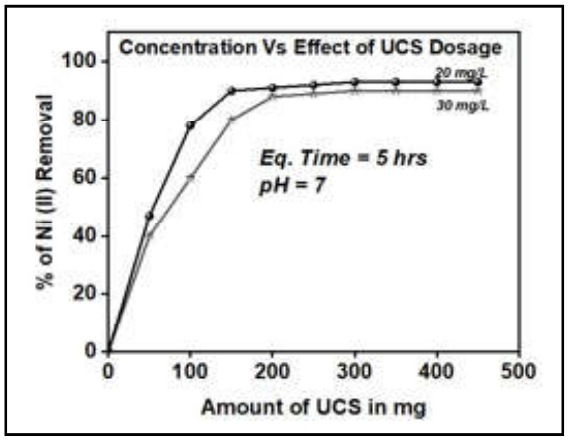

Fig.5. Effect of concentration Vs UCS dosage on % removal of Ni^{2+}

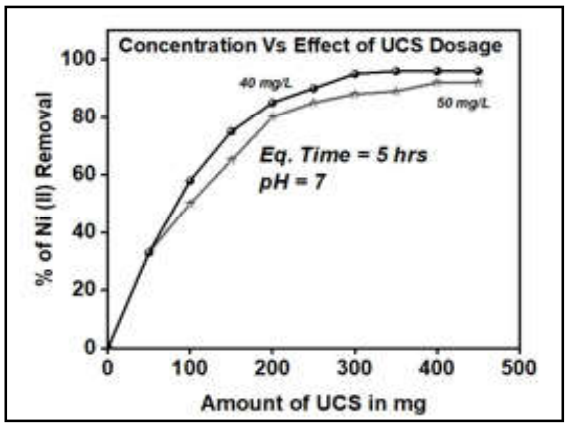

Fig.6. Effect of concentration Vs UCS dosage on % removal of Ni^{2+}

It could be seen from the figures, that a minimum of 250 mg of UCS was required for a maximum removal of 95% from 20 mg / L Ni^{2+} solution and 94% from 30 mg / L solution. A minimum of 350 mg and 300 mg of UCS was required for a maximum removal of 94% and 91% from 40 mg / L and 50 mg / L Ni^{2+} solutions respectively. It is thus clearly understood that, as the concentration of Ni^{2+} increases, the UCS dosage required for maximum percentage removal also increases.

4. CONCLUSION

As a result of extensive study on the effect of UCS on Ni^{2+} removal from aqueous medium, the following conclusion were derived,

- An effective ecofriendly biosorbents is developed for Ni^{2+} removal.
- UCS is found to be more efficient and capable of removing 95-97% of Ni^{2+} from aqueous systems.

REFERENCES

[1] Fluoride and Human Health, WHO, Geneva, 1970
[2] J.M. Wood, Environment, 1972. pp. 14-33.
[3] L.J. Carter, Science, Vol. 198, 1977, pp.1015.
[4] C.K. Jain, D.S. Malik and A.K. Yadav, "Applicability of Plant Based Biosorbents in the Removal of Heavy Metals: A Review", Environmental Processes, Vol. 3, 2016, pp. 495-523.
[5] R. Ayyappan, A.C. Sophia, S. Swaminathan and S. Sandya, "Removal of Pb(II) from Aqueous Solution Usingcarbon Derived From Agricultural Wastes", Process Biochem, Vol. 40, 2005, pp. 1293–1299
[6] J.C. Lee, Y.O. Son, P. Pratheeskumar and X.L. Shi, "Oxidative Stress and Metal Carcinogenesis", Free Radical Biol Med, Vol. 53, (2012), pp.742-757.
[7] P.C. Nagjyoti, K.D. Lee, T.V.M. Sreekanth, "Heavy Metals, Occurrence and Toxicity for Plants: A Review", Environ Chem Lett, Vol. 8, 2010, pp.199-216.
[8] Q. Manzoor, R. Nadeem, M. Iqbal, R. Saeed, T.M. Ansari, "Organic Acids Pretreatment Effect on Rosa Bourbonia Phyto-biomass for Removal of Pb(II) and Cu(II) from Aqueous Media", Bioresour Technol, Vol. 132, 2013, pp.446-452.
[9] U. Shafique, A. Ijaz, M. Salman, Wu. Zuman, N.R. Jamil and A. Javid, "Removal of Arsenic from Water Using Pine Leaves", J Taiwan Inst. Chem. Eng. Vol.43, 2012, pp. 256-263.
[10] D. Purkayastha, U. Mishra, S. Biswas, "A Comprehensive Review on Cd(II) Removal from Aqueous Solution", Journal of Water Process Engineering, Vol.2, 2014, pp.105-128.
[11] Nicholls, Comprehensive Inorganic Chemistry, Pergamon Press, Oxford, New York, Vol.3, 1973.

[12] M.J. Gauvin, Nickel In: Chemical Minerals Year Book, Environmental Department of Energy, Mines and Resources Paper No.33. Research Programme, 1976.
[13] S.P.Ed. Parker, "Encyclopedia of Environmental Sciences", 2nd ed. Mc Graw Hill, New York, 1980.
[14] Hassler, "Purification with Activated Carbon for the Examination of Water and Wastewater",Chemical Publishing Company, New York, 1974.
[15] L. Theim, J.T.O. Connor, "Removal of Barium, Cadmium, Mercury and Selenium from Drinking Water Supplies", University of Missouri, Columbia, 1977.
[16] G.S. Logsdon, J.M. Symons, Water Works Association, Vol.65, 1973, pp.554.
[17] M.R. Moghadam, N. Nasirizadeh, Z. Dashti and E. Babanezhad, "Removal of Fe(II) from Aqueous Solution Using Pomegranate Peel Carbon: Equilibrium and Kinetic Studies", International Journal of Industrial Chemistry, Vol.4, 2013, pp.19.
[18] Y. Gutha, V.S. Munagapati, S.R. Alla and K. Abburi, "Biosorptive Removal of Ni(II) from Aqueous Solution by Caesalpinia Bonducella Seed Powder", Sep. Sci. Technol, Vol.46, 2011, pp.2291-2297.
[19] A.H. Al-Dujaili, A.M. Awwad and N.M. Salem, "Biosorption of Cadmium (II) onto Loquat Leaves (Eriobotrya japonica) and Their Ash from Aqueous Solution, Equilibrium, Kinetics, and Thermodynamic Studies", International Journal of Industrial Chemistry, Vol.3, 2012, pp.22.
[20] B. Alyüz and S.Veli, "Kinetics and Equilibrium Studies for the Removal of Nickel and Zinc from Aqueous Solutions by Ion Exchange Resins", J Hazard Mater, Vol. 167, 2009, pp.482-488.

AN DESIGN AND ANALYSIS OF VAC LINE REAR SUB FRAME TANK MOUNTING

P. Vivek Kumar and E. Soundarpandian
Department of Mechanical Engineering,
Bannari Amman Institute of Technology, Sathyamangalam -638 401, Erode District, Tamil Nadu

Abstract

As we are designing tankers, we have to consider total load acting on each component. We want consider braking load, acceleration load, and load due to tipping angle. In these considerations, we have found an error in rear sub frame. In this vac-line rear sub frame tank, we had an issue of heavy load acting on a tipping assembly so, we have planned to newly design and deploy the tipping assembly by attaining the required FOS. In nominal products, FOS should be greater than 1.5 (150% efficiency) so, we can use the product with 100% efficiency for long period of time. The major considerations to be attained is to maintain a minimum FOS of 1.5 factor in order to ensure safety in all aspects and also to avoid failure at any cost. By comparing the initial considerations, several analyses were carried out. In order to reduce the stress acted on the bolts which would shear at some point, it is proposed to prevent the FOS not to be less than 1.5 by designing the tipping assembly to reduce the shear force acting on the bolt. During tipping, the entire load of the tanker act only on the fasteners. Hence through inserting a pin to the tipping assembly, the load completely applied on the bolts got reduced and the entire load can be equally spread through fasteners and pins, so after the attachment of pins we can attain the required FOS, then further proceeding it to the production and manufacturing department.

Keywords: *Acceleration load, Braking load, FOS, Tipping*

1. INTRODUCTION

As we are developing a new model for our new product the project assigned to me was the tipping assembly. The major consideration is to maintain a minimum of 1.5 factor of safety during all aspects to avoid the failure. The design will be construction from the tanks are in the International Organization for Standardization ISO 9001:2015[3]. The finite element analysis is mentioned as a legitimate approach for verifying the design of sewage tank in clause of ISO 9001:2015[7]. The standards specify the maximum sheet plate thickness, its needed for the tank's construction, and stress value to observe the tank or shell, and partitions, monitoring the tank's supporting structures and comparing the design's tensile stress. Additionally, the weldment is the standard factor used in ISO 9001:2015[10] for comparing minimum tensile stress values created on the weldment area for the weldment strength to high. The geometry tank used to transport flammable substances might be different.

The structural stability of the various supporting structures (Ss) used to place a tank will be fixed on a freight track has been observed in the current work. Despite the fact that the design of the tankers carrying sewage is specifically described in Standard and Regulation, mentioned above, there was no instructions about how this tank mounted on the chassis of the freight vehicle for providing the necessary support and transfer the weight of the tank to the vehicle efficiently [11].

To observe the effects of a tanker's number of Ss, geometrical models of preexisting box- shaped tank and its related finite element model were made using Solidworks® Computer- Aided Design (CAD) software. EN24 have a tensile strength 745MPa and a yield strength of 470MPa, Brinell hardness 217. The EN19 has a tensile strength is 655MPa and a yield strength of 415MPa, Brinell hardness 197. EN24 is a 1.5% nickel, 1% chromium, 0.2% molybdenum alloy steel which has a long history dating back over 100 years. EN24 can be heat treated to a wide range of tensile strengths from 850- 1000 N/mm² ('T' condition) up to 1550 N/mm² ('Z' condition).

3. FACTOR OF SAFETY (FOS)

The safety factor is defined as the ratio of the component material's ultimate stress to its working stress. In mathematics, the Factor of Safety is the ratio of material strength to permitted stress. The safety equation's factor is impacted by the material type.

Factor of safety = Ultimate strength/Working stress - brittle material (concrete) Factor of safety = Yield strength (óy)/Working stress - ductile material (steel) Examples: FoS for steel = Yield strength (óy)/Working stress (0.87óy) = 1.15 (appr) FoS for concrete = Yield strength (óy)/Working stress (0.67óy / 1.5) = 3 (appr) (5"As there is little quality control when the concrete is being prepared, a two times safety factor is used.)

In line with IS 456's Article 36.4.2, while assessing the strength and serviceability standards of the structures or structural members used in a limited state.

Material Limit state method Collapse Deflection Cracking Steel 1.15 1.0 1.0 Concrete1.5 1.0 1.3 Table 1.4 - Limit state method

Table 1 Limit state method

Material	Limit state method		
	Collapse	Deflection	Cracking
Steel	1.15	1.0	1.0
Concrete	1.5	1.0	1.3

Compared to concrete, steel has a lower safety factor. Concrete is made in industry because it is a brittle material and is generally less reliable than steel. Because concrete is prepared on site under various climatic conditions, the quality control is therefore better than with concrete.

4. OBJECTIVES AND METHODOLOGY

Developing a new design for the project assigned to me was the tipping assembly my role is to design the tipping assembly. The design should have a minimum FOS of 1.5. Maximum Stress 738 MPA act on Bolt area at Existing Model (without Pin) as shown in Figure 1.

With Our Existing Model We Have Undergone Certain Types of Modifications like changing material, increasing bolt count, changing bolt positions in Order to withstand all Kind of Loads.

Our Objective Is to Design the Tipping Assembly of the Vac-Line Subframe Rear Tank and Also to Reduce the Load By Applying on The Bolts in Order to Ensure Safety. It Is Mandatory to Attain the Required FoS. It Is Proposed to Use a Pin to Reduce the Load Applied on The Bolts by Analysing the Required Fos. Finally Assembling the Tank While Tipping the Entire Load Of the Tanker in Order to Ensure Safety and Avoid Failure.

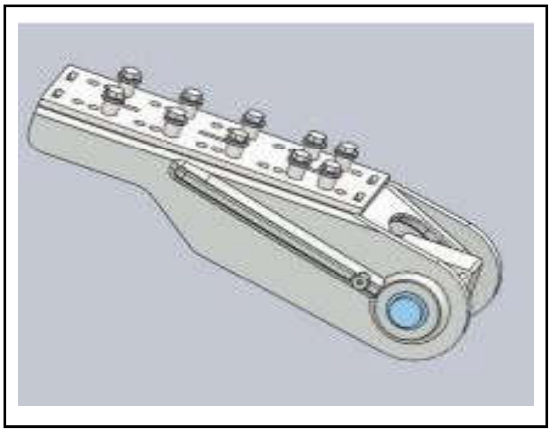

Fig 1 Existing Model

5. METHODOLOGY

In order to completely lessen the load applied to the bolt, our concept is to employ a pin. We will analyse our idea and, after achieving the necessary FOS, go on to the fabrication and manufacturing of the product. The primary consideration for this assembly is that during tipping, the tanker's whole load should only be focused on one component. After examining the necessary FOS, it is suggested that a pin be used to lessen the load placed on the bolts.To assure safety and prevent failure, assemble the tank in the end while tilting the tanker's load.

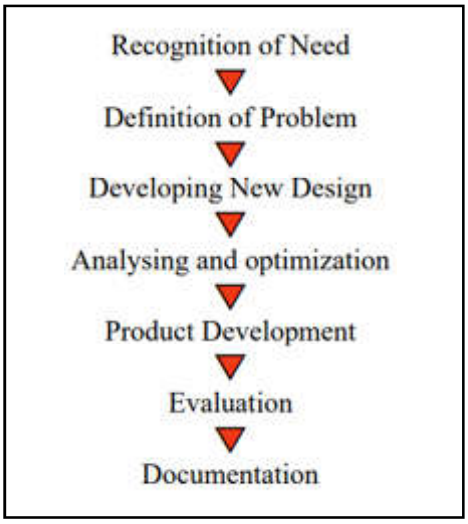

Flow Chart:

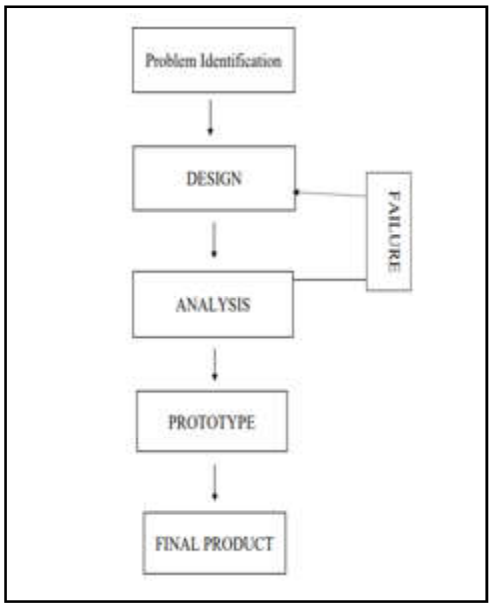

Fig .3 Process flow and methodology

5. CALCULATIONS

5.1 Static Load Consideration

Total tank capacity= 4200 Gallons 1 gallon = 3.78541 litre Tank Capacity consider as Filled with Water of 19093 Litres = 19093 Kg's Empty Weight of 3D Model of Tank = 3120 kg's Total Weight consideration taken for Analysis = 22213 Kg's

Since the tank must support the weight of the fully filled tank, we must first take into account the whole load operating on the hinge. To get the total load, we need to know the tank's capacity and total weight. Our tank has capacity of 4200 gallons, with the known values we have calculated total weight of tank.

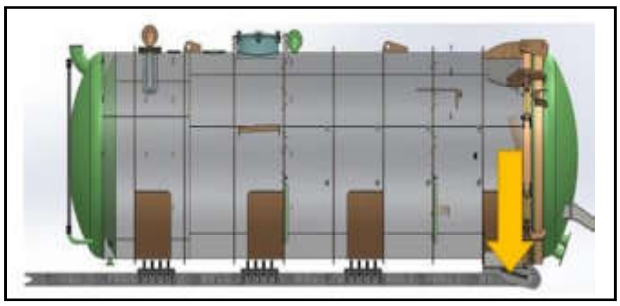

Fig 3 Static tank

5.2 Load due to 35 Degree Tipping of Tank

Load of Tank with Water = 22213 kg's
Tipping Angle = 35 Degree
Inclined force formulae,
F %" = mg sin (Ų)
Inclined Force Acting on Bracket
= Sin (35) x 22213
= 12618 Kg's
Load at Tipping as per calculation = 12613 Kg's
But We consider Load as 22000 kg's for Two Pivot Bracket
Acceleration Force 61000 kg's

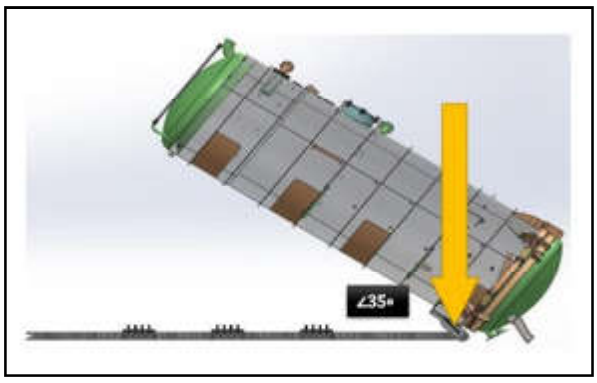

Fig. 4 Inclined tank

For Cross Verification, Hinge Profile Individual FEA Is Analyzed. Downward Force
= 5500 Kg's Side Force Due to Acceleration = 30500 Kg's.

5.3 Specification of Pins

YieldStrength of 10.9GradeBolt-940MPA(FOS-1.75)

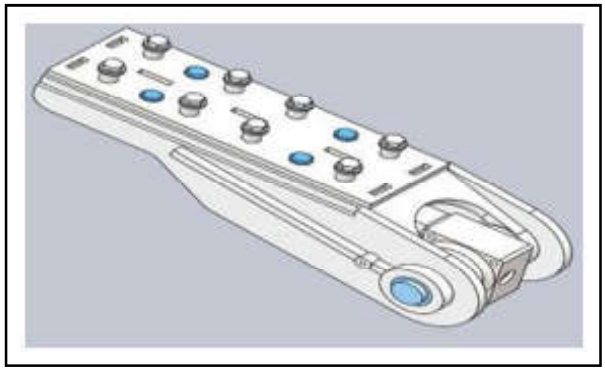

Fig. 5 Pins

5.4 Material

Material used is EN24. EN24 is a 1.5% nickel, 1% chromium, 0.2% molybdenum alloy steel. EN24 can be heat treated to a wide range of tensile strengths from 850-1000 N/mm² ('T' condition) up to 1550 N/mm² ('Z' condition). Heat treated EN24 offers high tensile strength combined with good ductility and resistance to shock. At low temperatures good impact values can be obtained. In this blog we explain a little about the characteristics and history of this well-established steel grade.

Table 2 EN24 Typical Analysis

Carbon	035-0.45%	Silicon	0.1.-0.35%
Nickel	1.30-1.80%	Manganese	0.45-0.70%
Chromium	0.90-1.40%	Phosphorous	0.05%max
Molybdenum	0.20-0.35%	Sulphur	0.05%max

6. RESULTS AND DISCUSSION

6.1 Result for Static & Acceleration Force (Without Pins)

We have done an FEA analysis, to know the position of maximum stress acted on the surface of body. From result, we have come to a conclusion that there is an error in distributing stresses on the hinge, so we have to design a project in a way to solve the problem. We have introduced certain ways like introducing new materials, increasing bolt count Etc.., to rectify the problem.

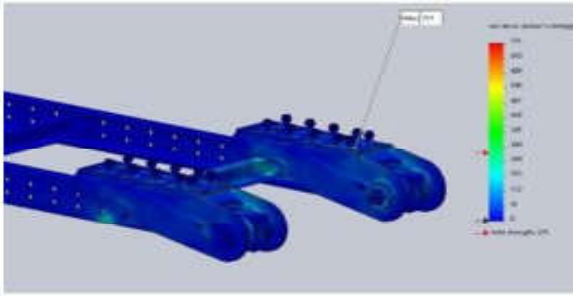

Fig. 6 Result for Static & Acceleration Force (Without Pins)

6.2 Results for Angle Load: MAXIMUM STRESS = 212 MPa

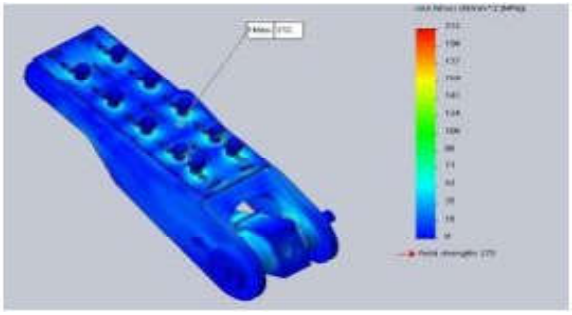

Fig .7 Results for Angle Load

6.3 Pivot Block Individual FEA Results

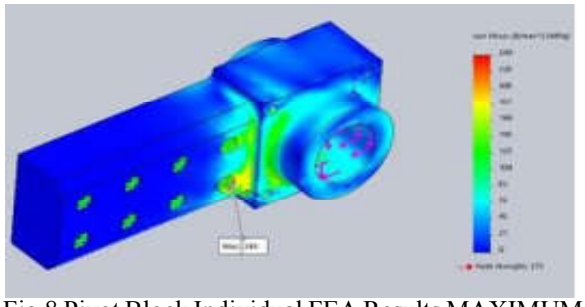

Fig.8 Pivot Block Individual FEA Results MAXIMUM STRESS = 249 Mpa

6.4 Hinge Profile Individual FEA Results

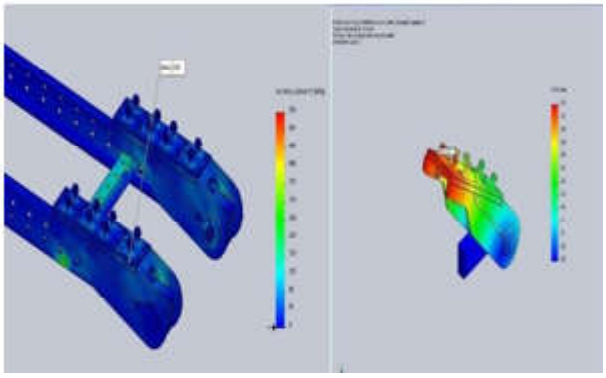

Fig. 9 Hinge Profile Individual FEA Results MAXIMUM STRESS = 290 Mpa RESULTS WITH PIN

6.5 Result for Static & Acceleration Force (With Pin)

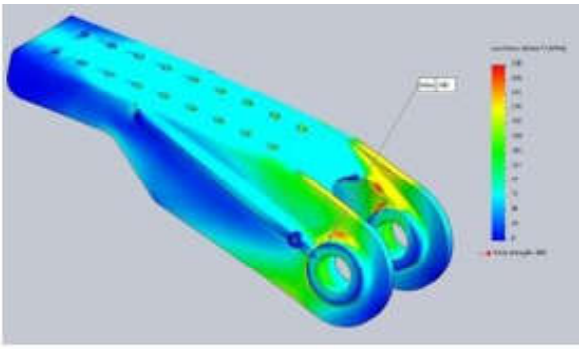

Fig. 10 Static Force (With Pin)

MAXIMUM STRESS = 538 MPa

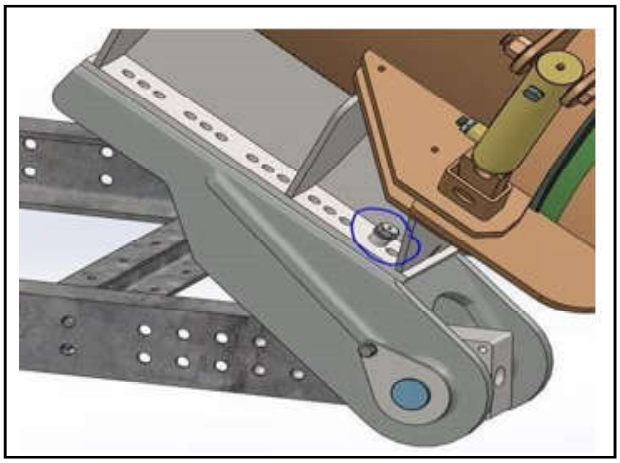

Fig.11 Final model with pin

This is our final design to develop a new product using pin as shown in Fig.4. (In Bolt mounting area)-Yield Strength of 10.9 Grade Bolt-940 MPA(FOS-1.75). By analysing the necessary FOS, it is suggested to utilise a pin to lessen the load put on the bolts.

7. CONCLUSION

As per Initial FEA Analysis. We facing failure in Complete Assembly. Maximum Stress occurred in Bolt Area 731 MPA (without Pin).

FOS= 1.28 So, we implement New Stopper Pins with Revised Bolt pitch in Pivot bracket. Maximum Stress occurred in Bolt Area 538 MPA (with Pin). FOS= 1.75. Our work is used for safety issues at tank mounting, with our product we can work with full efficiency. It can also withstand up to 1.5 of its weight. Many tankers can implement our project in order to reduce tear & wear stresses. It is also cost efficient, so they can be fabricated easily.

REFERENCES

[1] Jasvir Singh Dhillon and Priyanka Rao, "Design of Engine Mount Bracket for FSAE Car Using Finite Element Analysis", IJERA, Vol.4, No.9(version 6), 2014.

[2] "Asker H.K., Dawood T.S. and Said A.F., 2012, Stress Analysis of Standard Truck Chassis during Ramping on Block Using Finite Element Method", ARPN Journal of Engineering and Applied Sciences, Vol.7, No.6, pp. 641-648.

[3] E.Madenci and I. Guven, "The Finite Element Method and Applications In Engineering Using ANSYS, Springer Publisher Nor MAM, Rashid H, Faizul WM, Mahyuddin W, Azlan MAM, Mahmud J., 2012, Stress analysis of a Low Loader Chassis, Procedia Engineering, Vol.41, 2007, pp. 995-1001.

[4] Umesh S Ghorpade and Mahendra Gaikwad, "FEA and Natural Frequency Optimization of Engine Bracket", IJMIE, Vol.2, No.3, 2012.

[5] C. Karaoēlu and N.Kuralay, "Stress Analysis of a Truck Chassis with Riveted Joints, Finite Elements in Analysis and Design", Young, W, 1989 - Roark's Formulas for Stress and Strain, 6th edition. McGraw-Hill, Vol. 38, No. 12, 2002, pp. 1115-1130.

[6] J. Shigley and C. Mischke, "Standard Handbook of Machine Design", McGraw-Hill, 986 , pp.2-15.

[7] K. Chinnaraj, M.S.Prasad and C.L.Rao, "Experimental Analysis and Quasi Static Numerical Idealization of Dynamic Stresses on a Heavy Vehicle Chassis Frame Assay", Journal of Applied Mechanics of Materials, Vol.13-14, 2008, pp. 271-280.

[8] Pavan B. Chaudhari, "Comparison of Mg, Al and Cast Iron to Obtain Optimum Frequency of Engine Bracket using FEA", IJERA, Vol.2, Sep-oct 2012.

[9] IB. Zaman, "Study of Dynamic Behaviour of Truck Chassis, M.Sc. Thesis, Faculty of Mechanical Engineering, Universiti Teknologi Malaysia, Malaysia, 2005.

[10] P. Abhishek, S.M.Hardeep and G.Sarvocch, "Finite Element Analysis of Fuel Tank Mounting Bracket", International Research Journal of Engineering and Technology, Vol.5, 2018, pp.956-958.

[11] R.Rajappan and M.Vivekanandhan, "Static and Modal Analysis of Chassis by Using FEA", International Journal of Engineering and Science, Vol. 2, No. 2, 2013, pp. 63-73.

[12] D. Koulocheris and C.Vossou, "Exploration of Equivalent Design Approaches for Tanks Transporting Flammable", Computation, Vol. 8, No.33, 2020.

[13] N. K. Ingole and D.V.Bhope, "Stress Analysis of Tractor Trailer Chassis for Self-Weight Reduction", International Journal of Engineering Science and Technology, Vol.3, No.9, 2011, pp.7218-7225.

BIO MEDICAL WASTE CLASSIFICATION AND ITS DISPOSING METHODS USING ML

G. Gopi[1], S. Cibi Joshua[2], KI. Dass Prabu[3] and M. Janarthanan[4]
[1]Department of Physics, [2&3]Department of Mechatronics, [4]Department of Mechanical
Bannari Amman Institute of Technology, Sathyamangalam - 638 401, Erode District, Tamil Nadu
E-mail: gopi@bitsathy.ac.in, cibijoshua.mc19@bitsathy.ac.in, dassprabu.mc19@bitsathy.ac.in

Abstract

As demand increases, the supply of medical waste is increasingly surpassing the demand for health. The generation of various wastes increases as the population grows. Because the disease can spread to humans through the waste, the COVID-19 period saw a substantial increase in medical waste, which is exceedingly harmful. As a result, safe medical waste disposal is essential because it depends on preserving nature and the environment. In this paper, we present artificial intelligence and deep learning techniques for recognizing and classifying medical waste. AI is emerging as the computer industry's future. We have used the CNN algorithm, which is the best for image and audio recognition, to improve categorization. FRCNN is a suitable artificial neural network for real-world use. We pay special attention to the problem of classifying medical waste since it needs to be resolved right away given the current situation. With an epoch of 100 and a 96% accuracy rate, our research offers a high accuracy, AI-based image categorization method. A train dataset and a test dataset were created using the gathered image dataset. We trained the FRCNN model to deliver the best evaluation. A website that accepts images outputs information about the type of medical waste it is, how to dispose of it, and even the color code. Hence the power of artificial intelligence can be applied to simplify the classification of medical waste and could be used in all the healthcare centers.

Keywords: *Artificial Intelligence, Biomedical waste, FRCNN(Faster Regional Convolutional Neural Network), Recognizing and classifying*

1. INTRODUCTION

One of the main contributors to the spread of infections and disease is the inappropriate disposal of rubbish. It puts the public, patients, and hospital staff's health in danger. There is a chance of nosocomial infection. A large number of hospitals, nursing homes, and healthcare facilities regularly dispose of all of their waste at the garbage collection site, where it is subsequently picked up by trucks for final disposal. The majority of the locations are open to rag pickers, who run the danger of getting sick while touching such dirty items. The market where the items were sold that were picked up often recycles used needles, syringes, gloves, leftover pharmaceuticals, etc. Everyone who uses these goods runs the risk of contracting an infection. Storage, sanitization, and disposal come after the methods for processing and disposing of biological waste have been established.

Due to the COVID-19 Epidemic, there has been a delay in obtaining and submitting the information to State Boards and CPCB. Each State Board has, nevertheless, submitted the Annual Report Information on Biomedical Waste Management. A considerable amount of potentially infectious and dangerous waste is created every day in hospitals and other healthcare facilities around the world. A specific focus of environmental and humankind preservation is the efficient management of biomedical waste, which includes an appropriate waste reduction and neutralisation component. Together with this idea, a comprehensive strategy for dealing with biological waste is required since, without qualified leadership, the handling of hazardous medical waste could degrade the calibre of patient care.

(a) Biomedical waste: This term refers to waste products produced during veterinary procedures, animal slaughter, vaccines, research, diagnostics, and therapy.
(b) Medical waste: This term refers to any waste produced during diagnosis, treatment, immunization, animal care, research, biological production, and biological testing.
(c) Hospital trash: The trash generated or leaving hospitals is what may be 85% are non-hazardous, while 10% are infectious. Dangerous: 5%.

SAP Technical Modules are used to construct applications, debug issues, download and install upgrades, and plan and execute migrations. They are utilized on the back end of an SAP landscape. SAP functional modules offer business functions like handling orders, transforming unstructured data into intelligence, and managing human resources.

A hospital, nursing home, clinic, dispensary, veterinary institution, animal house, pathological laboratory, or blood bank are just a few examples of an establishment that generates bio-medical waste. According to the Gazette Notification dated July 20, 1998, it is the responsibility of every occupier (a person having control over an institution or premises) to take all necessary precautions to ensure that such waste is handled without having a detrimental effect on human health or the environment. By these guidelines,

- It is forbidden to mix bio-medical waste with other types of trash.
- At the point of creation, bio-medical waste must be divided into containers or bags according to its different classifications.
- More than 48 hours cannot be spent storing biomedical waste. Every occupant is required to either install the necessary bio-medical waste treatment facilities, such as an incinerator, autoclave, or microwave system, or to ensure that the necessary waste is treated at a shared waste treatment facility.
- Each occupier must submit an application to the designated authorities for authorization to be granted.

Each occupier is required to keep records of all biomedical waste generation, collection, reception, storage, transportation, treatment, and disposal.

2. OBJECTIVE

- To reduce the chance of infections spreading.
- To safeguard the community's health and well-being as well as those of the medical staff.
- To shield from harm and even lethal infections.
- To offer garbage management options that are environmentally sustainable.
- To advocate for the environment's sustainability and quality.
- Government and private hospitals, nursing homes, doctor's offices, dentistry offices, dispensaries, facilities for medical research and training, blood banks.
- Collecting sites, labs, animal shelters, and slaughterhouses are all potential sources of biomedical waste.
- To stop or lessen the generation of garbage and the level of risk associated with their re-use.

Utilizing trash as a source of energy or recovering waste through recycling or any other method to obtain secondary raw materials. The procedures and techniques utilized to dispose of waste shouldn't put anyone in danger.

Medical care is crucial for our wellbeing and survival, yet the trash it generates puts both the environment and humanity in grave danger. Ineffective waste management in healthcare facilities has a direct impact on the community, the medical community, and the environment. A considerable amount of potentially harmful and infectious waste is created each day in hospitals and other medical facilities around the world. Exposure to hospital or BMW waste and careless disposal represent serious threats to the environment and public health, needing careful control and treatment prior to final disposal.

Waste management is responsible for gathering, moving, and disposing of garbage, sewage, and other waste products. A variety of choices for recycling items that shouldn't go in the garbage are provided through the process of processing solid wastes, often known as waste management. The subject is recycling waste into valuable materials. The primary motivation for waste collection is the protection of the environment and the general public's health. Garbage and waste have the potential to pollute the air and water. It is also known that decomposing waste releases harmful vapours into the air that might make it difficult for someone to breathe. It is really concerning that hospital trash has not been handled correctly. Medical staff members lack sufficient training in hospital waste management practises. In addition, how people treat rubbish is hazardous in and of itself. The rubbish must be disposed of by hospital employees as quickly and cheaply as possible, without following hygienic procedures. The goal of this study is to increase the general people's and medical professionals' knowledge of the critical information needed to safeguard the environment and public health.

India's urbanisation is bringing numerous problems because as the population rises, so do the demands for resources such as utilities, food, and land. Also, 1.37 billion

more people than there are now produce more waste than they do now. The management of solid waste in urban settings is a serious challenge for the majority of countries in the globe. Tonnes of trash are produced each day in India. Only 5% of this massive amount of rubbish is recycled, though. One solution to this problem would be to identify and classify the garbage from the beginning. Waste segregation needs to be managed well in order to lower the risks to the ecosystem's safety and health. We can comprehend the economic value of waste better when we separate the waste elements. Different waste types cannot currently be separated using an effective approach. The objective of our project is to develop a simple, cost-effective, and user-friendly segregation system for Indian cities to handle waste management more effectively.

2. LITERATURE REVIEW

2.1 BIOBIN for Biomedical Waste Handling and Disposal During COVID '19:

Author: Akila V; Gayathri B

In year 2021, waste generated during covid 19 diagnosis and treatment must be managed individually in accordance with biomedical waste management (Bwm) rules and the central pollution control boards cpcb instructions the collection of this biomedical waste from quarantine wards, isolation wards, laboratories, covid test facilities and other facilities should be directed to the common bio-medical waste treatment and disposal facility as soon as possible after it has been kept separate cbwtf. This study proposes an internet of things (iot) enabled biobin for continuously monitoring and alerting the sanitary workers involved in this collection for routine cleaning and early disposal of this dangerous biological waste.

2.2 Biomedical waste classification, quantification, and management based on IoT:Author:

Dr. Pooja Raundale; SachinGadagi

In year 2017, This initiative's primary goal is Plans for waste segregation are proposed in order to increase recycling and properly handle non-recyclable waste. Biomedical waste is just one example of trash that does not fall under that category. As a result, this type of garbage is dealt with differently. As a result, such garbage is managed separately. This study looks at the current national practices as well as the various technologies that can be used to automate these procedures and handle biohazardous waste with care.

Using recent technological breakthroughs and wireless communication, the proposed solution could help to completely automate this system. Because IoT devices are inexpensive and simple to set up, they can be used to easily automate this system. COTS IoT components are commonly used. The current internet infrastructure is used for real-time data transport. When deployed at sources, the color-coded bags will be marked with RFID tags that are automatically issued and indexed by a system. Weighing sensors would be installed in the bins where these bags would be placed, and they would immediately start the van transporting the waste to CBM WTF. A 900-1900 MHz (2G spectrum) network connects a master bin and all slave bins.

2.3 Forward Supply Chain and Waste Management Using Block chain For COVID – 19 Medical Equipment and Supplies:

Author: Raja Wasim Ahmad; Khaled Salah

In the year 2021, The integration of the Ethereum blockchain with IPFS's decentralized storage aims to safely fetch, store, and exchange information on COVID-19 medical equipment waste management and its forward supply chain. We provide algorithms for the COVID-19 waste handling interaction rules and the sanctions to be applied to stakeholders in the event of infractions. They go over the system concept and its entire execution in great detail. They use cost analysis to assess the performance and affordability of the proposed solution.

They investigate our method from the standpoints of generality and application, while also presenting the security analysis to validate the dependability of smart contracts. In this work, we present a high-level design of the proposed block chain-based solution to manage COVID-19 medical equipment supply and waste after use, which implements four primary smart contracts: order management, lot and ownership management, waste shipment handling, and registration. Medical supply and equipment are used by hospitals and COVID-19 testing facilities (COVID-19 swab sticks). Medical waste is generated in hospitals and COVID-19 testing facilities and is transported to a waste treatment facility for processing and disposal by third parties. The manager's primary responsibility in a medical waste treatment facility is to ensure that people can safely handle medical waste while it is being treated and disposed of.

2.4 Device Coding Biomedical Diagnostic System:
Author: Carlos Alvarez; Ankur Agarwal

In year 2015, This study looks at what happens when a device malfunctions and is brought in for repair. When a biomedical device is returned to the customer (a hospital, healthcare facility, or medical Centre) after a period of testing with a diagnostic no testing "no problem found," this occurs (NPF). We will discuss our proposal with a valid solution to this problem based on our experience in the biomedical engineering field and the use of internally generated error codes. Our solution is optimized for Android mobile technology, but it can also be loaded on other mobile platforms such as iPhone, PDM, and so on. Our solution to this problem is to create a widely accessible database of medical equipment, error codes, what they mean, and how to resolve any issues that arise.

It is suggested in this article that a web application be developed to aid in this process. Itis designed to work with mobile devices and all major browsers. Users can search for specific devices and error codes, view the solution to the problem, and access all of the database's data. The application's goal is to allow anyone, regardless of level, to notice an error number on their biomedical device, look it up in the database, and decide how to best address it, if at all, either by themselves or by asking someone else to do it.

3. SYSTEM ANALYSIS

Biomedical waste has become a critical issue that is highly concerning to the general public because of its increasing and negative effects on public health. Because of the biomedical industry's tremendous technical development and the abundance of waste disposal, the volume of biomedical waste produced has significantly increased. This issue is becoming increasingly important as a result of the possible environmental risks posed by biomedical waste. Sadly, many underdeveloped nations lack the technology necessary to use the most popular systems, which are electrically driven. An effective and cost-effective device for remote healthcare, a solar thermal autoclave uses renewable energy to sanitize equipment. One of the most needed to control for businesses (HCF and CBMWTF) is the management and treatment of biological waste because improper handling could result in harmful outcomes like widespread infection. A effective BMW management system was either not present in 60% of secondary care facilities and 54% of tertiary care facilities, which indicated that they need major improvement. An effort is being made to automate trash management by using wireless technology. Strategies for waste separation are recommended in order to improve recycling and properly manage non-recyclable garbage. In the case of a wide variety of wastes, including biological waste, this classification would not be accurate. This type of trash is treated differently because of this. Such waste is managed by a separate unit as a result.Such waste is managed by a separate unit as a result. The current national practices and the various technologies that can be employed to automate these processes and carefully handle biohazardous waste are discussed in this article.

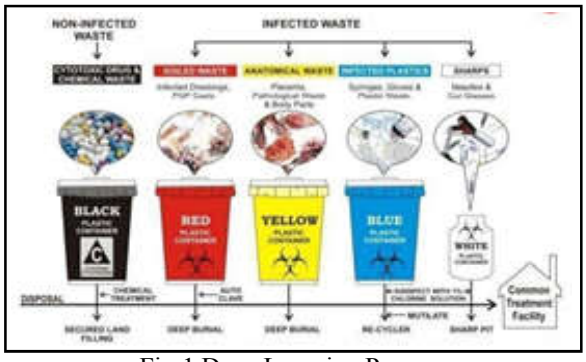

Fig.1 Deep Learning Process

4. MODULE DESCRIPTION

The UCI repository provided the data set needed to complete the specified work (Bio-medical waste management). The reduction of landfills, recycling, and trash reduction are all encouraged by waste separation. We took advantage of a medical waste dataset that was gathered in 2019 by the First Affiliated Hospital of Zhejiang University. This unusual collection includes labels, image data, and the medical waste border for 100 samples. These samples fall under many categories of medical waste. In this context, the proposed deep learning method is referred to as Deep MW (deep medical waste). The dataset contained some odd data, and some of the images contained trash from several categories. For example, the upper left corner of the gauze shows gloves, an infusion bottle, an infusion bag, an infusion apparatus, and a syringe. This kind of image was less precise in comparison. The original image's size and background, as well as other elements like quality, may have a significant impact on how well the categorization model performs. Real applications necessitate additional processes on the raw image, such as local sampling, cropping, etc. We used data pre-processing to ensure acceptable data quality and a constant sample size. This

is in conformity with the advice of medical experts. Namely, the dataset classification and corresponding sample size.

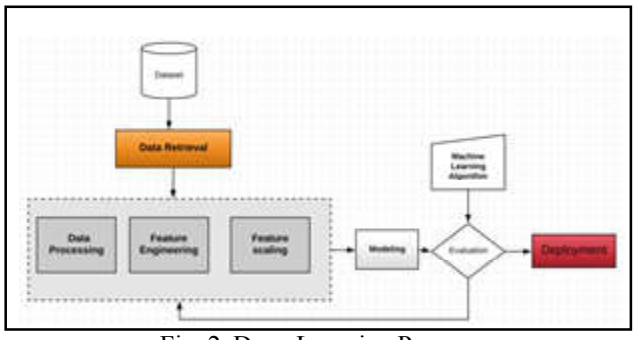

Fig. 2. Deep Learning Process

5. PERFORMANCE ANALYSIS

The result is counted as a true positive (TP) in this module; if the same result is mistakenly classified as a negative, it is counted as a false negative (FN). The outcome is counted as a true negative (TN) if the legitimate diagnosis is CHD absent and it is correctly labelled as negative; if the same outcome is wrongly classified as positive, it is considered as a false positive (FP).

Accuracy - A model's or algorithm's accuracy is a metric that indicates how well it operates and if it was trained appropriately. We ran 100 epochs, and the accuracy was 96%.

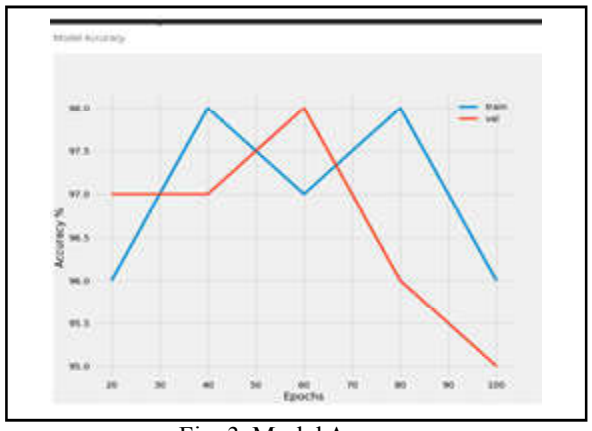

Fig. 3 Model Acuracy

6. PROPOSED WORKFLOW

FRCNN Based Biomedical Waste Management: The management of solid waste has become a major challenge in metropolitan places. Because different waste materials are produced in such large amounts, different ways to handle them are necessary. It is impossible to adequately treat all of this rubbish at once. One of the most important processes in waste management is waste classification. Waste separation currently involves physical effort, which could be highly harmful to the person doing the job. In the proposed system, an efficient automatic garbage disposal model has been added at the source itself. As a result, the technology will reduce the number of workers needed to sift waste. This will be accomplished by using the foundations of the Faster Region Convolutional Neural Network (FRCNN), a machine learning method. This system's objective is to take pictures of a single trash item, identify it, and successfully separate it in to biodegradable and non-biodegradable garbage.

7. SIMULATION

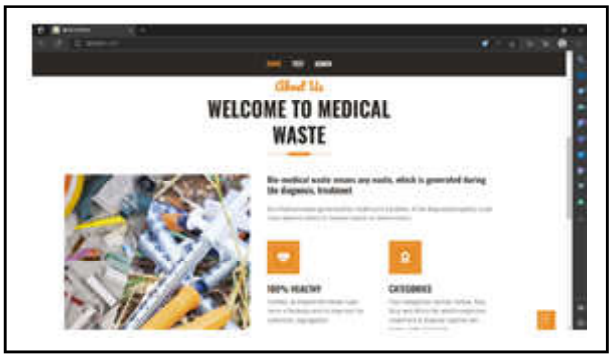

Fig. 4 Login Page

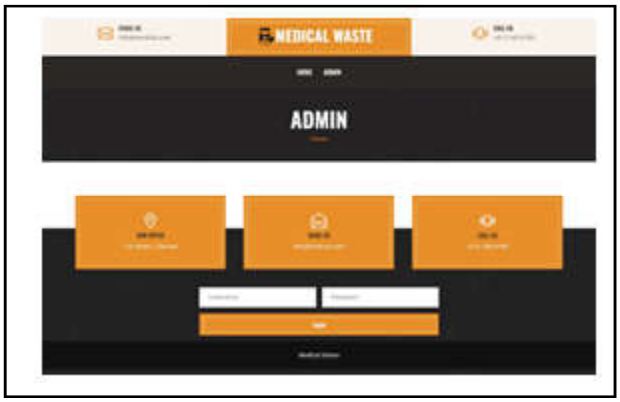

Fig.5 Admin Page

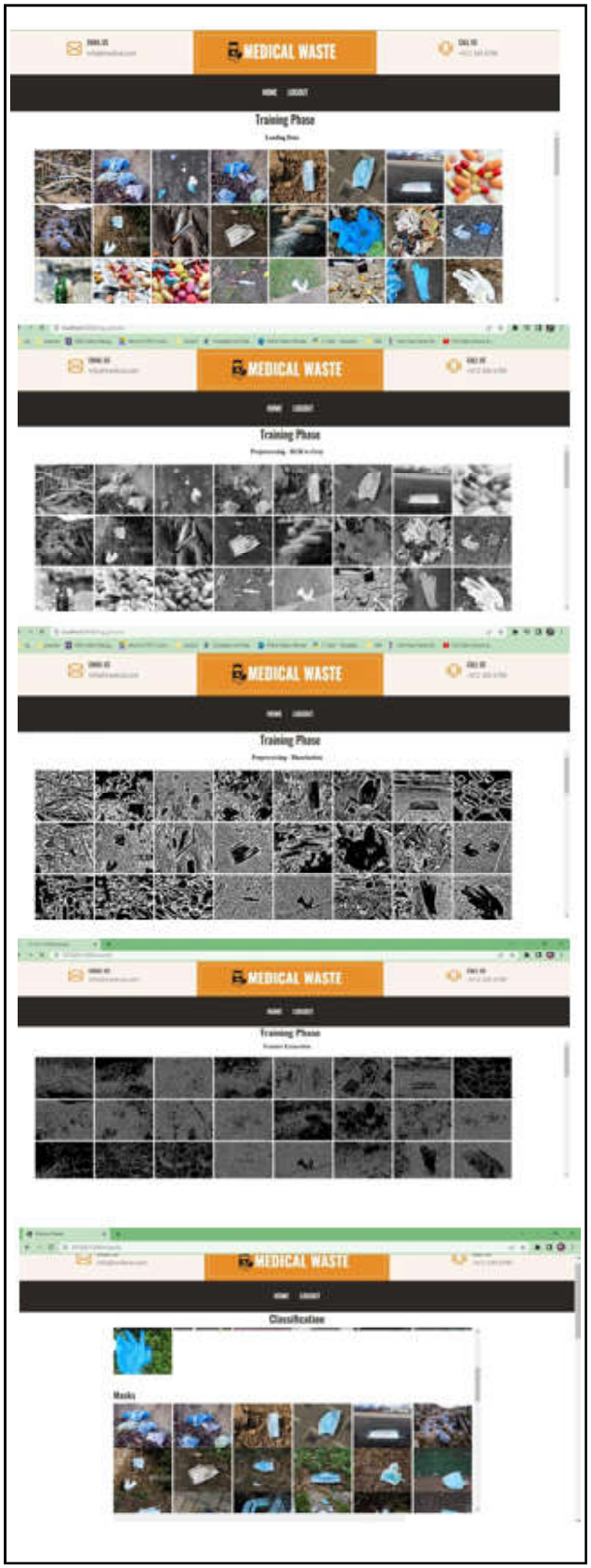

Fig. 6 Data preprocessing

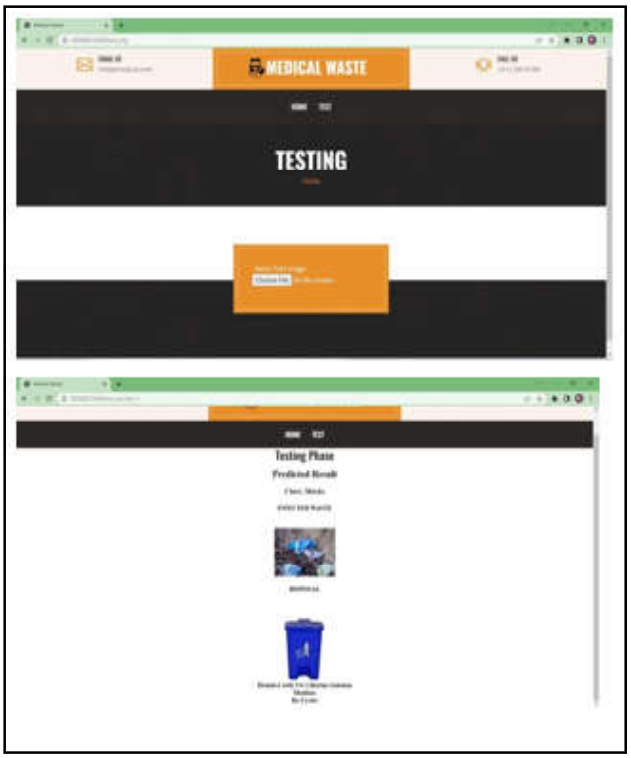

Fig.7 Testing phase

8. CONCLUSION

The results demonstrate that even with a small image dataset, sophisticated AI methods may be used for highly accurate automatic identification and classification of medical waste. The main objective of this study was to obtain the greatest classification accuracy possible utilizing a data set of only 100 photos of medical waste and the created AI system.

Thus, preventing overfitting because of the scant training data is the key problem. The results of the developed model will be reviewed in this section of the study. On the test data, the developed model performs reasonably. In conclusion, the model's accuracy rate is close to 96%. The model correctly classifies the various waste components by identifying the various categories of objects. The model correctly classifies the various waste components by identifying the various categories of objects. Using images from the testing data, the generated model's final output has been assessed. The test data images have been meticulously incorporated into the testing code for the waste element detection. The model's overall detection time to identify a single object from an image is close to 3.05 seconds. In order to determine the model's true correctness, the names of the images were actually provided so that it could be

physically observed how well the model's functions had performed in those pictures. Initially, during testing, it appeared as though many boundaries were being formed in the area of object detection, but this problem was resolved by lowering the threshold for picture prediction This study provided an automated framework for garbage detection using deep learning algorithms and image processing methods to decrease the effects of improper waste disposal. In order to implement the framework, training techniques, classification techniques, and a large photo collection were used. In this study, we show how the Faster R-CNN algorithm may be used to categorize waste products into different groups on many different objects in a single image.

In biomedical waste categories, gathered in the proper type of container, and designated color coding, the hospitals were segregating the biomedical waste every day. Although the quantity of hazardous waste has not decreased, the actions taken have resulted in its complete neutralization and safe disposal. The operation of the biomedical waste management system should be periodically redesigned in response to situational changes after study of hospital management. To reduce environmental pollution and protect the safety of the staff, patients, and general public, improvements over previous regulations in terms of improved segregation, transportation, and disposal techniques have been made. The dataset for our project, which contains photographs of regional waste products that are slightly diverse, was the main problem. It is the cause of the model's inaccurate predictions on a few local garbage photos. However, the datasets were improved by integrating images of locally collected trash. Images of the waste products in the training dataset that are unclean and appear dirty must be attached. In doing so, it may be possible to obtain improved categorization with a greater accuracy level.

REFERENCES

[1] P. Agamuthu, "Post-closure of landfill: Issues and Policy", Waste Manag Res, Vol.24, 2006, pp.503-4.

[2] V. Akila and B. Gayatri, "BIOBIN for Handling, Disposing Medical Waste during COVID19 Res. 2021.

[3] Block Chain and Waste Management for COVID 19 Medical Equipment, Res.2021.

[4] S.S.Block, "Disinfection, Sterilization and Preservation", 5th*ed.* Lippincott Williams and Wilkinspublication, 2001.

[5] Y. Chen, *et al., "*Application Countermeasures of Non-incineration Technologies for Medical Waste Treatment in China", Waste Manag. Res. J. Int. Solid Wastes Public Cleansing Assoc.Iswa **31**, pp.1237-1244.

[6] S. Gupta and R.Boojh, "Biomedical Waste Management Practices in Balrampur Hospital", Lucknow, India. Waste Manag Res.Vol.24, 2006, pp.584-91.

[7] Kannan Govindan and Arash Khalili Nasr, "Parisa Mostafazadeh; Mathematical Programming Model during Outbreak of Covid 19", Res.2019.

[8] GD. Meyers, G. McLeod and MA. Anbarci, "An International Waste Convention: Mmeasures for Achieving Sustainable Development", Waste Manag. Vol.24, Res.2006, pp.505-13.

EFH-CP-ABE SCHEME WITH MA-ABE AND KBE: EXTREMELY OPTIMIZED FILE HIERARCHY ATTRIBUTE-BASED CRYPTOGRAPHY

R. Ezhil, N.Nataraj and K.M. Madhumita
Bannari Amman Institute of Technology, Sathyamangalam - 638 401, Erode District, Tamil Nadu
E-mail:ezhilravikumar1997@gmail.com, n.nataraj08@gmail.com, madhumitha.se21@bitsathy.ac.in

Abstract

Customers can access, save, and retrieve their facts/data from a server remotely, which also provides on-demand services. The most effective technique to handle our information securely is through cloud garage. Data protection and privateers are important factors. There are several different encryption techniques used to securely percentage data. The issue with Constant data storage is typically resolved using (ABE). One-of the best ways to solve-issue of a reliable fact/resource-sharing system in cloud processing is through CP-ABE. Only authorised end-users/customers can encrypt and decode data. Each possesses a unique collection of traits. Hierarchically, a single access structure is paired with a layered access structure. The papers in the hierarchical structure are encrypted with built-in access control. For ciphertext time, the cost of encryption is reduced. Final Implementation provides significantly longer encryption times for a number of attributes. An Extremely Optimized File Hierarchy Attribute-Based Cryptography scheme (EFH-CP-ABE) with a few additional encryption techniques is suggested in this study. Cloud data can be secured by using different attributes and with additional features.

Keywords: *Attribute-based encryption, Cloud Computing, CP-ABE, Data Sharing, EFH-CP-ABE, File hierarchy Ciphertext-policy*

1. INTRODUCTION

Cloud-compute resource processing is a Model for offering easy, on-demand on-premise network access to customisable shared pools, relate to the Wikipedia definition. Deploy computer resources or any IT data transmission share (like networks, servers, storage, applications, and services) quickly with pay as you used. Cloud computing refers to on-demand computer data or supplies-resources that are available via interconnected N/W networks such as the internet and are delivered and dispersed with the least minimum of administrative effort or contact with service providers.

Cloud compute processing is an open-source, on-premise, on-demand resource that you may share and use of services from anywhere and payment only service for what use have use in time. Most cloud features and technologies are built on this service, and in the deployment, resource-shared, access-rapidly and they are the kind of access model. Cloud compute resource processing technique has advanced rapidly in recent years and has emerged as an important topic in computer science. It offers highly scalable and dependable storage on third-party servers for easy administration and deployment of services with pay as you go. Cloud compute is a centralised server resource with distributed servers on a scalable platform that provides on-demand computing supplies-resources (like: owner who provide called CSP) are offers on cloud-platforms-space for their-own customers to use and create any-of-their-services, and ISPs-offer high-speed broadband to access the internet. Cloud-Compute process, A concept that offers accessible, on-demand on-premises network access to a common pool of resources (such as networks, servers, storage, and applications) that can be created and deliver/server-resources quickly with-a little administration effort.

Cloud compute process provides a new business model for firms that want to implement IT services and other organisations like in the government sector, healthcare data management, education etc. This organisation service is simple to setup and requires no upfront expenditure. Security is the most primary concerns impeding cloud expansion. Users must encrypt their stored data before saving it on remote database servers to ensure that it is protected from other users or malicious websites.

2. CLOUD MODEL AND ITS BASIC OF CLOUD PROCESS, METHODS AND ISSUES

Recently, most research works on technology, business, sectors, the education field of agriculture, etc. Are they now based on cloud computing technology? During the covid-19 pandemic period, cloud technology was used in many fields that helped the IT workers, Students to process their work without any pending. Most software S/W and hardware H\W services are shared through the cloud because it is accessible, flexible, scalable, efficient with high availability, and then can be accessed from anywhere. The IaaS, PaaS, and SaaS which are the three primary cloud computing services. As a result, more data is accessible and shared across several businesses via the cloud-based network or services. It has more procs but also has drawbacks on the cloud during data transmission or data exchange. This cloud compute process built on two models: a service model and a deployment model, each of which has several variants based on its functions. Infrastructure, platform, and application-based service model Development-model based-on cloud-kinds(public/open-cloud,private/closed-cloud,hybrid/clone-cloud, community/organization cloud) depending on the characteristics of the cloud-models, They access data or on-demand resources that are shared by CSPs or service-providers are accessible to certain-data of authorised users. The use of cloud computing inside an organisation has almost always been expanded. However, with cloud adoption comes the urge to-ensure the organization's cloud security approach is capable-of being protective against the most serious cloud security risks. To address this, we employed a technique known as encryption technology, which-is used-to encrypt and decode data during cloud transfer and also to safeguard data from theft. Misconfigurations of cloud protection settings are a major cause of cloud records/resources breaches. Many firm's cloud protection posture control-strategies are in-adequate for safe-guarding their critical cloud infrastructure.

2.1 Issues in Data Sharing

This is affected by a number of things. Enterprises find it challenging to ensure that statistical data/resources are easily accessible to legal parties because cloud infrastructure is designed to be simple to use and to facilitate clean resource/data exchange. Additionally, organisations that use cloud-based infrastructure are unable to fully control and view their infrastructure; as a result, they are forced to rely on security measures supplied by their cloud service provider (CSP) to plan and maintain their cloud deployment. It is easy for a misconfiguration or security oversight to expose an organization's cloud-based resources to attackers because many organisations lack experience protecting cloud infrastructure and frequently have multi-cloud installations, each with an extraordinary array of vendor-supplied security measures.

Data Loss in Cloud-store-environment occurs due nature and by other external factors:

- Third party Access
- Undefine Interfaces/APIs
- Hacking of Accounts
- Unnoticed Security problem
- Sharing of Data with third party
- Malicious Insiders in the Cloud.
- Cyberattacks in the Cloud.
- Service loss or Attacks in the Cloud.

These are some of the issues that arise in the opensource-cloud when data/resources are shared and accessed using cloud-based models or form services.

- Encryption: It is method of rewriting the original data into duplicate data by using some cryptography text or character or symbols by using these the data are get hidden the original data called encryption
- Decryption: This is a method related to encryption that is diametrically opposed to encryption in that the changed data is converted to original information in this process known as decryption.

Cryptography is the combined process of encryption and decryption; the process explains in Fig 1. We can avoid data theft on-cloud by employing this strategy, method, and algorithm

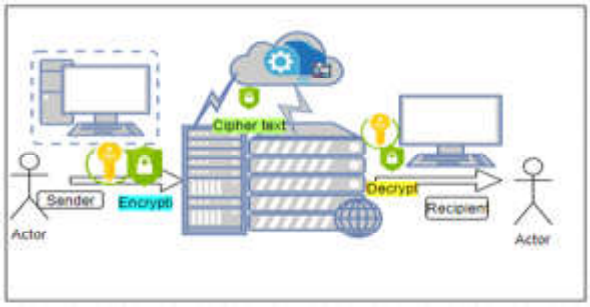

Fig.1 Basic Process of E&D (Encryption and Decryption)

Types and step process of E&D based on two types one is symmetric encryption Figure.2 and other one is asymmetric encryption Figure.3.

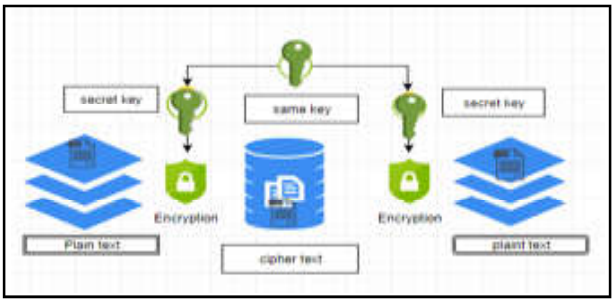

Fig.2 Symmetric encryption

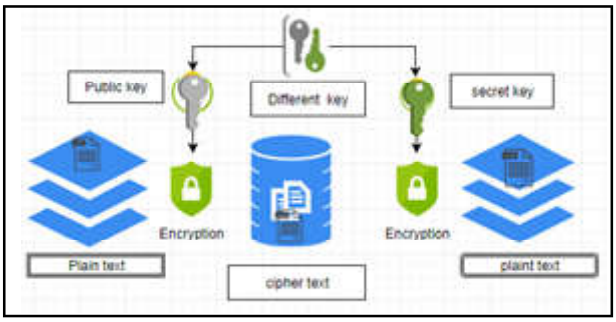

Fig.3 Asymmetric encryption

2.2 Comparison of Encryption Technique

Table 1 old-encryption technique VS Novel-encryption technique

Key difference	Order and old-encryption technique	Unorder and Novel-encryption technique
Cypher text size	The original plain text file is bigger than the encrypted text.	The encrypted text is bigger than the plain text file.
Data-size	Used to send enormous volumes of data.	Used to transmit small quantities of data
Resource obtained	Symmetric key encryption saves resources. Process as Fig 2.	Asymmetric encryption consumes a lot of resources. Process as Fig 3.
Key length	128- or 256-bit key sizes	RSA key size of at least 2048 bits
Security	Because it only employs one key for encryption, it is less secure.	Because encryption and decoding employ two keys, it is significantly safer.
Number Quantity of keys	In symmetric encryption, a single key is used for both encryption and decryption.	The usage of asymmetric encryption requires extensive resource use.
Method	Ancient technique.	Novel technique.
Confidentiality	When both encrypt and decode utilise the same key, key compromise is more possible.	To avoid having to share a key, two keys are generated separately for encryption and decryption.
Speed	A rapid approach that makes use of symmetric encryption.	Asymmetric encryption takes longer to perform.
Algorithm	DES, 3DES, AES, IDEA, RC4, and RC5.	RSA, Diffie-Hellman, DSA etc

2.3 Literature Survey

The EFH-CP-ABE Access-Control-Scheme with Attribute-Based Encryption, invented by J. LI, N. CHEN, and Y. ZHANG, provides many advantages over traditional methods. "Shulan- Wang, Junwei Zhou, Joseph K. Liu, Jianping-Yu, Jianyong-Chen, and Weixin Xie were the first to present the FH-CP-ABE approach". Compared to this approach, EFH-CP-ABE offers a few similarities, benefits, and drawbacks. We can therefore conclude that EFH-CP-ABE is the upgraded version of FH-CP-ABE. This cryptography policy scheme uses the same process level to encrypt multiple files. The method's security in the common model is formally established. Nonetheless, we think that the authority center-party may be completely trusted in the current arrangement. If the cloud authority becomes untrustworthy, his method might no longer be secure.

CP-ABE: [ABE Type] Initially presented by Sahai and Waters, to identify & address the ABE difficulties. Each user's identification is determined by a few attributes. Additionally, it developed a method for delivering "fine-grained access control" in a Cloud-Garage-Environment or in any other cloud storage procedures.

The two forms of ABE are key-policy-ABE (KP-ABE), which Goyal et al. first published. Furthermore, Bettencourt was the one who initially proposed the ABE ciphertext policy (CP-ABE). The [attribute set] and [access structure] in this scenario are appropriately associated with the private keys of the user/receivers and the CT (ciphertext). Only if a user's attribute set validates or satisfies the requirements of the access structure may they decode the ciphertext. Despite the unreliability of these cloud services, the CP-ABE system successfully forbids any unauthorised or untrusted user from accessing data garage-store on remote cloud servers.

Attribute-Based Multi-Authority Encryption: It (MA-ABE-secure scheme) is a stimulus of ABE-scheme in which the CA is dispersed widely over numerous independent parties. The first MA-ABE system based on prime-standard pairings that does not require a trusted setup. Prior to MA-ABE, (ABE) systems-module used characteristics for data encryption and decryption in secure state during data-transmission. The developers (Sahai and Waters) who devised an (ABE) scheme for the procedure. A single-access-tree-structure-authority has some disadvantages, some of which are as follows: The single-access-tree-structure-authority, CSP, manages all system attributes; failure-issue or corruption-data of the authority (Untrusted CA) affects the entire system. The Key-Escrow-problem is another weakness of a single-access-tree-structure-authority system. The single-access-tree-structure-authority distributes and shares private-keys so that the single-access-tree-structure-authority can decrypt any ciphertext in the system so here data can be loss. To address the shortcomings of a single-authority-attribute-based system-module, a multi-authority-attribute-based-encryption (MA-ABE-scheme) system was developed. This MA-ABE-scheme system employs a central-authority (CA) as well as several attribute-authorities (A-As). The (MA-ABE)-system is the CA-trusted-authority can decrypt-text and diminish the user-privacy and confidential-data of user, information, and resources, etc., so it may lead to problem or theft of data, which has an effect on cloud storage and also loss-data.

A multiple-authority based ciphertext encryption method A single central authority and a number of attribute authorities make up the attribute-based, multi-authority ciphertext policy encryption approach developed by Sascha Muller, Stefan Katzenbeisser, and Claudia Eckert. The method's disadvantage is that any ciphertext that is present in the network may be decoded by the central authority. A multi-authority ciphertext policy attribute-based encryption method is employed for monotonic access structures. This approach gets rid of the reliable central authority.Key-Management-Attribute-Based-Encryption is an alternative to the traditional ABE paradigm. Customers and users who has granted authorization-key can examine the data attributes in a tree-structured view. The end user's secret key is defined-order to reproduce the ATS- (access tree structure). To limit which cypher texts a user may decode, private keys are combined with monotonic access structures. Sets of features are pinned or pointed to in cypher messages.

Green *et al.* suggested outsourcing the CPA-secure CP-ABE initially in 2011. Only one modular exponentiation was left for the user to complete because the majority of Waters' expensive decryption methods were outsourced to a decryption proxy (such as Cloud Server). For each user enrolled with the Trusted-Authority, a process-get generates a public transformation key and a private decryption key (). The user submits his ciphertext to the decryption proxy, which uses the ElGamal algorithm to condense it into a brief ciphertext. The user then uses the decryption key to decrypt the new ciphertext. The user sends the decryption proxy, which converts the ciphertext into an El-Gamal short ciphertext, in order to decode it. The user then uses the decryption key to decrypt the new ciphertext. The success of this process also depends on the reliability of a third party. the format advised by Chun-I and colleagues ABE. The generation of keys is processed via identity-based encryption. System settings and keys are created and maintained by the root-authority. Data owners, cloud storage servers, domain authorities, and data consumers are given tasks by the approach. This has the benefit of making access control more precise possible. HIBE and CP-ABE are combined to accomplish full cloud delegation. Chun Yan et al. suggested combining (MA-ABE) with (EFH-CP-ABE) from (IBE) for CCA security and anonymity to boost security effectiveness.

In order to create distinct, obvious data security for both used and stored data, Vasily Sidorov. Transparent-Data-Encryption (TDE), which had previously been restricted in its ability to address privacy and security challenges, was improved by him. A secure, straightforward, and fine-grained question-result confirmation system was created by Hui Yin and Zheng Qin. a straightforward signature method is employed to confirm the reliability of the authentication item. For secure distributed massive data storage to accomplish privacy in cloud computing, Yibin Li et al. presented an intelligent cryptography-based method. To prevent your cloud administrator provider from receiving inaccurate data, it saves data in sporadic documents. The knowledge packets are split up to speed up processes. By developing a governing body that controls communication from user to server and back to the enquiring user, Palivela Hemant aimed to address security and backup difficulties. A database for user-server connections is provided by the routing-table, which is connected to the end and middle servers.

Lai *et al.* proposed decrypting and then validating the user's identity. Decrypts the encrypted text first, then validates its accuracy. The (ABE), which Jiguo Li and colleagues introduced in 2016, generates outsourced decryption with a strong focus on verity and then decrypts when the user first examines the cypher text after verification, indicating that the scheme-method is CPA. Plaintext attacks are safe. They added a delegation mechanism-scheme so that several-users may attest to the integrity of the encrypted material without access-to original file. Qi Li and colleagues focused on multi-authority-access-control for software storage. As a result, cloud storage now includes a secure, scalable, and reversible multiple authority access control mechanism.

J. Li, W. Yao, J. Han, Y. Zhang, and J. Shen, "CP-ABE With Efficient Attribute Revocation" Since each user has multiple attributes and numerous users have the same characteristics, CP-ABE techniques are used. This shows that in addition to preventing user collection, removing a single property can also have an impact on other system users. It also raises certain security concerns.

2.4 Preliminaries

The process of our work studies is referenced on CP-ABE-Scheme, FH-CP-ABE-Scheme, EFH-CP-ABE-Scheme, MA-ABE-Scheme And KBE- Scheme.

2.5 Related Work and Existing Studies with Problem Definition

The scheme FH-CP-ABE when compared to this method EFH-CP-ABE has some similarities, pros and cons, we can say that EFH-CP-ABE is the advanced level or next level of FH-CP-ABE. Then flexible access control (save time, computational cost of user) this method has developed to overcome one access level at a time in encryption, However-this approach has certain security flaws, so to improve that we move on to proposed work for develop and improvement security and level in one process by using M-ABE and KBE.As process mention on Figure 4.a, Figure 4.b, Figure 4.c.

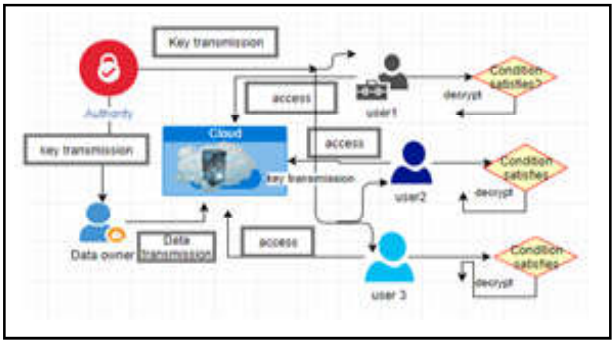

Fig.4 a) Existing system FH-CP-ABE with single-access level

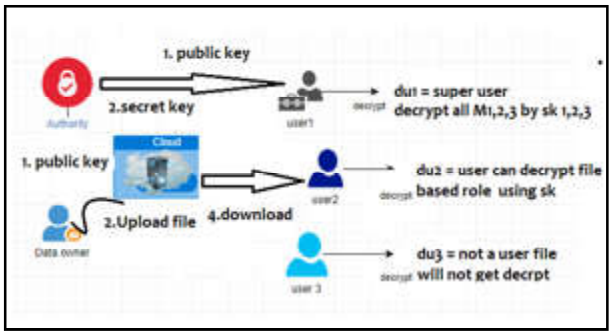

Fig.4 b) Existing system FH-CP-ABE with multi-access level

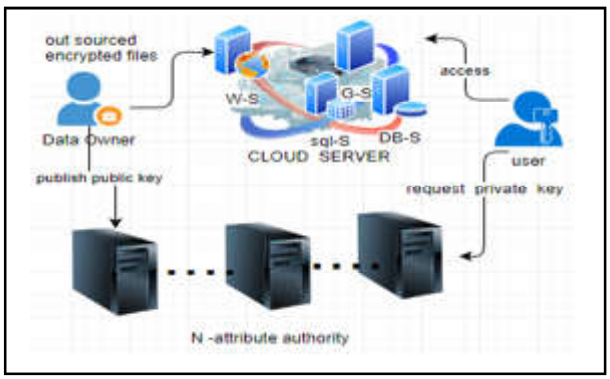

Fig.4 c multi-authority-attribute-scheme-based encryption

2.6 WHY TO PREFER MA-ABE, Multi-Authority Attribute-scheme-Based Encryption

It (MA-ABE-scheme) is a generalisation of ABE based on a stimulus where the CA is widely distributed across numerous independent parties. A trustworthy setup is not required for the first MA-ABE technique derived from prime-order pairings.

Attribute associated-encryption (ABE) is flexible encryption-approach used in the context of cloud-process computing, IOT, social-networks, other technological-resources where security-protection and privacy are critical needs of the cloud system (like EFH-CP-ABE method-based systems). The advantages and characteristics of the multi-authority-attribute-based-encryption-scheme (MA-ABE) method, which is one of numerous Attribute-Related-Encryption (ABE) techniques, are demonstrated in this study. A multi-authority-ABE system can have an unlimited number of attribute-authorities and user-types are differed. The system specifies two global public parameters. An end user can receive the appropriate decryption keys by selecting an attribute authority. Prior to MA-ABE, attribute-related-encryption (ABE) systems employed attributes to encrypt and decode data. (Sahai and Waters) they proposed an attribute-based model in 2005.A centralised-authority-system has various drawbacks, some of them are as follows: All system characteristics is managed by a single root-authority, CSP, Failure or corruption of the authority (Untrusted CA) impacts the entire system. Another vulnerability of a single authority system is the Key-Escrow dilemma. The single root-authority distributes and shares private-keys are order-to decipher any ciphertext in the system. A multi-authority-attribute-based-encryption-scheme (MA-ABE) system was created and solve the drawbacks of a single root-authority attribute-based-system. A central root-authority (CA) and many-attribute-authorities (AAs) used in MA-ABE system Chase and Chow proposed a method that would enable a multi-authority-attribute-based-encryption-scheme solution without full-access to central- authority. The system then leverages distributed pseudo random function approaches (PRF).

2.7 Proposed Method

Because we believe that this suggested work technique or scheme can enhance EFH-CP-ABE and also be utilised for (CP-ABE) for Big-Data-Access-Control in the Cloud-compute process, we have initiated a proposed effort to improve-resource-process. Extended-File-Hierarchy-Access-Control Scheme with Attribute-Based Encryption outperforms FH-CP-ABE. When compared to this approach, we can say that EFH-CP-ABE has certain similarities, as well as advantages and disadvantages, and that EFH-CP-ABE is the advanced level or next level of FH-CP-ABE.A Cryptography policy mechanism that encrypts multiple-files, data at the same-access level. In the standard model, it officially verifies the method's security. It allows safe and flexible-access-control in cloud-storage while also decreasing computation time for cloud clients. Nonetheless, we consider that the authority-centre-party is completely trustworthy in its current form. His technique may no longer be secure if the cloud authority becomes untrustworthy. All decrypted-keys can be obtained and decrypted-data or resources by an untrustworthy-CSP/untrustworthy authority centre. To eliminate the vulnerability created by a single authority centre, a multi-authority ABE system or any-other method (like KBA) that can be developed would be an appropriate strategy secure-cloud. A Cryptography policy approach in which numerous-files are encrypted on the same computer. Because the key-generation procedure of this approach is nearly identical with that of the CP-ABE method, we can extend it to a multi-authority scheme and also employ the Knowledge Based Authentication scheme for added security. Hierarchical-files are encrypted-data or resources with some condition of symmetric session-keys, and then session-keys are encrypted as well. These encrypted files/documents and encrypted-session-keys are all kept on cloud servers, which are virtual environments. The system's framework consists of four entities:

- Data Ownership (DO): The data holder/owner must keep and distribute a specific quantity of data on the CS. Files are divided-into various data-blocks based-on-access level permissions.
- Central Authority (CA): The central authority initiates the system process and creates the system's masters secret key and public parameters. It also generates the private key () of each attribute set at the same time. Where it is fully defined as a trustworthy entity.
- Cloud Server (CS): A cloud-server is a trustworthy yet perplexing entity in the world of cloud-resource computing technologies. It conducts ciphertext store and transfer services in the virtualized cloud environment with confidence.
- Data Client (DU): Data users can download the ciphertext from the CS and decode individual files/

documents/resources or the whole ciphertext into plaintext. Then, after obtaining the ciphertext, it performs the decryption procedure as follows: If its properties match those of a certain level node, it decrypts the relevant session keys using the EFH-CP-ABE encryption technique. Then, at the nodes, it handles all level nodes in the subtree of rooted nodes and obtains all related session keys. Finally, it obtains data-blocks, an-appropriate lower-level data blocks through the benefit-use of a symmetric encryption technique.

When compared-related to the FH-CP-ABE scheme approach, this procedure of EFH-CP ABE encryption may encrypt numerous files on the same access level, making it more practical, especially for more hierarchical sectors and large company growth and service businesses. It reduces storage space and compute costs in CS, and it also provides safe and flexible-access-control for users in cloud. store. However, if the CA is untrustworthy, it may result in data theft. To over-come this issue, we may use/add the different-kind of multi authority-based encryption and decryption policy attribute technique, adding protection through Knowledge Based Authentication as process mention in Figure 5.

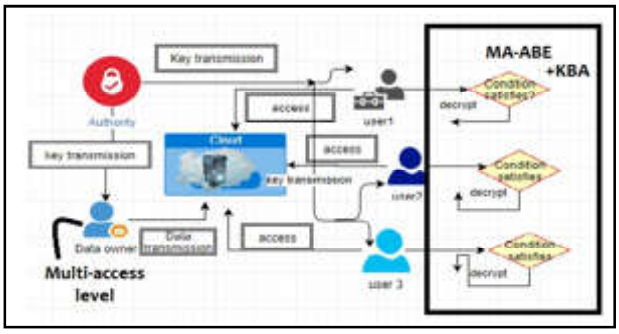

Fig. 5 Proposed system process

2.8 Compare the integrate access structure of EFH-CP-ABE and FH-CP-ABE

The majority of these systems' operations and outcomes are equivalent. The sole distinction is that EFH-CP-ABE supports different encryption methods at the similar access level (flexible access control), but FH-CP-ABE does not. When this method compares and related to EFH-CP-ABE, FH-CP-ABE provides more secure conditions for users to download data; nevertheless, in EFH-CP-ABE, the parent node of data can decrypt the data of child node files; to over-come this issue, we can utilise a multi-authority-based technique.

3. CONCLUSIONS

Throughout this study, we evaluate the FH-CP-ABE scheme to the EFH-CP-ABE scheme is order to-improve encryption access from one to multiple accesses at same-time, same-access-level. In addition to improve safe data transmission and security of cloud-store, we use (MA-ABE) Multi-attribute authentication is used, and we may strengthen security by using KBA, which improves access and allows users to use CS securely without the necessity for a CA or outside access.

4. FUTURE WORK

By utilizing the study concept of our paper work method and procedure, we will attempt to resolve these concerns (Analysis and Implementation of algorithm) in our future work.

REFERENCES

[1] J. Li, N. Chen and Y. Zhang, "Extended File Hierarchy Access Control Scheme with Attribute-Based Encryption in Cloud Computing," in IEEE Transactions on Emerging Topics in Computing, doi: 10.1109/TETC.2019.2904637, Vol. 9, No. 2, 1st April-June 2021, pp. 983-993.

[2] S. Wang, J. Zhou, J. K. Liu, J. Yu, J. Chen and W. Xie, "An Efficient File Hierarchy Attribute-Based Encryption Scheme in Cloud Computing," in IEEE Transactions on Information Forensics and Security, doi: 10.1109/TIFS.2016.2523941, Vol. 11, No. 6, June 2016, pp. 1265-1277.

[3] Shulan Wang and Junwei Zhou, Member, IEEE, Joseph K. Liu, Member, IEEE, Jianping Yu, Jianyong Chen, and Weixin Xie, "An Efficient File Hierarchy Attribute-Based Encryption Scheme in Cloud Computing", IEEE Transactions on Information Forensics and Security, Vol.11, No. 6, June 2016.

[4] A Study on CP-ABE-Based Medical Data Sharing System with Key Abuse Prevention and Verifiable Outsourcing in the IoMT EnvironmentYong-Woon Hwang and Im-Yeong Lee*

[5] Li and H. Zhu, "Multi-authority Attribute-Based Access Control Scheme in Mhealth Cloud with Unbounded Attribute Universe and Decryption Outsourcing", 2017, 9th International Conference on Wireless Communications and Signal Processing (WCSP), 2017, pp.1-7, doi: 10.1109/WCSP.2017.8171106.

[6] M. Green, S. Hohenberger and B. Waters, "Outsourcing the Decryption of ABE Ciphertexts", in Proceedings of the 20th USENIX Conference on Security, Berkeley, CA, USA, August 2011, pp.34.

[7] B. Waters, "Ciphertext-Policy Attribute-Based Encryption: An Expressive, Efficient, and Provably Secure Realization", in Proceedings of the IACR International Conference on Public-Key Cryptography, Taormina, Italy, March 2011, Vol. 6571, pp. 1-25.

[8] T. Elgamal, "A Public Key Cryptosystem and a Signature Scheme Based On Discrete Logarithms", IEEE Transactions on Information Theory, Vol. 31, 1985, pp. 469-472.

[9] M. Green, A. Akinyele and M. Rushanan, Libfenc, The Functional Encryption Library.

[10] E. Fujisaki and T. Okamoto, "Secure Integration of Asymmetric and Symmetric Encryption Schemes", in Proceedings of the Annual International Cryptology Conference, Santa Barbara, CA, USA, August 1999, pp.537-554.

[11] PalivelaHemant,Nitin Gawande,*et al.,* "Development of Servers in CC to Solve Issues Related To Security and Backup", 2011,IEEE.

[12] Chun-I Fan Attribute Based Encryption from Identity Based Encryption, Journal of LATEX class files,September 2016.

[13] VasilySidorov and WeeKeong Ng, "Transparent Data Encryption for Data-in-Use and Data-at-Rest in a Cloud-Based Database-as-a- Service Solution", 2015, IEEE.

[14] HuiYin and ZhengQin, *et.al.*, "Achieving Secure, Universal,Fine Grained Query Results Verification For Secure Search Scheme Over Encrypted Cloud Data", 2016, IEEE Transactions on Cloud, Jiang Schuci,GuoWeibin *et al,*"Hierarchy Attribute-BasedEncryption Scheme to Support Direct Revocation in Cloud Storage", 2017, IEEE.

[15] T.Khodadadi, Y.Javadianasl, F.Rabiei, M.Alizadeh, M.Zamani and SS.Chaeikar, "A Novel Graphical Password Authentication Scheme with Improved Usability", In 2021, 4th International Symposium on Advanced Electrical and Communication Technologies (ISAECT) 2021, Dec 6, IEEE, pp. 01-04.

[16] SS. Patel, A. Jaiswal, Y. Arora and B.Sharma, "Survey on Graphical Password Authentication System", Data Intelligence and Cognitive Informatics: Proceedings of ICDICI 2020, 2021, pp.699-708.

Indian Journal of Engineering, Science, and Technology (IJEST)

(ISSN: 0973-6255)
(A half-yearly refereed research journal)

Information for Authors

1. All papers should be addressed to The Editor-in-Chief, Indian Journal of Engineering, Science, and Technology (IJEST), Bannari Amman Institute of Technology, Sathyamangalam - 638 401, Erode District, Tamil Nadu, India.
2. Two copies of manuscript along with soft copy are to be sent.
3. A CD-ROM containing the text, figures and tables should separately be sent along with the hard copies.
4. Submission of a manuscript implies that : (i) The work described has not been published before; (ii) It is not under consideration for publication elsewhere.
5. Manuscript will be reviewed by experts in the corresponding research area, and their recommendations will be communicated to the authors.

Guidelines for submission

Manuscript Formats

The manuscript should be about 8 pages in length, typed in double space with Times New Roman font, size 12, Double column on A4 size paper with one inch margin on all sides and should include 75-200 words abstract, 5-10 relevant key words, and a short (50-100 words) biography statement. The pages should be consecutively numbered, starting with the title page and through the text, references, tables, figure and legends. The title should be brief, specific and amenable to indexing. The article should include an abstract, introduction, body of paper containing headings, sub-headings, illustrations and conclusions.

References

A numbered list of references must be provided at the end of the paper. The list should be arranged in the order of citation in text, not in alphabetical order. List only one reference per reference number. Each reference number should be enclosed by square brackets.

In text, citations of references may be given simply as "[1]". Similarly, it is not necessary to mention the authors of a reference unless the mention is relevant to the text.

Example

[1] M.Demic, "Optimization of Characteristics of the Elasto-Damping Elements of Cars from the Aspect of Comfort and Handling", International Journal of Vehicle Design, Vol.13, No.1, 1992, pp. 29-46.

[2] S.A.Austin, "The Vibration Damping Effect of an Electro-Rheological Fluid", ASME Journal of Vibration and Acoustics, Vol.115, No.1, 1993, pp. 136-140.

SUBSCRIPTION

The annual subscription for IJEST is Rs.600/- which includes postal charges. To subscribe for IJEST a Demand Draft may be sent in favour of IJEST, payable at Sathyamangalam and addressed to IJEST. Subscription order form can be downloaded from the following link http:// www.bitsathy.ac.in./ ijest.html.

For subscription / further details please contact:

IJEST
Bannari Amman Institute of Technology
Sathyamangalam - 638 401, Erode District, Tamil Nadu Ph: 04295 - 226340 - 44
Fax: 04295 - 226666 E-mail: ijest@bitsathy.ac.in Web:www.bitsathy.ac.in

Indian Journal of Engineering, Science, and Technology
Volume 14, Number 1&2, January - December 2020

CONTENTS